Doctoral Dissertation

Numerical Study on the Time-dependent Flow Behaviors of Fresh Concrete

フレッシュコンクリートの流動挙動の時間依存性に関する

解析的研究

March, 2018

Guodong Cao

Computer Science and Design Engineering
Graduate School of Science and Engineering
Yamaguchi University

Acknowledgements

Studying as a Ph.D student in Yamaguchi University is a challenge and opportunity for me. I have learnt a lot in Japan. During my doctoral course, there are many people had given me help and support.

First of all, I would like to express my gratitude to my supervisor Prof. Zhuguo Li for interesting discussion and advise. He not only gave guidance in my study, but also helped me in my life. His positive and optimistic attitude, strong research skills are my learning objects.

I am thankful to Prof. Masanori Fujita, Prof. Hideaki Nakamura, Prof. Katsuhiko Takami, and Prof. Takashi Saeki for their invaluable suggestions and advice.

Special thanks to Mr. and Mrs. Nagayama. who taught me Japanese.

Furthermore, I wish thank my colleagues, Yingdan Zhang, Sha Li, Zhisong Xu, Kun Guo, Qing Tian, Tatsuya Kitada etc. who have provide help and company in these years. I am grateful to Sosuke Ishida, and Naoki Maeda. They helped me do the concrete test, even though in summer and winter.

At last, I wish to thank my parents and my friends for their support and encouragement in my study and life.

Abstract

Concrete is one of the most widely used construction materials. The performances of hardened concrete is greatly dependent on the construction quality. Pump is widely used to transport concrete in construction site, and maximum pumping distance and height become greater and greater as high-rise buildings increase. And the amount of reinforcing steel bars in concrete member has been increased for achieving earthquake-resistant structure. Therefore, proper evaluation and prediction of the workability of fresh concrete, including flow ability, segregation resistance, and passing ability, etc., are essential to consider the structural, construction and environmental conditions. Numerical simulation is thought to be a rapid, inexpensive, and time & labor saving method for workability design.

Fresh concrete is a kind of viscous particle material that contains water, cement and aggregate particles. Interactions among the particles may lead to inter-particle tructure at rest, which are physical flocculation and cement hydration. The physical flocculation originates from a combined action of van der Waals attraction, electrostatic repulsion and steric hindrance, is a reversible process. The flocculated structure would be broken down by an agitation. When the hydrates are generated, there are linkages formed between particles. Since these lining structures are not easily destroyed by an external force, the formation of hydrate-linkage structure is an irreversible process. With the advance of degrees of cement hydration and physical flocculation, the flow ability of fresh concrete drops, i.e. shows standing time-dependent behavior.

Except for physical flocculation and cement hydration, the particle arrangement, which is usually described by the distribution and mean value of particle contact angles, also affects the rheological properties of fresh concrete. The movement of particles under external fore or own weight causes a change in the particle arrangement of fresh concrete. Hence, the flow behavior of fresh concrete is shearing time-dependent. Moreover, particle contact results in inter-particle frictional resistance that is dependent on the vertical pressure or normal stress on the shear plane. Therefore, fresh concrete's flow behaviors are not only shearing time-dependent but also vertical pressure-dependent.

Up till now fresh concrete is usually regarded as a viscous fluid, and the Bingham model is used as its constitutive model in the numerical flow simulation. But Bingham model is unable to describe the time-dependence, and pressure-dependence of flow behaviors. The standing and shearing time-dependences of fresh concrete are barely reflected in the numerical simulation.

This research aims to develop analytical methods for the time-dependent flow behaviors of fresh concrete. Fresh concrete is a kind of particle material as stated above, and its flow is a large deformation problem. Thus two particle methods were used in this study to simulate the flow behaviors of fresh concrete. First, a standing time-dependent Discrete Element Method (td-DEM) was proposed to investigate the standing time-dependence of fresh concrete. The td-DEM is a mesh free particle method and can directly express the contact model and describe the contact action change between

particles. The parallel contact model was adopted to describe the contacts between the physically flocculated particles, and the standing time-dependent sitffnesses of the parallel contact model were obtained by theoretical investigation. The effect of cement hydration was considered in the td-DEM by introducing the clumped particles that are particle group linked by the hydrates. In this td-DEM, the effects of cement's fineness and constitutes and the addition of mineral admixtures were also considered. For verifying this new td-DEM, the numerical simulation of the gravity-induced funnel flow of fresh mortar was performed. The numerical and experimental results at different standing time after mixing were well consistent.

Smoothed Particle Hydrodynamics (SPH) is also a mesh free particle method. Large deformation problem of free surfaces, such as flow of fresh concrete, can be easily and accurately tracked by the Lagrangian motion of particles. A numerical approach was proposed to investigate the shearing time-dependence of fresh concrete, on the basis of SPH and VGM (viscous granular material) model. The VGM model is a newly developed constitutive model, which can describe the nonlinear, shearing time-dependent, and pressure-dependent flow behaviors of fresh concrete. And the visco-plastic model, proposed by Murata, was adopted to treat the slippage resistance of fresh concrete at the flow boundary in this SPH. L-flow tests of three types of fresh mortar with different water cement ratio were simulated by using the proposed SPH. In order to discuss the effect of using different constitutive models, the numerical simulations using SPH and Bingham model were also performed for the mortar mixtures. It was found that the numerical results using VGM model were more consistent with the experimental ones than the Bingham model for low fluidity mixture since the VGM model can reflect the change of internal structure of fresh concrete during the flow process.

The numerical methods proposed in this paper would provide useful guidelines for optimizing the mix proportions of concrete to ensure it with suitable time-dependent flow behaviors.

Contents

List of Figures

List of Tables

Chapter 1
Introduction

1.1 Background of Research

The concrete pump is widely used to transport concrete in construction site, and maximum pumping distance and height become greater and greater as high-rise buildings increase. Amount of reinforcing steel bars in concrete members has been increased for achieving earthquake-resistant structure. The use of various admixtures results in the diversity of fresh concrete's properties. The properties of fresh concrete have significant effects on the mechanical performance, durability, surface appearance and so on. Therefore, proper workability, e.g. flow ability, passing ability and segregation resistance etc., is required for fresh concrete to build concrete construction efficiently with high-quality and to improve the quality of hardened concrete. The workability is not only dependent on rheological behaviors, but also related with the structural, construction and environmental conditions. So far, a lot of studies on the rheological test method have been performed to try to evaluate the flow ability of fresh concrete [3, 4], but since the workability is not only dependent on flow ability, but also related with the structural, construction and environmental conditions. The workability would not be properly judged if only based on the rheological test results. Moreover, there are no doubts that designing workability of concrete by experiment is costly
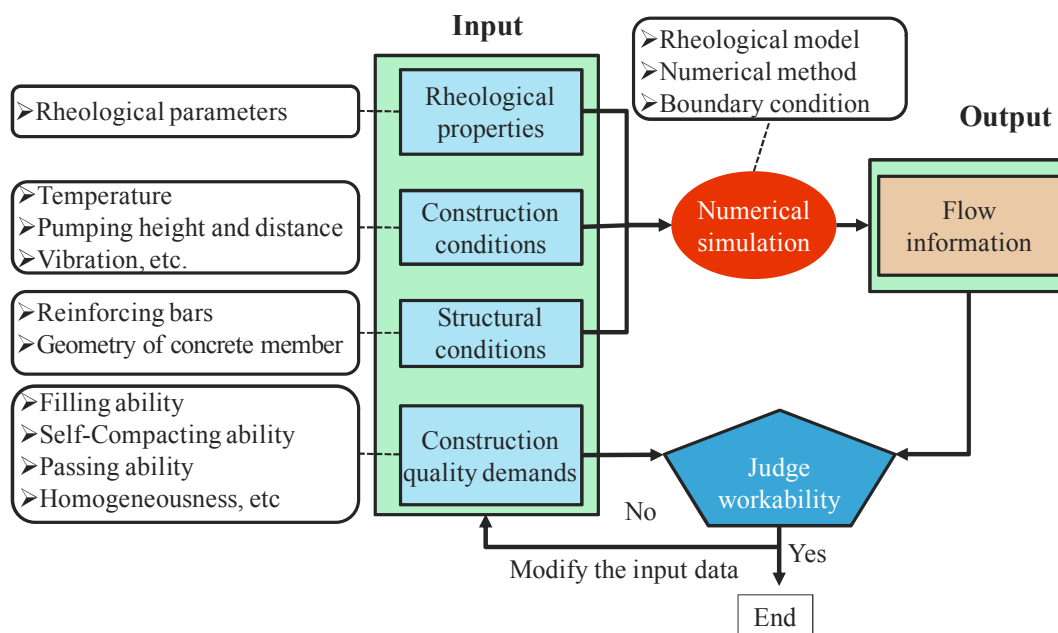
Fig. 1.1 Evaluating and designing workability of fresh concrete based on numerical simulation [2].

and labor intensive. With the development of computer technology, numerical simulation has increasingly become a more and more important tool for solving practical and complicated problems in engineering and science. Therefore, it is a alternative approach to evaluate and design the workability of fresh concrete based on numerical simulation [2, 5, 6], as shown in Fig. 1.1.

The rheological behavior of fresh concrete ongoing changes during the mixing, transporting, placing, casting and finishing (Fig. 1.2) [7]. The viscosity and yield stress decrease when fresh concrete is sheared and increase when fresh concrete is at rest. This is the so-called time-dependent flow behaviors of fresh concrete. It contains two aspects: standing time-dependence (at rest) and shearing time-dependence (shearing). Better understanding the time-dependent flow behaviors is necessary to improve the quality of hardened concrete.

Fresh concrete is a particle materials in water, interactions among the particles may lead to microstructures formation in the suspension at rest [8]. The microstructures are caused by thixotropy and cement hydration. As sand and gravel are inert non-colloidal particles, cementitious particles are the only potential source of thixotropy in a given concrete The thixotropy of fresh concrete is related to process of flocculation and dispersion and re-flocculation of cement particles [9, 10], as shown in
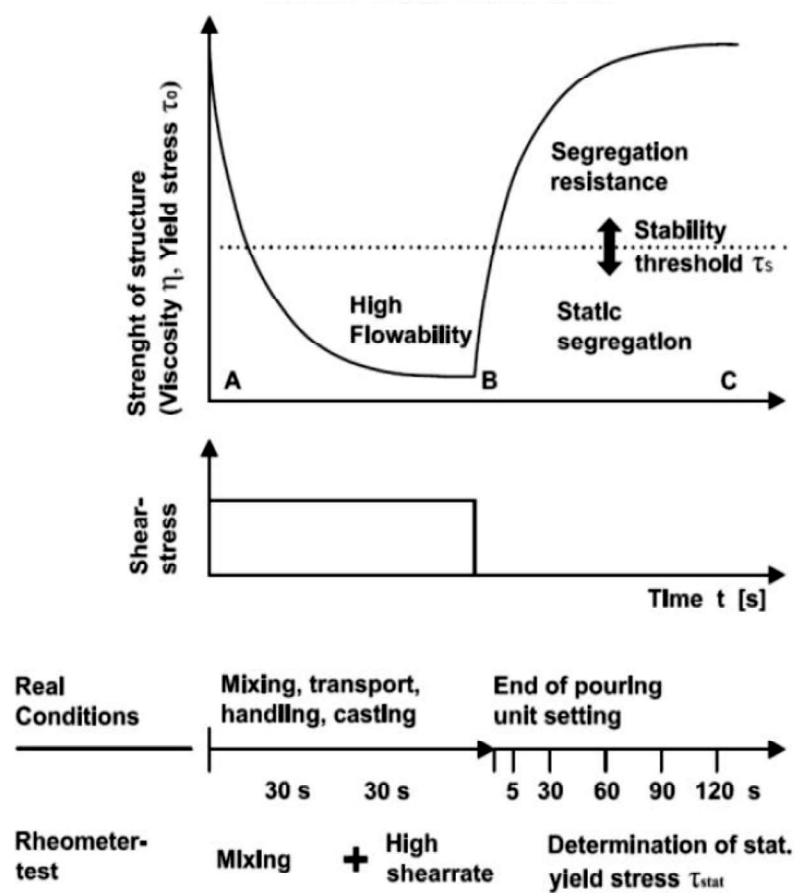
Fig. 1.2 Rheological parameters of fresh concrete depending on time
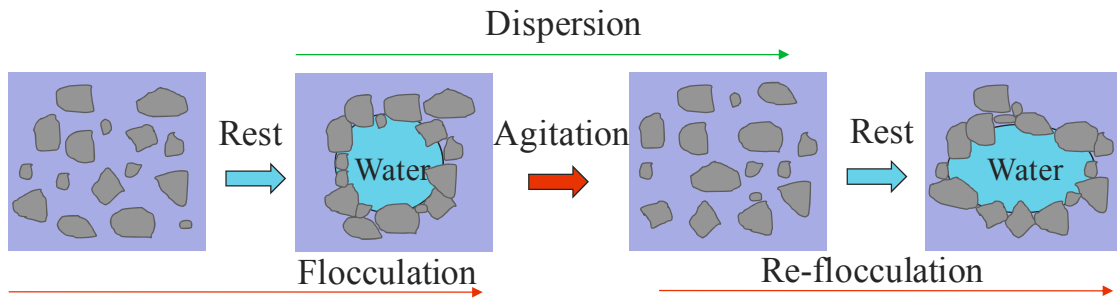
Fig. 1.3 The process of physical flocculation

Time
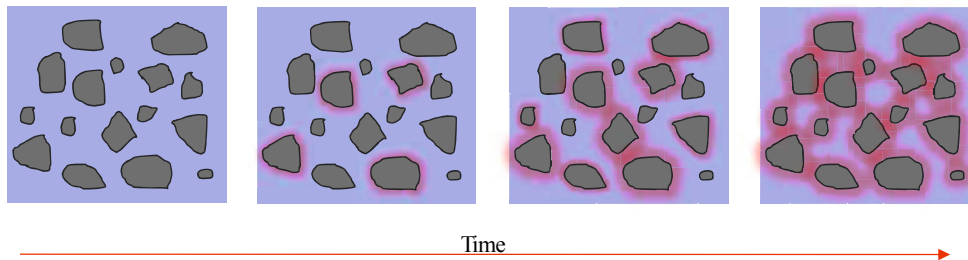
Fig. 1.4 The process of cement hydration

Fig. 1.3. The cementitious particles contact when flocculation occurs at rest and are separated when fresh concrete is sheared. They will contact again when fresh concrete is at rest again (Fig. 1.3). That is to say, the thixotropy is a reversible process. When two cement particles contact together by flocculation, the interaction of total potential energy exists between them. It originates from combined of forces of van der Waals attraction, electrostatic repulsion and steric hindrance [11, 12]. When cement is mixed with water, hydration happens and the surfaces of the cement particles are covered by sulphoaluminate hydrate (see Fig. 1.4), that is to say, there are linkages formed between
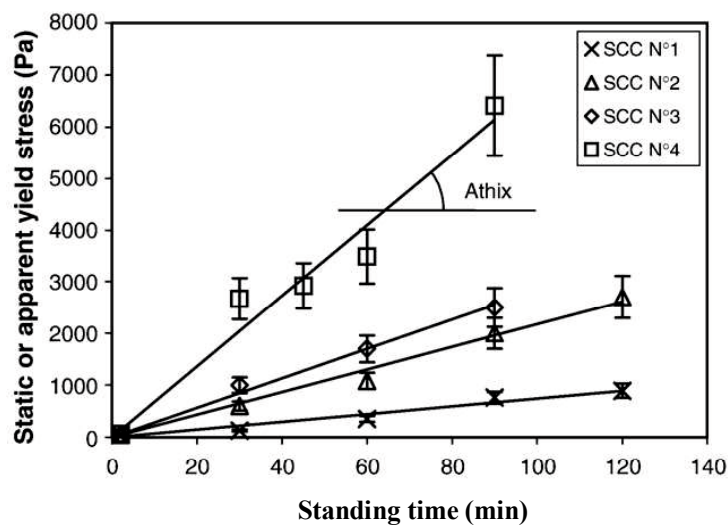
Fig .1.5 Static or apparent yield stress increases with standing time

3
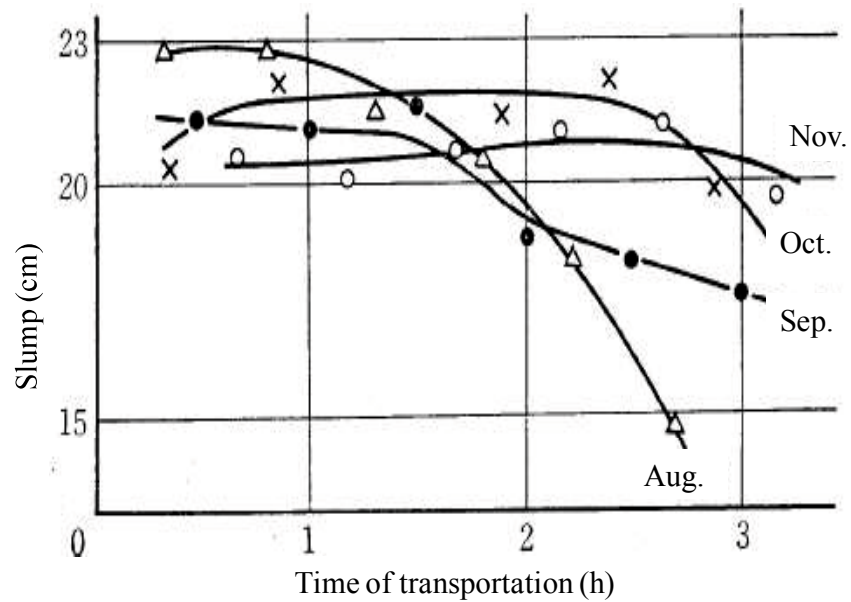
Fig. 1.6 The relationship of slump and time of transportation at different season [1].

cement particles. As soon as the cement agitated, the linkages may be broken [11]. No recovery of structure was measured for such case, i.e. the hydration of cement is a irreversible process. With the advance of cement hydration and flocculation at standing time, the static or apparent yield stress increased [13], as shown in Fig .1.5.

Because there is standing time-dependence, during the transportation process of fresh concrete, the slump is change with transportation time, as shown in Fig. 1.6. There are different slump loss at different months.

As shown in Table 1.1, according to the survey, about 30% blockage and pipe's damage are caused by slump loss. During the 3D concrete printing process, if the build-up rate is too small, the fresh concrete can't support the next materials, collapse happens, as shown in Fig. 1.7(a). if build-up rate is too large and the apparent stress increases above a critical value, then the two successive
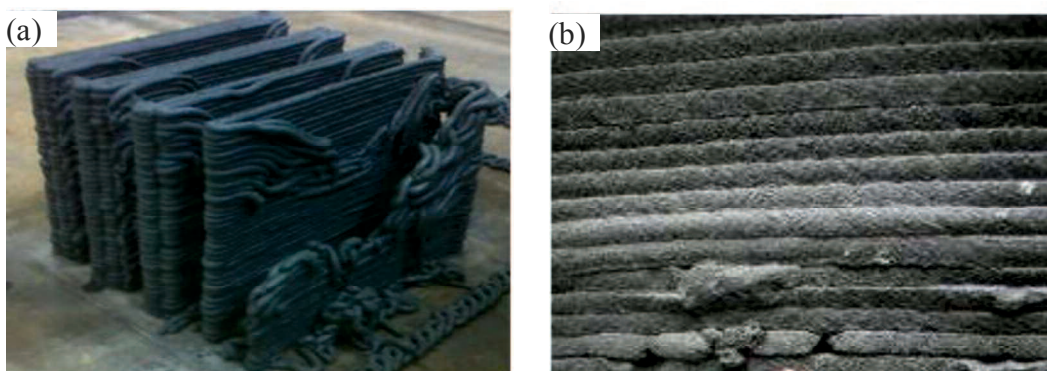
Fig. 1.7 (a) Collapse (b) Cold joints in 3D concrete print

Table 1.1 Types and reasons of trouble in concrete pumping

Types of trouble		Reasons of trouble			
		Construction conditions		Materials conditions	
Blockage	66%	Concrete supply stop	66%	Segregation	51%
		Insufficience of pump capacity	17%	Slump loss	31%
		Excessive pumping speed	8%	Excessive viscosity	15%
Pump failure	12%	Bad maintenance	56%		
		Aging	42%		
		Others	2%		
Pipe's destruction	11%	Thinness	62%	Slump loss	37%
		Excessive pumping speed	13%	Segregation	28%
		Concrete supply stop	10%	Excessive viscosity	28%
Tip hose's destruction	4%	Aging	62%	Segregation	43%
		Concrete supply stop	19%	Excessive viscosity	43%
		Excessive pumping speed	6%	Slump loss	14%

layers do not mix at all, and a weak interface, for example, cold joints, between the concrete layers may appear in the hardened concrete, as shown in Fig. 1.7(b).

The physical flocculation and cement hydration at rest will increase the number of contacts between particles. Accordingly, the contact forces increase. Except for physical flocculation and cement hydration, the inter-locking and friction between particles of fresh concrete also have important effects on the rheological behaviors of fresh concrete. The particle arrangement, i.e. the structure of granular body, which is usually described by the distribution and mean value of particle contact angles, can be quantificationally describe by the particle contact angle, as shown in Fig. 1.8.
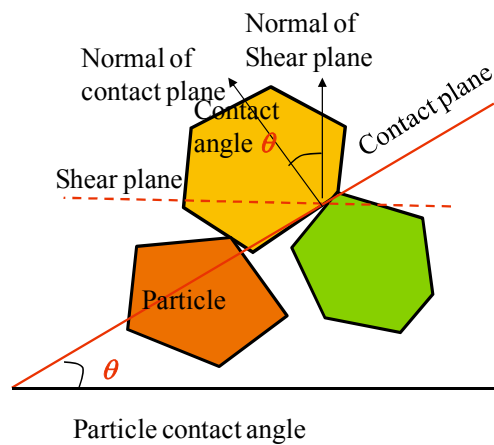
Fig. 1.8 Concept of particle contact angle
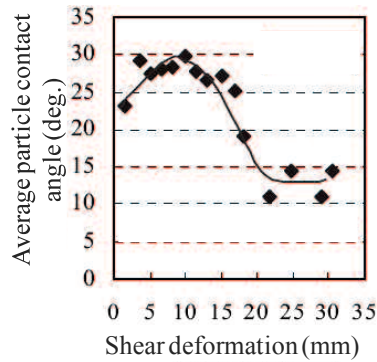
Fig. 1.9 The relationship of average particle contact angle and shear stress
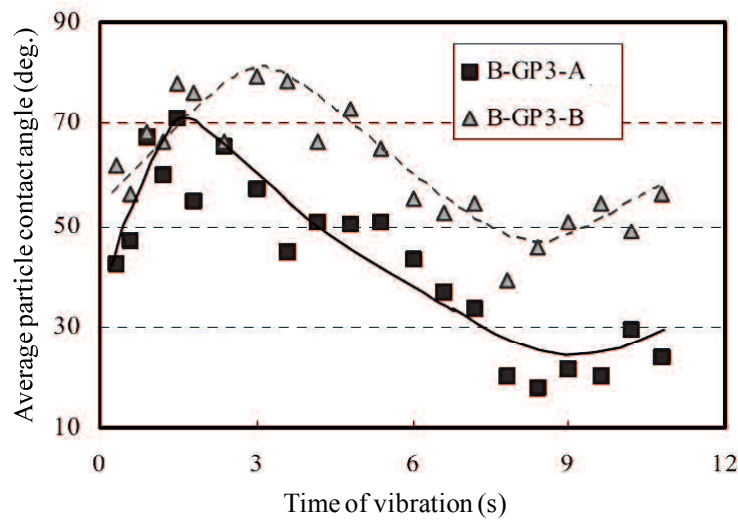
Fig. 1.10 The relationship of average particle contact angle and time of vibration

Before yield, the average particle contact angle increases and decreases when shear failure occurs [14]. Li et.al found that the average particle contact angle evolved with shear deformation and vibration, as shown in Fig. 1.9 and 1.10, respectively. [15]. That is to say, fresh concrete is shearing time-dependence. Because there is shearing time-dependence, when measuring the rheological behavior of concrete, the up-curve and down-curve do not coincide (Fig. 1.11(a)). When concrete is sheared at constant and low rate, the torque increases to a maximum value and then decreases to a certain value (Fig. 1.11(b)). Moreover, particle contact results in inter-particle friction. The inter-particle frictional resistance is dependent on the vertical pressure or normal stress on the shear plane. Hence, the deformation resistance of fresh concrete is pressure-dependent [16, 17]. The change of average particle contact angle results in the nonlinear flow behavior of fresh concrete.

Therefore, the time-dependences have important effects on the workability fresh concrete, but the numerical simulations of fresh concrete in the references fewly taken the time-dependences into account. And Bingham model is always used as the constitutive model, but it is unable to describe

(a) various shear rate   (b) constant and low shear rate
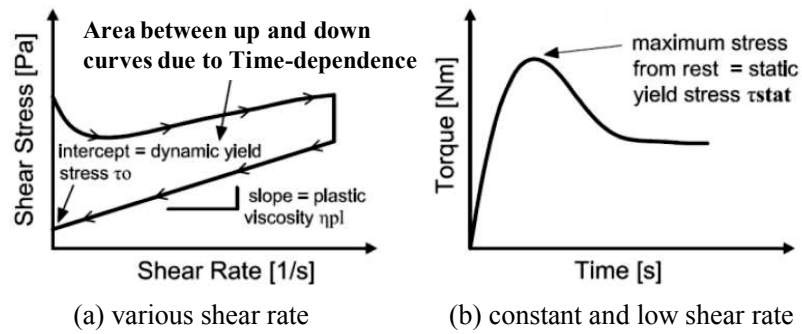
Fig. 1.11 The flow curve of fresh concrete

the nonlinear, and normal stress-dependent flow behaviors of fresh concrete, and it can't describe the change of rheological property with standing and shearing time.

1.2 Objectives of Research

The main objectives of the present research are as follows:

1. Develop a numerical method based on Discrete Element Method (DEM) to predict the standing time-dependent flow behavior of fresh concrete with or without mineral admixture. The effects of hydration and physical flocculation on rheological behavior were taken into account.

2. Develop a numerical method based on Smoothed Particle Hydrodynamics (SPH) and Viscous Granular Materials (VGM) model to study the shearing time-dependent flow behavior of fresh concrete. The shearing resistance at boundaries was considered.

1.3 Originality of Research

1. A standing td-DEM model is proposed to study the standing time-dependence of fresh concrete. Our standing td-DEM model is different from general DEM at two aspects: one is that the clumped particles with irreversible bonds were introduced to reflect the effect of hydration, which grow in quantity with time. The second is to permit the normal and shear stiffness (k_n, k_s) to change with time due to the hydrates' formation and particle flocculation, whereas in general DEM model the normal and shear stiffness are constants.

2. The VGM model, which can not only describe shearing time-dependence but also the nonlinear, pressure-dependent characteristics, was used as the constitutive model in the SPH simulation. The shearing time-dependent, nonlinear and pressure-dependent characteristics of fresh concrete can be accurately described.

1.4 Structure of Research

The frame of this dissertation is as follows:

Chapter 1 relates background, objectives and originality of the research.

Chapter 2 introduces the present researchers about time-dependences, constitutive models. The measuring method of parameters of VGM model is presented. The numerical approaches of fresh concrete are summarized. The problems in the current numerical simulation of fresh concrete are be summarized.

Chapter 3 experimentally investigates the standing and shearing time-dependent flow behaviors of fresh concrete. Firstly, the slump table test acting as the calibration test of input parameters of time dependent DEM was performed. Then the funnel flow under self-gravity of fresh mortar was carried out to evaluate the standing time-dependence. L-flow test of fresh mortar was used to investigate the shearing time-dependence. At last, the Ring Shear under Normal Stress (RSNS) rheometer test was performed to measure the parameters of Bingham model and VGM model.

Chapter 4 proposes a standing td-DEM model of fresh concrete. The parallel bond model was employed to express the physical dispersed-flocculation behavior of particles, and the clumps of particles were used to represent the bond particles due to the cement hydration. A viscous damping model was used for the viscous force. The changes of the numbers of the clumped particles and the flocculation particles with the standing time were investigated theoretically. The increase of degree of cement hydration was represented by the increase of number of clumps. The effect of physical flocculation was described by the change of normal and shear stiffness in parallel bond model. We assumed that the normal and shear stiffness changed linearly with standing time. Then the simulation of the flow table test of the fresh mortar was carried out to calibrate the input parameters of standing time-dependent DEM. Based on the obtained input parameters, the funnel flows, which were done at different moments after the mortar mixed, were simulated. The numerical results of the funnel flow were compared to the experimental data. The effect of mineral admixture on standing time-dependence of fresh mortar was investigated.

Chapter 5 proposes a shearing time-dependent SPH approach. The VGM model, which can describe the non-linear flow behavior, and pressure-dependence of the rheological behaviors of fresh concrete besides the shearing time-dependence, was used as constitutive model. The slippage resistance was also taken into account at the flow boundaries. Then input parameters of VGM model measured in chapter 3 were used, the numerical simulation of L-flow test was conducted. In order to contrast, numerical simulation based on SPH and Bingham model were also done for the same mortars.

Chapter 6 draws the global conclusions of the dissertation, and provides recommendations for future works.

References

[1] S. Karasuda, Transport planning and management of ready mixed concrete for concreteconstruction, *Summaries of Cement and Concrete, Japan Cement Association (JCA),* 277 (1970) 28-34.

[2] Z. Li, State of workability design technology for fresh concrete in Japan, *Cement and Concrete Research,* 37 (9) (2007) 1308-1320.

[3] C. F. Ferraris, F. de Larrard, Modified slump test to measure rheological parameters of fresh concrete, *Cement, Concrete and Aggregates,* 20 (2) (1998) 241-247.

[4] C. F. Ferraris, Measurement of the rheological properties of high performance concrete: state of the art report, *Journal of Research of the National Institute of Standards and Technology,* 104 (5) (1999) 461.

[5] R. Deeb, S. Kulasegaram, B. L. Karihaloo, 3D modelling of the flow of self-compacting concrete with or without steel fibres. Part I: slump flow test, *Computational Particle Mechanics,* 1 (4) (2014) 373-389.

[6] H. Lashkarbolouk, A. M. Halabian, M. R. Chamani, Simulation of concrete flow in V-funnel test and the proper range of viscosity and yield stress for SCC, *Materials and Structures,* 47 (10) (2014) 1729-1743.

[7] D. Lowke, Superplasticizers and Thixotropy of Fresh Concrete,[In:] 9th ACI International Conference on Superplasticizers & 10th International Conference on Recent, *Seville, Spain, October,* (2009) 11-37.

[8] N. Roussel, Steady and transient flow behaviour of fresh cement pastes, *Cement and concrete research,* 35 (9) (2005) 1656-1664.

[9] J. E. Wallevik, Thixotropic investigation on cement paste: Experimental and numerical approach, *Journal of non-newtonian fluid mechanics,* 132 (1) (2005) 86-99.

[10] J. E. Wallevik, Rheological properties of cement paste: thixotropic behavior and structural breakdown, *Cement and Concrete Research,* 39 (1) (2009) 14-29.

[11] G. H. Tattersall, P. Banfill, The rheology of fresh concrete, Pitman London, 1983.

[12] R. J. Hunter, Foundations of colloid science, Oxford University Press, 2001.

[13] N. Roussel, F. Cussigh, Distinct-layer casting of SCC: the mechanical consequences of thixotropy, *Cement and Concrete Research,* 38 (5) (2008) 624-632.

[14] Z. Li, Rheological model and rheometer of fresh concrete *Journal of Structural and Construction Engineering, Transaction of Archcitectural Instistue of Japan,* 80 (710) (2015) 527-537.

[15] Z. Li, Y. Tanigawa, Investigation on granular characteristics of fresh concrete based on visualized experiment using alternative materials, *Journal of Structural and Construction Engineering, Transaction of Archcitectural Instistue of Japan,* 77 (678) (2012) 1175-1184.

[16] Z. Li, T. Ohkubo, Y. Tanigawa, Yield model of high fluidity concrete in fresh state, *Journal of Materials in Civil Engineering,* 16 (3) (2004) 195-201.

[17] H. Mori, M. Tanaka, Y. Tanigawa, Experimental study on shear deformational behavior of fresh concrete, *Journal of Structural and Construction Engineering,* 427 (1991) 1-10.

11

Chapter 2
Review of Previous Research

2.1 Introduction

The previous research relating to this dissertation is summarized and commented in this chapter. Section 2.2 summarized the previous research about the time-dependent flow behaviors of fresh concrete. Section 2.3 introduced the constitutive models of fresh concrete. The calculations of shear stress and shear strain rate of VGM model were also presented. Section 2.4 concluded the numerical simulation of fresh concrete and analyzed their advantages and disadvantages. The problems in the numerical simulation of fresh concrete were summarized at section 2.5. The reasons why DEM and SPH were chosen to study the time-dependent flow behaviors were also given.

2.2 Measurement and Evaluation of Time-dependent Flow behaviors

The physical flocculation and cement hydration have important effects on the properties of fresh concrete, including static stability, air entrapment, surface finish, maximum formwork pressure and its decay after casting, and interlayer bond strength during multi-layer casting in the absence of vibration [1-4]. The viscosity of fresh concrete is dependent on the average particle contact angle during flow process, the flow velocity increases without the consideration of physical flocculation and cement hydration. It is necessary to measure and evaluate the time-dependent flow behaviors of fresh concrete. In the literatures, a lot of researchers have been done for measuring and evaluating the time-dependences of fresh concrete.

Lapasin et.al measured the difference $\Delta\tau$ of maximum shear stress τ_{max} needed to initial flow and the equilibrium τ_e at different rotation speeds ω at a constant shear rate. The thixotropy of a cement paste can be represented quantitatively by the area comprised between the maximum stress and the equilibrium stress curves in the shear stress and rotation speed diagram (Fig. 2.1) or by the area comprised between the difference of maximum and equilibrium stress and rotation speed (Fig 2.2) [5]. This curve can be represented by the following equation

$$\Delta\tau = \frac{\omega}{a+b\omega} \tag{2-1}$$

where, the coefficients a and b are functions of the compositive flow behaviors of the mixture.

Yim. et al. developed a laser backscattering instrument (Fig. 2.3) to monitor the flocculation and deflocculation of cement clusters when cement paste was under Couette flow. The change of cement grains was continuously observed with the change of shear stress under specific shear strain
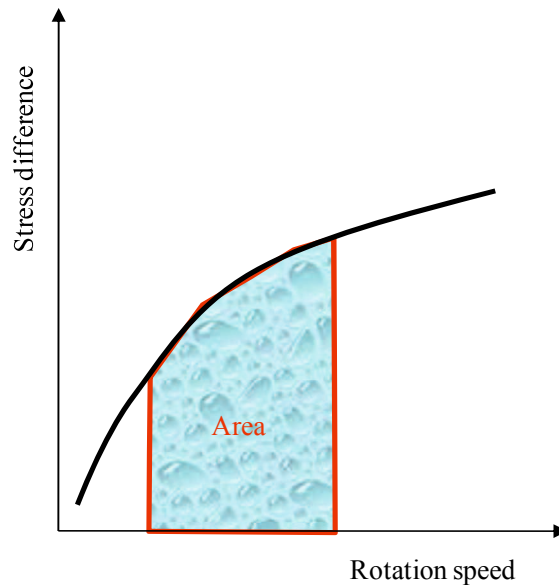
Fig. 2.1 Equilibrium and maxima shear stresses difference vs. rotation speeds
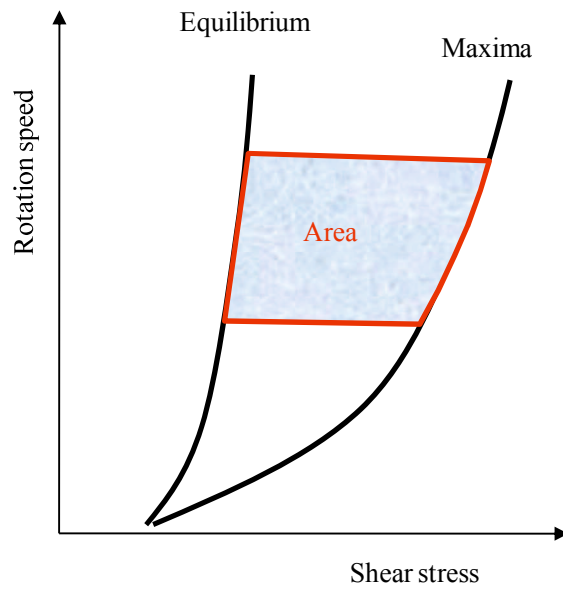
Fig. 2.2 Equilibrium and maxima shear stresses under different rotation speeds
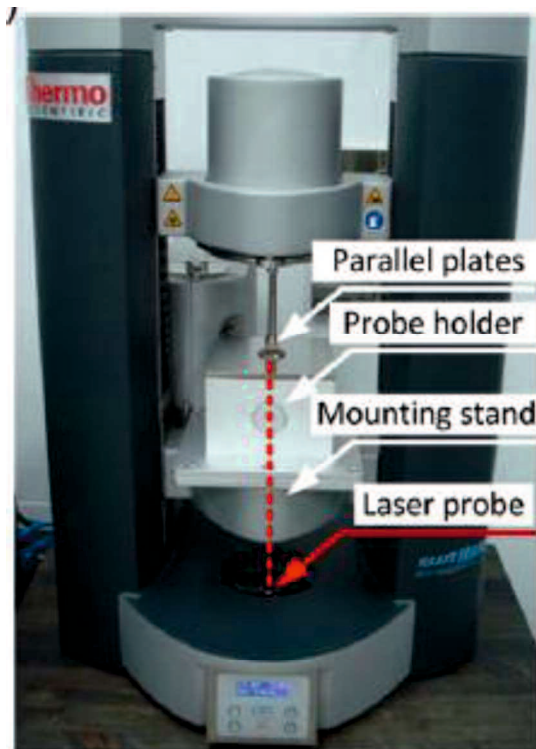
Fig. 2.3 Laser backscattering instrument

rates of 1 s^{-1}, 10 s^{-1}, and 100 s^{-1} [6]. The change of distribution of cement or binder was continuously observed, showing flocculation or deflocculation. The change of the shear stress was simultaneously measured. It reveals that flocculation depends on the shear strain rate.

Khayat et al. [7] expanded the inclined plane technique (Fig. 2.4) for estimating the structural

14
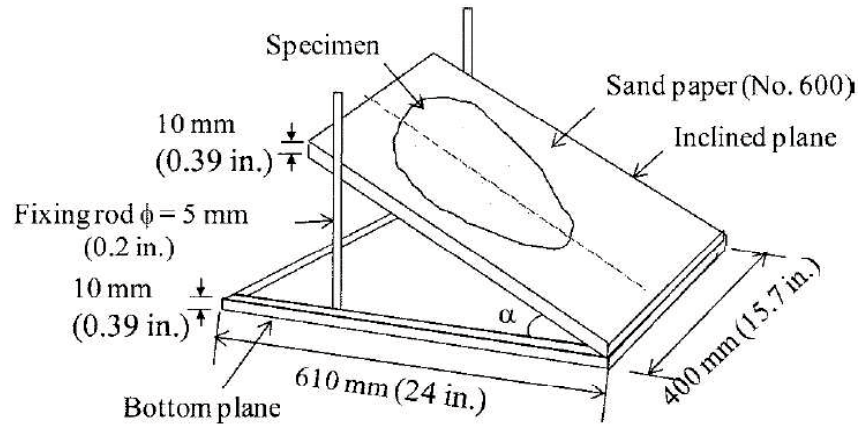
Fig. 2.4 Schematic of inclined plane test

buildup of highly fluidity self-leveling mortar and SCC mixtures. The sheared mass of the cementitious material on the plane with an angle of α and an effective height of h begins to flow downward due to gravitational acceleration g. Considering ρ as the density of mixture, the shear stress is calculated by

$$\tau = \rho g h \sin \alpha \qquad (2\text{-}2)$$

The shear stress of 29 SCC mixtures were measured by the inclined plane technique and compared to the experimental results using a concrete rheometer, the correlation coefficient R^2 is 0.82.

Li et.al theoretically analyzed the time-dependence of high fluidity concrete by considering the effects of both hydration and physical flocculation of cement particles [8] and proposed numerical models to quantitatively predict the fluidity of high fluidity concrete in any time and under any stress state. A series of numerical analyses were carried out based on the proposed models, the variations of apparent viscosity or Bingham parameters with standing time of stationary state or agitated state were discussed under different conditions, such as temperature, hydration rate of the cement, superplasticizer dosage, dispersion degree of cement particles, the dependence of the fluidity on standstill time and stress duration, as well as the influencing factors of the dependence, were quantitatively clarified.

Roussel presented a thixotropy model for fresh fluid concretes [9]. The model was agreement with the experimental observations reported in the literature. The predictions of the model were successfully compared with various experimental measurements obtained with a BTRHEOM rheometer.

Recently, Jarny et al. have shown using MRI velocimetry that, over short timescales flocculation and de-flocculation processes dominate, which lead to rapid thixotropic effects, while

15

over larger timescales hydration processes dominate, which lead to irreversible evolutions of the behavior of the fluid [10]. These two effects work simultaneously at any time of fresh state, but they appear to have very different characteristic times.

2.3 Constitutive Models of Fresh Concrete

The rheological behaviors of fresh concrete play a significant effect on concrete construction. The rheological behaviors of fresh concrete are usually described by a constitutive model. The model parameters are generally estimated from the relationship of shear stress and shear rate. Using a proper constitutive model in the simulation to thoroughly characterize the rheological behaviors can improve the accuracy of numerical approach. The constitutive models of fresh concrete in the references are given below.

2.3.1 General Models

(1) Bingham model

Bingham model is the most widely used to describe the rheological behaviors of fresh concrete, and is expressed by

$$\tau = \tau_0 + \eta_b \dot{\gamma} \tag{2-3}$$

where, τ is shear stress, τ_0 is yield stress, η_b is plastic viscosity, and $\dot{\gamma}$ is shear strain rate.

The constitutive law shown in Eq.(2-3) is discontinuity when shear stress τ approaches to the yield stress τ_0. When subjected to the τ_0, the apparent viscosity ($\eta_{app}=\tau/\dot{\gamma}$) becomes infinite so that numerical divergence occurs in the computation. Hence, it is difficult to introduce directly Bingham model into the numerical simulation. A regularized Bingham model or Bingham type model is used [11].
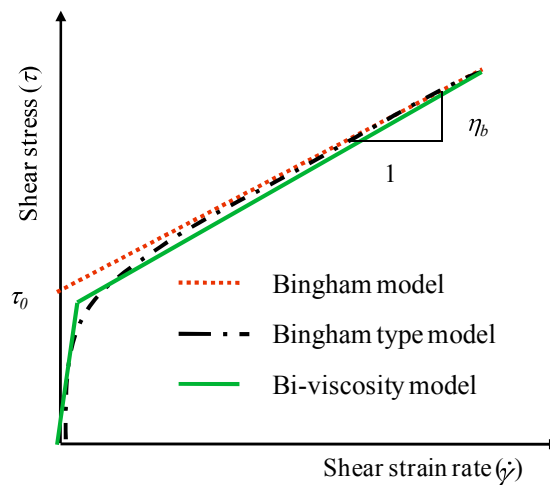
Fig. 2.5 The Bingham model, Bingham type model and bi-viscosity model

$$\tau = \left(\eta_b + \tau_0 \frac{\left[1 - e^{\beta \dot{\gamma}} \right]}{\dot{\gamma}} \right) \dot{\gamma} \qquad (2\text{-}4)$$

where, β is a parameter related to the transition between the solid and fluid regimes. The larger the β, the sharper the transition [12].

The other way to avoid the numerical divergence is to used a so called bi-viscosity model. It assume the viscosity is very large before yield, and it likes Bingham fluid after yield. The Bingham model, Bingham type model and bi-viscosity is shown in Fig. 2.5.

(2) Eyring model [13]

$$\tau = a\dot{\gamma} + b \sinh^{-1}(\dot{\gamma}/C) \qquad (2\text{-}5)$$

where, a, b and C are constants, previously applied to simple fluids and subsequently extended to suspensions. This model does not include the yield value term.

(3) Herschel-Bulkley model [14]

$$\tau = \tau_0 + K\dot{\gamma}^n \qquad (2\text{-}6)$$

where K is the viscous and n is the power index, which represents the deviation from Newtonian behavior. n > 1 for shear thickening fluid and n < 1 for shear thinning fluid. This model leads to the Newton law when $\tau_0 = 0$ and n=1, to the Bingham model when n=1, and to a power law when $\tau_0 = 0$.

The Herschel-Bulkley model was applied to cement pastes by Jones and Taylor [15]to correlate data obtained by measurements conducted with a cone and plate viscometer and successfully used by Atzeni [16].

(4) Vom Berg model [17]

$$\tau = \tau_0 + B \sinh^{-1}(\dot{\gamma}/C) \qquad (2\text{-}7)$$

where, B and C are constants.

It was successfully tested by Lapasin er al. [18] and appeared to be the most suitable state equation for explaining cement paste shear-dependent behavior.

(5) C. Atzeni model[16]

$$\gamma = a + b\tau + c\tau^2$$
(2-8)

where, a, b and c are constants

(6) Shangraw-Grim-Mattocks model [19]

$$\tau = \tau_0 + \eta_\infty \dot{\gamma} + \alpha_1 [1 - \exp(-\alpha_2 \dot{\gamma})]$$
(2-9)

where α_1 and α_2 are adjustable parameters, η_∞ is viscosity at initial shear rate.

(7) Casson model [20]

$$\tau = \tau_0 + \eta_\infty \dot{\gamma} + 2(\tau_0 \eta_\infty)^{1/2} \dot{\gamma}^{1/2}$$
(2-10)

This equation was derived by supposing the aggregation of the dispersed phase particles into hypothetical chains having their length depending on the interaction forces among the particles and on the shear stress.

The constitutive models from Eq. (2-3) to (2-10) do not describe the time-dependence and pressure-dependence of fresh concrete.

(8) Pressure dependent model [21]

There is friction when particles in fresh concrete contact. Mori et al [21] confirmed that the shear stress was dependent on the normal stress acted on the fresh concrete, and a pressure dependent model was proposed and is given by

$$\tau = \dot{\gamma}(\eta' \sigma_n + \tau_0) + (\tau'_y \sigma_n + \tau_0)$$
(2-11)

where, σ_n is normal stress acting on the shear plane that is caused by external force, τ'_y and η'_y are coefficients.

Although the model can describe the pressure-dependence, the self-gravity is not considered. And the coefficients are difficultly measured.

(9) Thixotropy model [9]

The yield stress of fresh concrete is dependent on the interaction between particles. The cement hydration and physical flocculation have effect on the interaction. A thixotropy model was proposed by Roussel [9] and is expressed by

$$\tau = (1 + \lambda_0 e^{-\alpha \dot{\gamma} t})\tau_0 + \eta \dot{\gamma}$$

(2-12)

where, α, λ_0 are coefficients.

Although the thixotropy model can describe the change of shear stress with time, but the change of plastic viscosity doesn't be expressed. So it is hardly used for ordinary concrete, especially for low fluidity concrete.

2.3.2 VGM Model

2.3.2.1 Introduction of VGM Model

At present, Bingham model is generally used to describe the rheological behavior of fresh concrete. Almost all the rheological tests are designed to measure the two parameters: yield stress and plastic viscosity of Bingham model to evaluate the consistency of fresh concrete [22]. And Bingham model is commonly used as a constitutive model of fresh concrete in numerical simulation [23, 24]. High fluidity concrete has a fluid flow behavior, and thus its flow behaviors are usually described approximately by Bingham model [25]. However, since fresh concrete is composed of cement and aggregate particles with inter-friction, and its deformation is time-dependent, it has the flow behaviors of both granular material and viscous material. Hence, fresh concrete is exactly a kind of viscous granular material rather than a viscous fluid, it is impossible that all the particles suspend in the mixing water without any contact [26].

Particle contact results in inter-particle friction. The inter-particle frictional resistance is dependent on the vertical pressure or normal stress on the shear plane. Hence, the deformation resistance of fresh concrete is pressure-dependent [21, 26]. On the other hand, the particle arrangement, i.e. the structure of granular body, which is usually described by the distribution and mean value of particle contact angles, also affects the deformation resistance of fresh concrete, while mean particle contact angle changes with the deformation so that dilatancy occurs [27]. The existence of particle contact angle amplifies the pressure-dependence of the deformation resistance. Once the dilatant deformation is restrained, normal stress and accordingly deformation resistance increase [28]. Fresh concrete is essentially a kind of particle material that contains water. The physical flocculation, dispersion and hydration of cement particles cause the change in the particle arrangement of fresh concrete. It is considered that the change of fresh concrete's particle arrangement, during the rheological tests, results in that the flow curve of fresh concrete is nonlinear

[25, 29], and shearing time-dependent [8]. Due to the same reason, measuring value of yield stress varies with the shearing time [9].

Obviously, Bingham model is unable to describe the nonlinear, and normal stress-dependent flow behaviors of fresh concrete, and it can't describe the change of rheological property with rest time and shearing time, i.e. the time-dependences of rheological property. The Herschel-Bulkley model, which is polynomial and quadratic function, was proposed to describe the nonlinear flow behavior [30, 31], but other flow behaviors are not expressed and the parameters in the model are lack of physical meanings and test methods [32].

As stated above, Bingham model can't exactly describe various rheological behaviors of fresh concrete overall since fresh concrete has granular flow behavior. For this reason, Li proposed the VGM model based on a series of theoretical analyses [25, 33] and experimental investigations[34, 35], as shown in Eqs. (2-13) and (2-14) [33, 36]. It was verified that this model is able to describe various rheological flow behaviors of fresh concrete [37]. When shear stress (τ) and shear strain (γ) are smaller than the shear failure limit stress (τ_f) and limit strain (γ_f), fresh concrete is in visco-elasto-plastic state, and the shear strain γ under a shear stress τ is expressed by Eq. (2-13). When $\tau \geqq \tau_f$ and $\gamma \geqq \gamma_f$, fresh concrete enters into the shear failure state, the τ–$\dot{\gamma}$ relationship is described by Eq. (2-14). The relationship of shear stress and shear strain is shown in Fig. 2.6

if $\tau < \tau_f, \ \gamma < \gamma_f$

$$\gamma = \frac{c_6\tau}{c_2 + c_3\tau} \cdot \frac{1}{\sigma_n + C_{w2}} \cdot [1 - \exp(-qt)] = \gamma_\infty \cdot [1 - \exp(-qt)]$$

$$\dot{\gamma} = \frac{c_2 c_6 s_1 / (\sigma_n + C_{w2})}{(c_2 + c_3\tau)^2} \cdot \left[1 - \exp\left(-q\frac{\tau}{s_1}\right)\right] + \frac{c_7\tau(c_2 + c_3\tau)}{\exp(q\tau/s_1)}$$

$$c_2 = \phi + \theta_0, \ c_3 = \frac{\theta_f - \theta_0}{\tau_f}, \ c_6 = \frac{1}{2}N\Lambda_0$$ (2-13)

$$q = c_8(\sigma_n + C_{w2})\left(\frac{c_2 + c_3\tau}{c_6}\right)^2, \ C_{w2} = Nf_{wm}\cos\theta_0$$

$$\gamma_\infty = \frac{c_6\tau}{c_2 + c_3\tau} \cdot \frac{1}{\sigma_n + C_{w2}}, \ c_8 = \frac{2\Lambda_c c_6^2}{hNc_2 \exp(E/kT)}$$

if $\tau \geq \tau_f, \ \gamma \geq \gamma_f$

$$\tau = \sigma_n \tan(\theta_f e^{-\kappa \cdot \dot{\gamma} \cdot (t - t_f)} + \phi) + C_{w1} + \frac{\eta}{\cos(\theta_f e^{-\kappa \cdot \dot{\gamma} \cdot (t - t_f)})}\dot{\gamma}$$ (2-14)

where, σ_n is normal stress acting on the shear plane, N is amount of particle contacts on unit area of the shear plane, κ is a parameter related to shearing time-dependence, t_f is shearing time before shear failure, s_1 is loading speed in case of stress growth control, θ_0, θ_f is average particle contact angle at

21

the initial state, and the shear failure point, respectively, Λ_0, Λ_c is average moving distance of all particles in the beginning, and average moving distance of cement particles for overcoming potential barrier, respectively, E is mean potential energy barrier of cement particles that results in a viscous resistance, T is absolute temperature, h is Planck constant, ϕ is average inter-particle frictional angle, C_{w1}, C_{w2}, f_{wm} is shear resistance, vertical stress, and adhesive force caused by the surface tension and suction of mixing water, respectively, η is the essential viscosity that is associated with temperature and potential energy of cement particles when there is no particle contact in fresh concrete.

Rewriting the VGM model into Bingham form, Eq. (2-15) is obtained.

$$\tau = \tau_f^* + \eta_t \dot{\gamma}$$
$$\tau_f^* = \sigma_n \tan(\theta_f e^{-\kappa \cdot \dot{\gamma} \cdot (t - t_f)} + \phi) + C_{w1}, \quad \eta_t = \frac{\eta}{\cos(\theta_f e^{-\kappa \cdot \dot{\gamma} \cdot (t - t_f)})} \qquad (2\text{-}15)$$

The shear failure limit stress τ_f is mainly dependent on normal stress σ_n, mean particle contact angle θ_f, and mean inter-particle frictional angle ϕ, and is expressed by Eq. (2-15) [36].

$$\tau_f = \sigma_n \tan(\theta_f + \phi) + C_{w1} \qquad (2\text{-}16)$$

Because almost all the present rheometers of fresh concrete adopt the rotational speed sweep control method, it is impossible to evaluate the deformation behavior of fresh concrete before yield. VMG model not only describes the flow behaviors of fresh concrete in shear failure state, i.e. in yielded state, but also provides the information about the deformation before yield.

Eq.(2-14) contains the parameters of ϕ and σ_n so that VGM model can reflect the granular and pressure-dependent flow behaviors of fresh concrete. Moreover, the term $\theta_f \exp[-\kappa \dot{\gamma} (t-t_f)]$ in the Eq.(2-14) expresses actually the change of mean particle contact angle with shearing time, i.e. reflects the change in the flocculent or interlocking structure of particles, when fresh concrete deforms or flows. If rewriting Eq.(2-14) in the form of Bingham equation, yield stress τ_f^* and plastic viscosity η_t of VGM model are not constants, varying with shear rate $\dot{\gamma}$ and shearing time t. Hence,
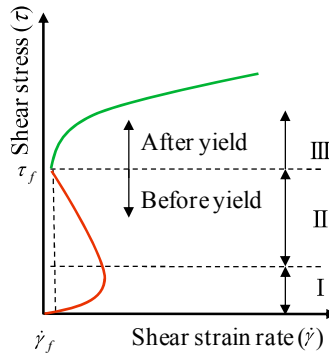
Fig. 2.6 The τ-$\dot{\gamma}$ relationship of VGM model.

VGM model can describe the non-linear and shearing time-dependent flow behaviors of fresh concrete.

The relationships between shear stress and shear strain rate consists of three parts. In the first part I, the particle contacts are loose, thus whole system is easy to deform, and the shear strain rate increases with shear stress. However, because the particles have to move to the positions with higher resistance for matching with subjected external force, the particle contacts become denser and denser with deformation, thus the shear strain rate begins to decrease at a certain shear stress even shear stress is increased (see Part II in Fig. 2.6). There is a limit in the increase of particle interlocking. If shear stress is increased continually and exceeds the stress limit τ_f of shear failure, the interlocking structure will be broken, the system enters into the shear failure state, and thus the shear strain rate increases with shear stress again (see Part III in Fig. 2.6). At the shear failure point, the average particle contact angle (θ) reaches to the maximum value θ_f, but decreases with the increase of the shear deformation in the shear failure state. Also, at the shear failure point, the shear strain rate $\dot{\gamma}_f$ is very small, nearly approaches to zero.

2.3.2.2 Measurement Method of Parameters of VGM Model

A rheometer shown in Fig. 2.7, called RSNS rheometer, was recently developed by Li for measuring the parameters of VGM model [36]. The RSNS rheometer has a motionless axis, thus fresh concrete or mortar sample is subjected to ring shear between two blades in radial pattern. Also, the RSNS rheometer can be operated by toque growth or rotation speed sweep control method, and the vertical pressure, acting on the shear plane, can be freely adjusted by two air cylinders. The

(a) apparatus   (b) planform of lower blade   (c) 2-D diagram
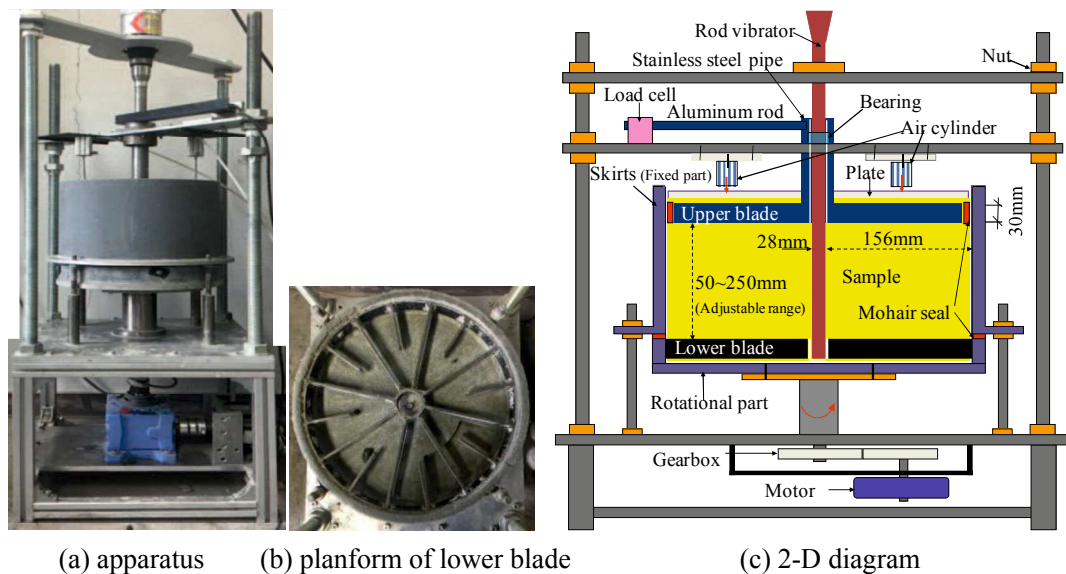
Fig. 2.7 RSNS rheometer

thickness of sample can be adjusted within 50 ~ 250 mm, and the diameters of sample's periphery and inner circumference are 340 mm and 28 mm, respectively. For low fluidity concrete, there is void near the blade. The sample is vibrated by a rod vibrator to eliminate void.

The VGM model describes both the rheological behaviors before and after yield. Hence, the measurement also divides into two parts: toque growth or rotation speed sweep control method [36]. The average shear stress is calculated by Eq. (2-17)

$$\tau_m = \frac{3\Gamma}{2\pi(R_2^3 - R_1^3)} \qquad (2\text{-}17)$$

where, Γ is torque exerted on sample, R_1 and R_2 are the diameters of inner circumference and sample's periphery, respectively.

The average shear strain and shear strain rate are at the middle position between rod vibrator and skirt. And they are calculated by

$$\gamma_m = \frac{\pi(R_1 + R_2)\varphi}{360h}, \qquad \dot{\gamma}_m = \frac{\pi(R_1 + R_2)\Omega}{360h} \qquad (2\text{-}18)$$

where, φ is rotational angle, Ω is angular velocity, h is the height of sample. The average shear stress, shear strain and shear strain rate are used in civil engineering to describe the mechanical performance of sand and soil [38, 39]. Hence, they will be used to describe the rheological behaviors of fresh concrete.

The detailed measurement and calculation of parameters of VGM model will be introduced at Section 3.6.

2.4 Numerical Approaches Simulating Fresh Concrete

With the development of computer technology, the numerical simulation becomes a novel and important tool to solve the practical problems in engineering. Based on it, the geometry of concrete structures, the mixture proportions can be optimized. Since 1992 Mori and Tanigawa firstly used numerical approach for concrete flow [40], there were a lot of simulations conducted for concrete test, e.g. slump [23], L_flow [41], V-funnel test [24, 42], etc. and concrete production and construction e.g. mixing [43], transportation [44], pumping [45] and casting [46], etc. Bingham model or Herschell Bulkley models are always used as constitutive model and fresh concrete is assumed to be a homogeneous fluid. The numerical approaches (Table 2.1) of fresh concrete that can be found in the literature may be divided into main series: single fluid simulation, simulation of discrete particle flow and coupling method of fluid and particle. The numerical approaches are almost about mixing, transportation, pumping, casting and concrete tests. There is few numerical study concerning the time-dependent flow behaviors of fresh concrete.

2.4.1 General Numerical Approaches
2.4.1.1 Single Fluid Simulations

Table 2.1 Numerical methods and commercial software used by researchers

Contact name	Country	Research group/institution	Commercial Software	Numerical method
Liberato Ferrarra	Italy	Polytechnico di Milano	None	CFD-particle Finite Element method
Nicolas Roussel	France	IFSTTAR	FLOW 3D	CFD-Volume of Fluid method
Ksenijia Vasilic	Germany	BAM	ANSYS Fluent	CFD-Volume of Fluid method
Annika Gram	Sweden	CBI	OpenFOAM	CFD-Volume of Fluid method
Jon Spangerberg	Denmark	DTU	FLOW 3D	CFD-Volume of Fluid method
Knut Krenzer	Germany	IAB Weimar	PFC 3D	Distinct Element method
Viktor Mechtcherine	Germany	TU Dresden	PFC 3D	Distinct Element method
Jan Skocek	Denmark	DTU	None	Lattice Boltzman method
Bhushan Lal Karihaloo	UK	Applied and Computational Mechanics	None	Smoothed Particle Hydrodynamics
Jon Elvar Wallevik	Iceland	Innovation Center Iceland	None	Viscometric-ViscoPlastic-Flow

1) Viscoplastic Finite Element Method and Viscoplastic Divided Element Method

Viscoplastic Finite Element Method (VFEM) is developed based on FEM by introducing a frictional interface law [47]. In VFEM, the fresh concrete is divided into discrete elements, then the individual elements are connected together by a topological map, which is usually called a mesh. The interpolation functions are built upon the mesh, the displacements of nodal points of mesh represent the deformation of fresh concrete. In Viscoplastic Divided Element Method (VDEM), space is divided into elements and cells, which are either empty or full, and the flow is described by the displacement of virtual markers. The fixed position of nodal points allows reinforcement and complicated structure to be simulated.

Mori and Tanigawa used the VFEM and VDEM to simulate flow of fresh concrete [40], both of these two numerical methods can simulate various concrete tests. Kurokawa et.al used the VFEM to study the effect of volume fraction of coarse aggregate on Bingham's parameters of fresh concrete [48]. Theane et.al assuming that the fresh concrete is a continuum fluid, using the Bingham model describing the rheological behavior, simulated the L-flow based on Galerkin FEM formulation of the Navier-Stokes equation [49]. The BML rheometer was used to measure the Bingham parameters When blockage don't occurs, it is possible to simulate the flow in the L-box with reinforce steel bars by a continuum mechanical approach and the Bingham model. It is not reasonable to simulate the plane of symmetry in a 3-d model (8-node brick elements) by that of a 2-d (4-node quadrilateral
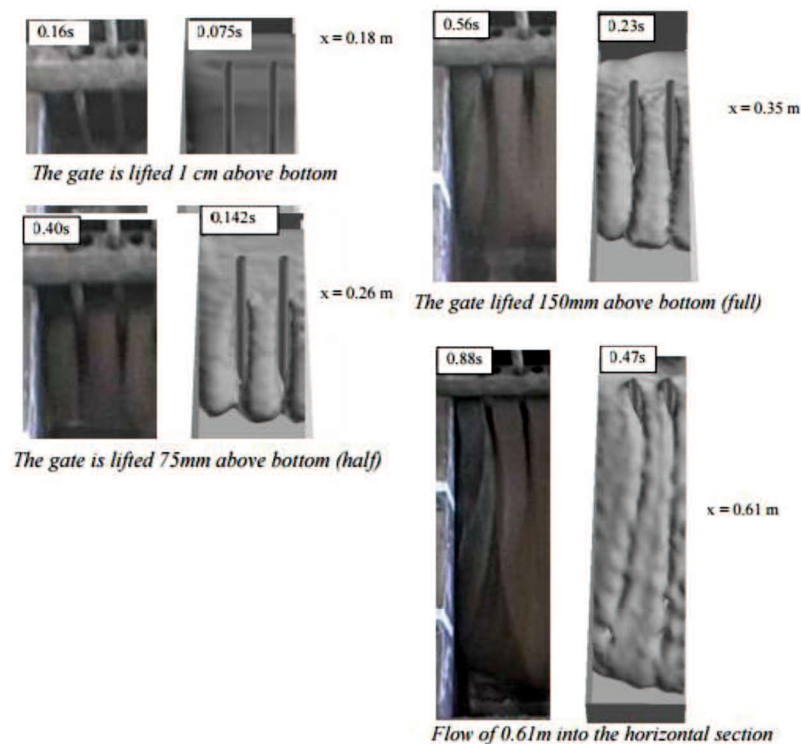
Fig. 2.8 Experimental results (left) and numerical simulations (right) at the same flow distance but different times

26

elements) model due to the effect of viscous. It is necessary to take the effect of lifting rate of gate and slid at the boundary into account in numerical simulation, otherwise, the numerical simulation does not seem to correspond to the experimental results, as shown in Fig. 2.8. However, it can't assess the blocking resistance due to the absence of particles in a continuum approach.

2) CFD-particle Finite Element method

A single fluid approach has been employed, using Polyflow, a CFD code developed by ANSYS, by Ferrara to assess the correlation between fundamental rheological properties of cementitious suspensions acquired through rheometer tests and field test parameters, a wide set of numerical simulations of both the mini-slump flow and the EN445 cone tests have been performed [50]. The Bingham model had been employed to describe the rheology behavior of fresh concrete. With reference to the mini-slump flow test, both the final slump diameter (Fig. 2.9(a)) and the time to final spread (Fig. 2.9(b)) of numerical and experimental results were compared. With reference to EN445 cone test, the flow times corresponding to different volumes of fluid cement paste flown out of the cone nozzle of numerical and experimental results were compared.

3) CFD-Volume of Fluid Method

Flow 3D code [11] is a general purposed computer program and is user friendly when dealing with complex free surface transient flow of non Newtonian fluids. Rouseel [51] performed 3D simulations of different slump test methods using the computational fluid mechanics code Flow 3D. The materials was assumed to behave as an incompressible elastic solid before yield, beyond which
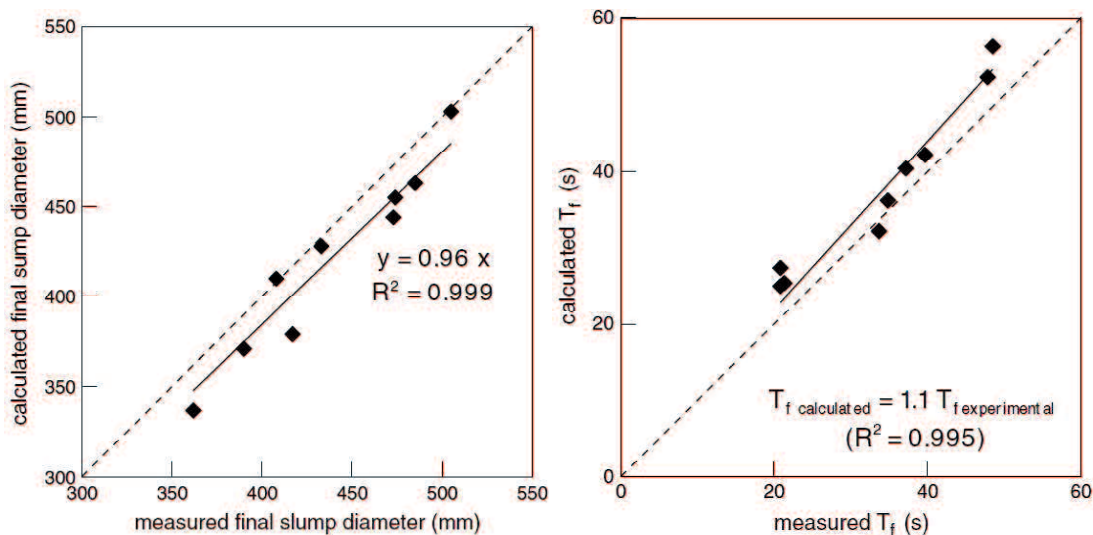
(a) final slump diameter (b) the time to final spread

Fig. 2.9 Experimental results and numerical simulation of min-slump flow test
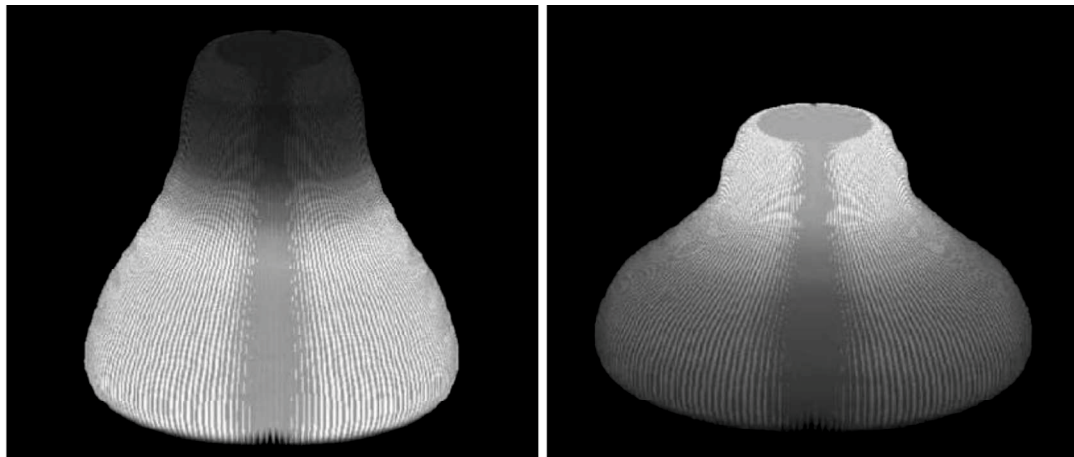
(a) yield stress= 2600Pa   (b) yield stress=2000Pa

Fig. 2.10 Examples of obtained shapes of numerical results of ASTM slump test

it behaves as a Bingham fluid. The invariant generalization of fresh concrete was the one proposed by Oldroyd [52] based on the three dimensional von Mises yield criterion. The numerical simulation performed for two asymptotic cases (Fig. 2.10): when there is a very small slump value(purely extensional flow, yield stress is equal to 2600pa) and when there is a large spread diameter (purely shearing flow, yield stress is equal to 2000pa). Inertia effects were neglected, that is to say, the influence of lifting speed or the plastic viscosity was not taken into consideration. Tatersall and Banfill [53] experimentally concluded that the slump of fresh concrete is indeed highly correlated with yield stress but is not significantly affected by the plastic viscosity. The numerical results of mini cone test and ASTM slump test were in agreement with corresponding experimental results.

4) Lattice Boltamann Method

Lattice Boltamann Method (LBM) [54]has developed into simulate single and multi phase fluid flows. It is based on microscopic models and mesoscopic kinetic equations. The fundamental idea of the LBM is to construct simplified kinetic models that incorporate the essential physics of microscopic or mesoscopic processes so that the macroscopic averaged properties obey the desired macroscopic equations. Space is commonly discretized into square (2D domain) or cubic Eulerian cells forming a fixed Cartesian grid (see Fig. 2.11(a)). Eulerian nodes are placed into the centre of each cell and a lattice is formed by connecting the nearest Eulerian nodes. The movement of themicroscopic particles is restricted onto the lattice directions, which results in a discretization of continuous particle distribution functions into only a few particle distributions associated with lattice velocities (Fig. 2.11(b)). The detail calculation of LBM can be found in Ref [55].

Svec et.al [56] performed numerical flow simulation of SCC containing fibers using the LBM. The effect of particles' shape such as round or elongated on rhelogical behavior was taken into
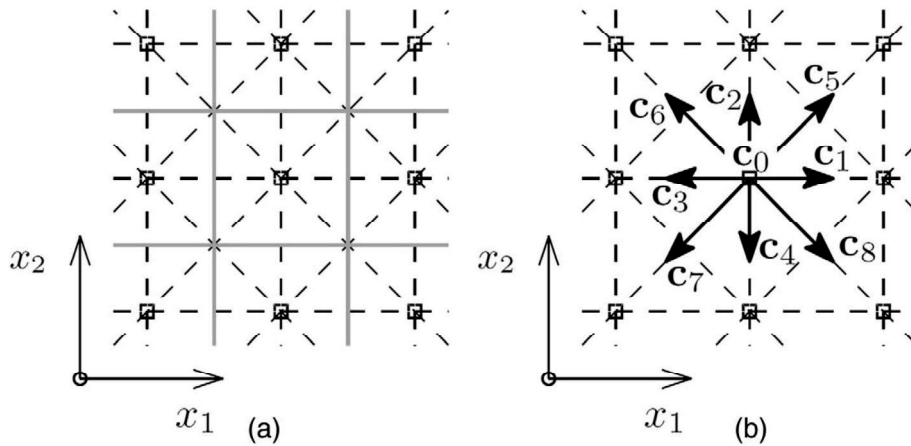
Fig. 2.11 Scheme of D2Q9 lattice for LBM. Square marks stand for nodes, grey lines for cell boundaries and dashed lines for lattice. (b) Set of corresponding lattice velocity vectors in a node

account by using a modified Immersed Boundary Method [57]. The fresh concrete was regarded as a Bingham fluid (yield stress = 5Pa and plastic viscosity = 10 Pa.s). The slump test was simulated to present the capabilities of LBM.

2.4.1.2 Discrete Particle Flow Simulations

When fresh concrete is of high fluidity and the content of coarse aggregate is low, it flows like a fluid. Whereas, in case of low fluidity and large amount of coarse aggregate, the interaction between coarse aggregate is obvious, that is to say, the behavior is dominated by the granular nature. Therefore, it is advantage to simulate the flow of fresh concrete using the discrete element method.
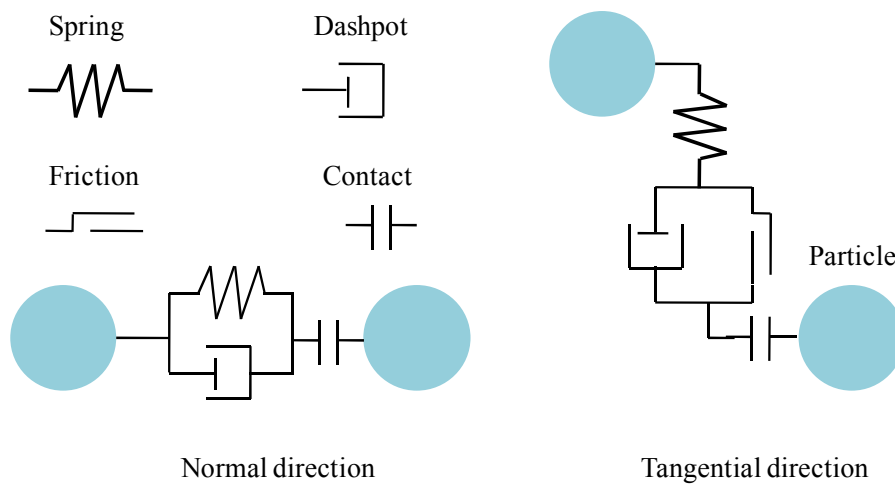
Fig. 2.12 Standard contact model between particles in DEM

The numerical simulation of fresh concrete based on discrete particle flow are summarized as follows.

1) DEM

The DEM is a particle approach, of which a fundamental assumption is that the analyzed material consists of separate discrete particles: circular particles (2D) or spherical particles (3D). The boundary is represented by the wall. At every calculation cycle includes two steps: according to Newton's second law to calculate the motion of each particle and deciding the contact forces by the force-displacement law [58-60]. The contact force at each contact point is divided into normal and shear direction. Spring, dashpot, friction are used to express the elastic, viscous and friction component, as shown in Fig 2.12. As a complement to laboratory experiments, discrete particle numerical simulation applied to granular materials gives access to mesostructure or even microstructure at the scale of the grains and contacts, and improves our understanding of macroscopic mechanical behavior from the microscopic point. The detailed introduction of DEM
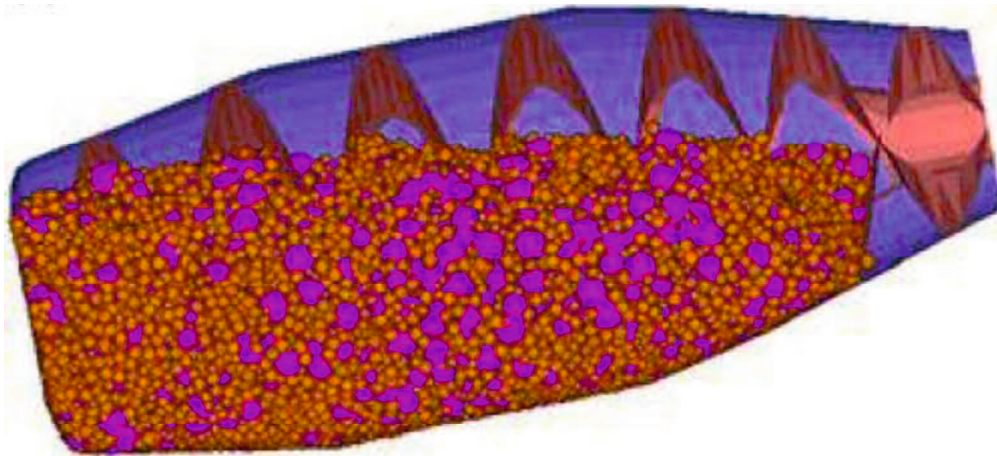
Fig. 2.13 Simulation of the mixing process of fresh concrete in drum
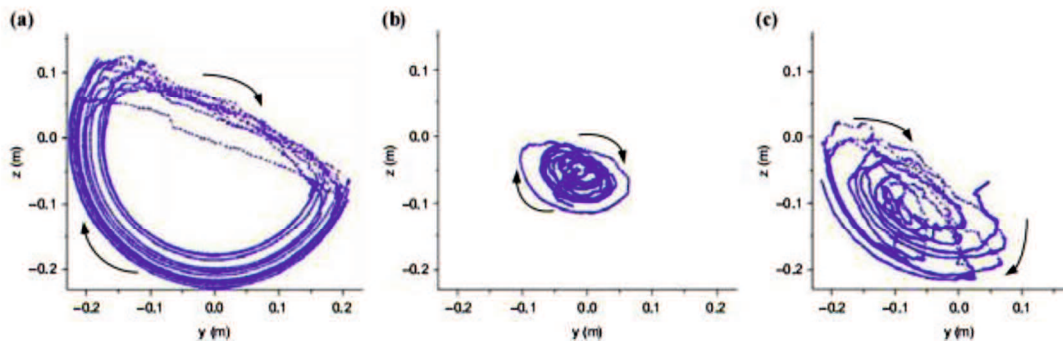
Fig. 2.14 The different movement cases of particles in drum (a)outer circulation, (b) inner circulation, (c) irregular circulation

will be given in Section 4.2.

Based on the work in Ref. [61], Noor and Uomoto [62] used the PFC3D code to simulated behaviors of SCC under various states. Various consistency and rheology tests of SCC were performed using this numerical method. In DEM calculation, the increase of phase numbers and small particle sizes like sand and cement extremely time and calculation consuming. Hence, the two phase model: coarse aggregate and mortar were used. The contact parameters, such as contact stiffness and bond strength both for normal and tangential direction were verified by the lifting sphere viscometer test. The method proposed by Noor and Uomoto was also adopted by Petersson [63] and Hakami and Petersson [64] to simulate the flow in L-box. It proves that the 3D model and 2D model (depending on type of simulation) are very suitable for the simulation of SCC flow and simulation of tests for passing ability.

Tan et.al [65] used a two-phase DEM model to simulate the mixing process of fresh concrete in truck mixer. The contact parameters between particles was calibrated by the ICAR rheometer test. It can study both the flow of fresh concrete as a whole (Fig. 2.13) and the displacement of its individual particles (Fig. 2.14).

2) SPH

SPH is a meshfree particle method based on Lagrangian formulation. It was first invented to solve astrophysical problems [66, 67]. The state of a system is represented by a set particles, which possess materials properties and interact with each other within the range controlled by a weight function or smoothing function [68]. The discretization of the governing equations is based on these discrete particles, and a variety of particle-based formulations have been used to calculate the local
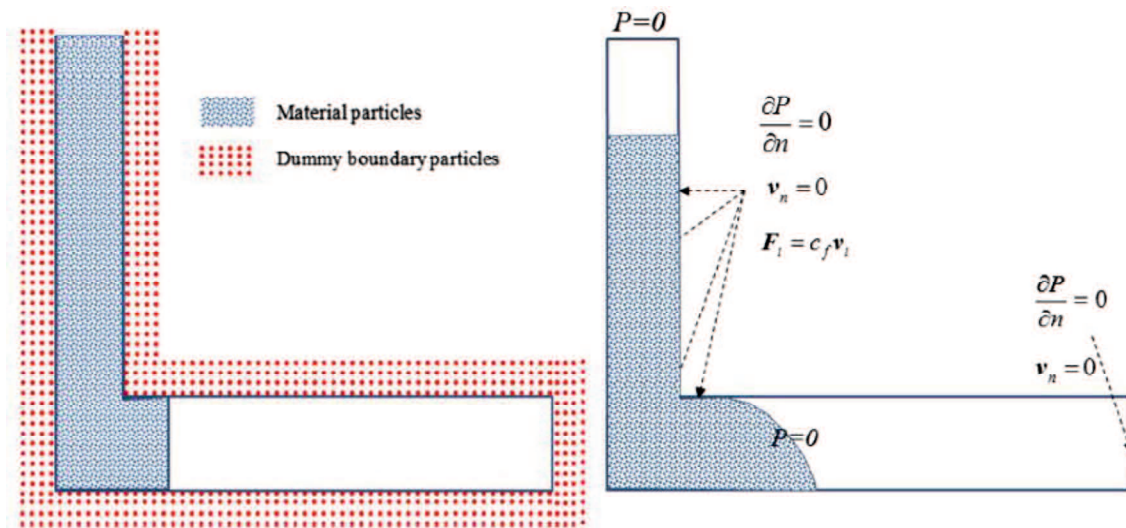
Fig. 2.15 Boundary conditions used in SPH

density, velocity and acceleration of the fluid. The fluid pressure is calculated from the density using an equation of state, the particle acceleration is then calculated from the pressure gradient and the density. SPH, without using a grid/mesh, allows a straightforward handing of very large deformation, since the connectivity between particles are generated as part of the computation and can change with time. So it is appropriate to simulating the flow of fresh concrete using SPH. The numerical simulation of fresh concrete using SPH will be given below and the detailed calculation of SPH will be introduced at Section 5.2.
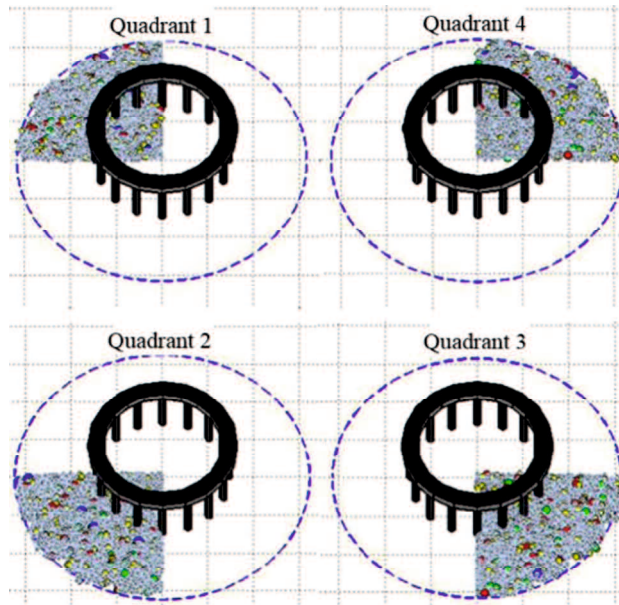
Fig. 2.16 Four quadrants of pancake to determine the distribution of coarse aggregate
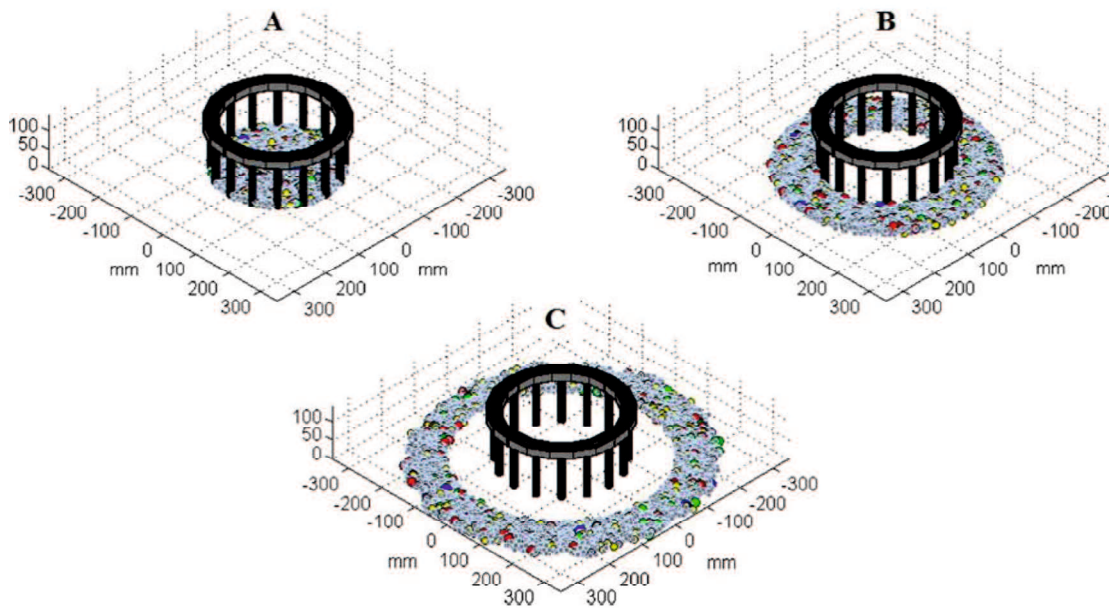
Fig. 2.17 The three concentric regions to evaluate the distribution of coarse aggregate

32

Kulasegaram [69] developed a numerical method using SPH to determine how the fibres distribute and orient themselves during the flow process of ultra-high performance and SCC. A Bingham-type constitutive model [11] was used to described the constitutive relation of fresh concrete containing short steel fibres and inserted into the incompressible SPH. A number of simulations were presented to demonstrate the effectiveness of the numerical method. The same method was also used by Deeb to simulate the flow of fresh concrete containing fibres or not in slump test [23]and L-flow test [70]. But the fresh concrete was represented by three types particles with different diameters and their constitutive behavior was described by a Bingham-type model. Three types of boundary conditions were considered, a zeor pressure condition on the free surface, Dirichlet boundary condition at boundaries, and Neumann conditions on the pressure gradient, as shown in Fig. 2.15. The 3D simulation of fresh concrete without fibres was focused on the distribution of coarse aggregate (diameter is larger than or equal to 8 mm). The distribution of fibres and their orientation was concerned when fresh concrete contained fibres . The simulation results were able to predict accurately the distribution of fibres and their orientations during the flow, but because of the effect of lifting gate, there was a delay in the flow time between numerical simulation and experiment. Dhaheer et.al used the incompressible SPH method the predict the flow of SCC mixes through gaps in reinforcing bars. Also, the Bingham-type model used as the constitutive model. Six mixes with nominal 28-day cube compressive strengths of 30, 40, 50, 60, 70 and 80 MPa were used. The distribution of coarse aggregates was examined along several cut sections of the flow pancake, as shown in Fig 2.16 and Fig 2.17. The numerical results were in very good agreement with experiment results for all mixes.

Sakihara et.al [71] simulated the flow of fresh concrete using SPH and a bi-viscosity model (see Section 2.3). It was assumed that fresh concrete was a fluid with a very large viscosity before yield and behaves like Bingham fluid after yield. The Dam break of water test was performed to valid the numerical method. The final shape of L-flow of fresh concrete can be accurately simulated.

3) Moving Particle Semi-implicit

Moving Particle Semi-implicit (MPS) method is presented by Koshizuka and Oka for incompressible fluid [72]. The motion of each particle is calculated through interactions with neighboring particles covered with the kernel function. Deterministic particle interaction models representing gradient, Laplacian, and free surfaces are proposed. Fluid density is implicitly required to be constant as the incompressibility condition, while the other terms are explicitly calculated. The Poisson equation of pressure is solve by the incomplete Cholesky conjugate gradient method.

Cho et.al [73] develop a numerical approach using the MPS and a viscous -plastic flow constitutive law to simulate the flow analysis of fresh concrete. Yamada et.al [74, 75] inserted a new
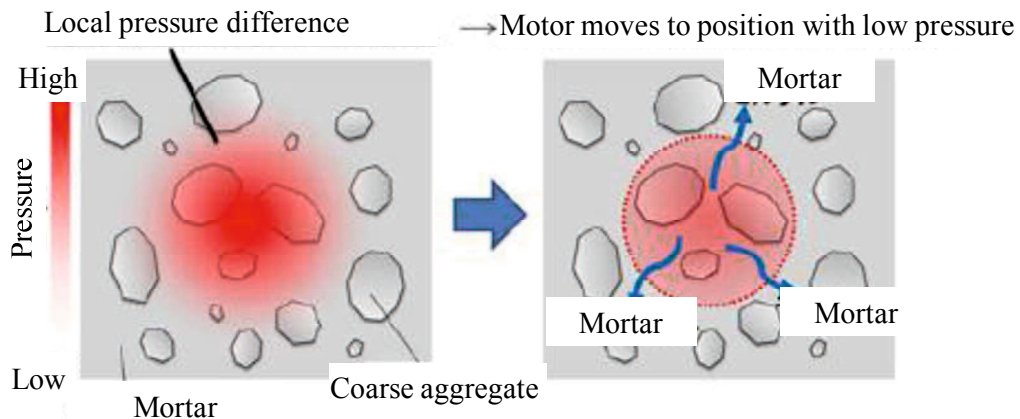
Fig. 2.18 Boundary conditions used in MPS

materials segregation model into MPS to numerical analysis the flow of fresh concrete. The content graph of materials segregation model is shown in Fig. 2.18. Because of the density's difference between coarse aggregate and mortar in fresh concrete, pressure difference occurs. Mortar moves from position of high pressure to where pressure is low, but coarse aggregate is leaved behind. Hence, segregation of coarse aggregate happens. The local volume of mortar is dependent on the pressure difference. The parameters of materials segregation model is measured by slump cone test. The 2D simulation of slump was performed. The mass of coarse aggregate at different position was calculated and compared to experimental results.

2.4.1.3 Simulation of Coupling Method of Fluid and Discrete Particle

The fresh concrete is regarded as particles suspended in a fluid.

1) Viscoplastic Suspension Element Method

A Viscoplastic Suspension Element Method (VSEM) was used by Mori and Tanigawa to simulate the flow of concrete in various tests [40]. Two phase: mortar and coarse aggregates (monosize spheres) was used. A viscoplastic equation was introduced to describe the viscoplastic interactions between particles.

2) Finite Element Method with Lagrangian Integration Points

A finite element method with Lagrangian integration points(FEMLIP) [76] is a code based on an Eulerian grid of finite element and a set of Lagrangian particles or tracers inside the mesh. The different point of FEMLIP and FEM, SPH and DEM is that the materials points and computational points do not coincide , as shown in Fig. 2.19. The grid is usually kept fixed except in the case of
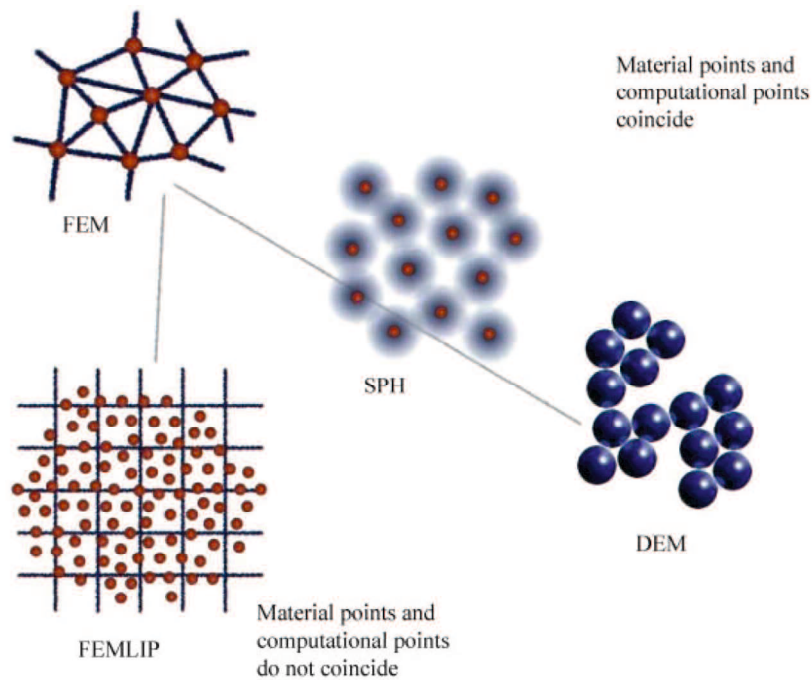
Fig. 2.19 Different ways to discretize a system with particles and/or grid

moving boundary conditions. The retained approach uses an Eulerian finite element grid (fixed) as a computational set of points and a set of Lagrangian particles embedded in the mesh which are used as integration points for any given configuration. Material properties are initially set on particles. The nodal unknowns of grid are computed using the integration over particles, then the velocity of particles was calculated by interpolated of nodal information. The position of particles will be undated according their velocities.

When using FEMLIP modeling concrete as a heterogeneous material made of mortar and aggregate (see Fig. 20(top)), the scale should be smaller than the form scale since aggregates must be discretised by several finite elements in order to be properly modeled as rigid compared to mortar.

FEMLIP was used by Dufour and Cabot to simulate flow of fresh concrete [77]. Three types of fresh concrete, ordinary concrete, high performance concrete and SCC were used. The constitutive relationship of fresh concrete was described by a Bingham-type model and friction was not considered at the boundary. They fitted the two Bingham parameters from the slump test with flow time to calibrate the model parameters, as shown in Fig. 2.20(bottom). Then the final shape of L-flow of 2D numerical simulation and experiment were compared.

2.4.2 Numerical Study on Time-dependences

2.4.2.1 Standing Time-dependence

Fresh concrete is of standing time-dependent flow behavior. When simulating concrete test,

35
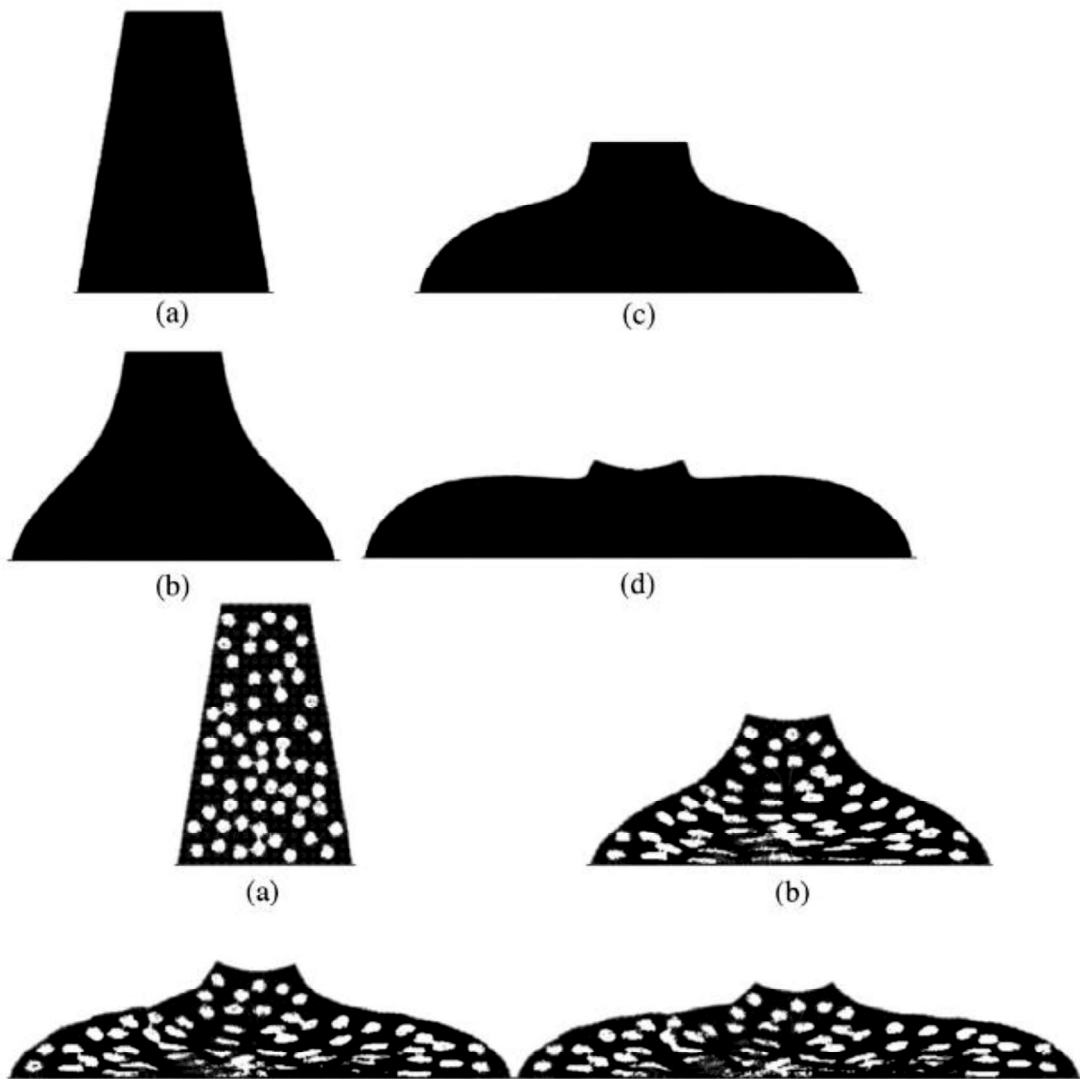
Fig. 2.20 Numerical simulation of the slump flow test using a homogeneous approach (top) and using a heterogeneous approach (bottom)

such as slump flow and L-flow test, the testing time is short and the effect of standing time-dependence could be neglected. But for simulating multi-casting process, predicting the formwork pressure, the standing time-dependent flow behavior has to be considered. At rest, the network is formed by hydration and flocculation of cement. It can support part of self-gravity to reduce the pressure on the formwork. A thixotropy model derived from the Bingham model was proposed by Roussel [4, 78]. During placing, the internal time between two contiguous layers of casting is short. If the thixotropic rate is too large, the apparent yield stress increases above a critical 2.value, then these two layers do not mix at all, and weak interface is formed, even crack may occurs for harden concrete. Roussel proposed numerical simulations using the thixotropy model to predict the occurrence of the phenomenon. For different resting time, Fig. 2.21 shown that a distinct interface could or not be spotted.
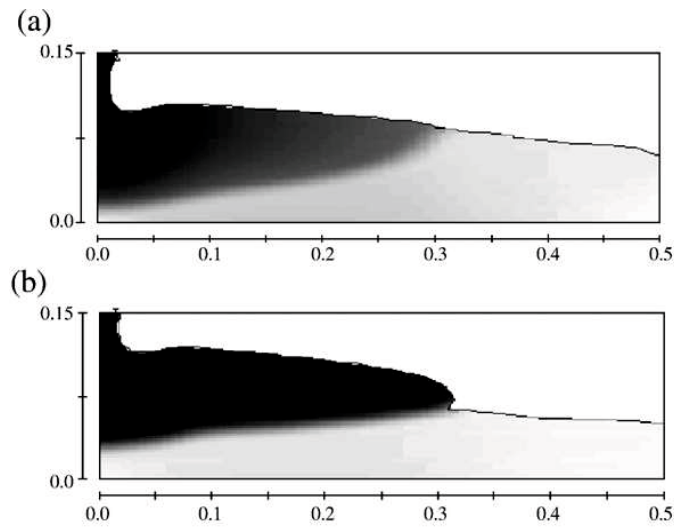
Fig. 2.21 Numerical simulations of the multi-layer casting phenomenon (a) For a 5 min. resting time, the two layers mix perfectly (b) for a 20 min. resting time, the two layers do not mix at all

2.4.2.2 Shearing Time-dependence

Based on Bingham model, Wallevik presented a rheological equation to simulate the thixotropic behavior of cement paste [79]. The model is an extension of the previous MHI-theory presented in [80] and can explain transient effects commonly observed in cement pastes. The cement hydration and physical flocculation were simultaneously taken into account. The numerical results of the relationship of torque and angular velocity after different rest time, as shown in Fig. 2.22.
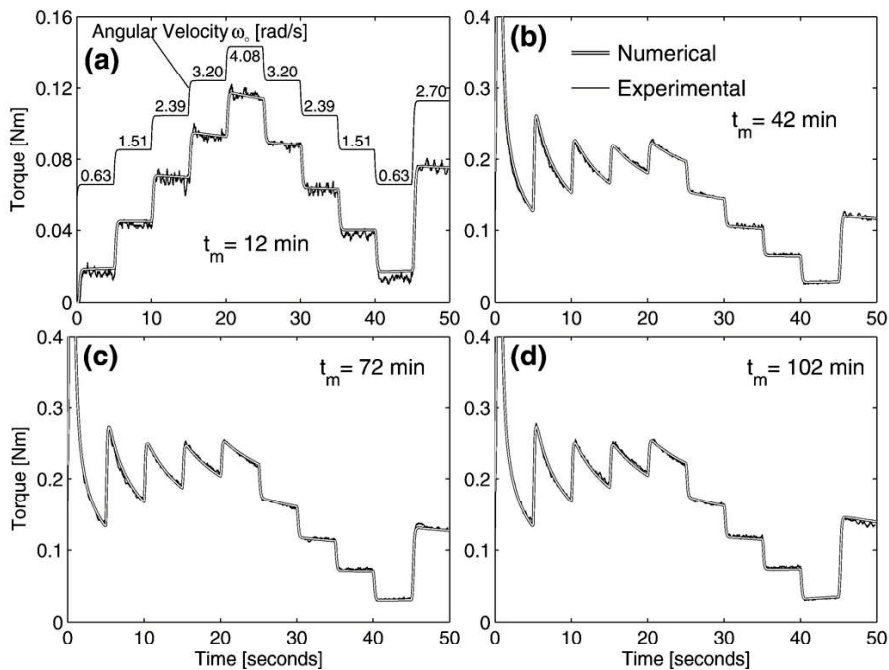
Fig. 2.22 Numerical and experimental results of ConTec Viscometer 4

2.5 Summary

In this chapter, the evaluation and measurement method of time dependent flow behavior of fresh concrete were summarized. The constitutive model of fresh concrete and its evolutionary type used in numerical simulation were concluded. At last, the numerical simulation of fresh concrete in the references were investigated. Main summary are stated as follows:

1) Fresh concrete is not only standing and shearing time-dependent but also nonlinear, pressure-dependent.

2) Bingham model is unable to describe the change of rheological property with standing and shearing time, and it can't describe the nonlinear, and normal stress-dependent flow behaviors of fresh concrete. The Herschel-Bulkley model, which is polynomial and quadratic function, was proposed to describe the nonlinear flow behavior, but other flow behaviors are not expressed and the parameters in the model are lack of physical meanings and test methods. Pressure dependent model can describe the normal stress-dependent flow behavior, but it do not consider the self-gravity of fresh concrete and its coefficient is difficult to measure. The thixotropy model can describe the change of shear stress with time, but the change of plastic viscosity can't be expressed. The measurement of parameters ,such as γ_0 and α is not introduced.

3) The VGM model can describe not only the shearing time-dependence but also the nonlinear, and normal stress-dependent flow behaviors of fresh concrete. The parameters of VGM model can be measured rather than assumed.

4) Fresh concrete is assumed as a homogeneous fluid and the Bingham type model is usually used as constitutive model in the numerical simulation. But Bingham model is unable to describe the nonlinear, and normal stress-dependent flow behaviors of fresh concrete, and it can't describe the change of rheological property with standing and shearing time. The time dependence of fresh concrete, especially shearing time-dependence are barely considered in the numerical simulation.

5) When fresh concrete is of high fluidity and the content of coarse aggregate is low, it flows like a fluid. It is possible to simulate the flow of fresh concrete using single fluid simulations. However, the two main numerical difficulties in connection with single fluid simulations are the yield stress behavior of the material and the free surface displacement. Moreover, as any continuum mechanics methods, single fluid simulation requires a clear definition of the boundary conditions. Fresh concrete displaying a moving free boundary is thus particularly delicate to simulate using single fluid simulation. Numerical simulation using coupling method of fluid and discrete particle capture the real nature of the fresh concrete. But it need to compute all the space where the fresh concrete is and will move to. It is time-consuming. Fresh concrete is a particle materials, the interaction between particles is significant. So it is advantage to simulate the flow of fresh concrete using particle method, which is good at the large deformation problem.

6) The standing time-dependence of fresh concrete is resulted from the hydration and flocculation of cement particles at rest. Structure builds-up and the contact forces and number of contacts evolve with standing time. It is hard to find the explicit relationship of rheological parameters and standing time. DEM is a mesh free particle method and it directly uses the contact relationship between particles. It is easy to change the contact relationship and revise the contact force between particles. Numerical simulation of fresh concrete using DEM gives access to mesostructure or even microstructure at the scale of the grains and at the view of contacts. It can study both the flow of fresh concrete as a whole and the displacement of its individual particles. Therefore, DEM was chosen as the numerical tool to investigate the standing time-dependence of fresh concrete.

7). The shearing time-dependence of fresh concrete is the change of rheological behaviors during the flow process. In addition, fresh concrete is nonlinear and pressure-dependent. The VGM model can used as the constitutive model in the numerical approach to describe the shearing time-dependent, nonlinear and pressure-dependent flow behavior. SPH, a open source code is also a mesh free particle. Large deformation of free surfaces, such as flow of fresh concrete, can be easily and accurately tracked by the Lagrangian motion of particles in the SPH method. Hence, we numerical study on the shearing time-dependence of fresh concrete using SPH method and VGM model.

References

[1] K. H. Khayat, M. Saric-Coric, F. Liotta, Influence of thixotropy on stability characteristics of cement grout and concrete, *Materials Journal,* 99 (3) (2002) 234-241.

[2] J. Assaad, K. H. Khayat, H. Mesbah, Variation of formwork pressure with thixotropy of self-consolidating concrete, *Materials Journal,* 100 (1) (2003) 29-37.

[3] N. Roussel, F. Cussigh, Distinct-layer casting of SCC: the mechanical consequences of thixotropy, *Cement and Concrete Research,* 38 (5) (2008) 624-632.

[4] G. Ovarlez, N. Roussel, A physical model for the prediction of lateral stress exerted by self-compacting concrete on formwork, *Materials and Structures,* 39 (2) (2006) 269-279.

[5] R. Lapasin, V. Longo, S. Rajgelj, Thixotropic behaviour of cement pastes, *Cement and Concrete Research,* 9 (3) (1979) 309-318.

[6] H. J. Yim, J. H. Kim, S. P. Shah, Cement particle flocculation and breakage monitoring under Couette flow, *Cement and Concrete Research,* 53 (2013) 36-43.

[7] K. H. Khayat, A. F. Omran, T. V. Pavate, Inclined Plane Test to Evaluate Structural Buildup at Rest of Self-Consolidating Concrete, *ACI Materials Journal,* 107 (5) (2010).

[8] Z. Li, T. Ohkubo, Y. Tanigawa, Theoretical analysis of time-dependence and thixotropy of fluidity for high fluidity concrete, *Journal of Materials in Civil Engineering,* 16 (3) (2004) 247-256.

[9] N. Roussel, A thixotropy model for fresh fluid concretes: theory, validation and applications, *Cement and Concrete Research,* 36 (10) (2006) 1797-1806.

[10] S. Jarny, N. Roussel, S. Rodts, et al., Rheological behavior of cement pastes from MRI velocimetry, *Cement and Concrete Research,* 35 (10) (2005) 1873-1881.

[11] T. C. Papanastasiou, Flows of materials with yield, *Journal of Rheology,* 31 (5) (1987) 385-404.

[12] H. Zhu, N. S. Martys, C. Ferraris, et al., A numerical study of the flow of Bingham-like fluids in two-dimensional vane and cylinder rheometers using a smoothed particle hydrodynamics (SPH) based method, *Journal of Non-Newtonian Fluid Mechanics,* 165 (7) (2010) 362-375.

[13] H. Eyring, Viscosity, plasticity, and diffusion as examples of absolute reaction rates, *The Journal of chemical physics,* 4 (4) (1936) 283-291.

[14] W. Herschel, R. Bulkley, Measurement of consistency as applied to rubber-benzene solutions, in: Am. Soc. Test Proc, 1926, pp. 621-633.

[15] T. Jones, S. Taylor, A mathematical model relating the flow curve of a cement paste to its water/cement ratio, *Magazine of Concrete Research,* 29 (101) (1977) 207-212.

[16] C. Atzeni, L. Massidda, U. Sanna, Comparison between rheological models for portland cement pastes, *Cement and Concrete Research,* 15 (3) (1985) 511-519.

[17] W. V. Berg, On the flow behaviour of cement pastes. Influence of the granulometric composition of cement and of the concentration of solids, *Magazine of Concrete Research,* 31 (1979) 211-216.

[18] R. Lapasin, A. Papo, S. Rajgelj, The phenomenological description of the thixotropic behaviour of fresh cement pastes, *Rheologica acta,* 22 (4) (1983) 410-416.

[19] R. Shangraw, W. Grim, A. M. Mattocks, An Equation for Non‑Newtonian Flow, *Transactions of the Society of Rheology,* 5 (1) (1961) 247-260.

[20] N. Casson, Rheology of dispersed systems, *Mill CC ed,* (1959).

[21] H. Mori, M. Tanaka, Y. Tanigawa, Experimental study on shear deformational behavior of fresh concrete, *Journal of Structural and Construction Engineering,* 427 (1991) 1-10.

[22] C. F. Ferraris, F. de Larrard, Modified slump test to measure rheological parameters of fresh concrete, *Cement, Concrete and Aggregates,* 20 (2) (1998) 241-247.

[23] R. Deeb, S. Kulasegaram, B. L. Karihaloo, 3D modelling of the flow of self-compacting concrete with or without steel fibres. Part I: slump flow test, *Computational Particle Mechanics,* 1 (4) (2014) 373-389.

[24] H. Lashkarbolouk, A. M. Halabian, M. R. Chamani, Simulation of concrete flow in V-funnel test and the proper range of viscosity and yield stress for SCC, *Materials and Structures,* 47 (10) (2014) 1729-1743.

[25] Z. Li, T. Ohkubo, Y. Tanigawa, Flow performance of high-fluidity concrete, *Journal of Materials in Civil Engineering,* 16 (6) (2004) 588-596.

[26] Z. Li, T. Ohkubo, Y. Tanigawa, Yield model of high fluidity concrete in fresh state, *Journal of Materials in Civil Engineering,* 16 (3) (2004) 195-201.

[27] Z. Li, J. Li, Granular material characteristic of fresh concrete, *Proceedings of 6th International RILEM Symposium on Self-Compacting Concrete,* (2010) 423-433.

[28] J. Li, Z. Li, Effect of boundary restraint on the flow of fresh concrete through opening, *Journal of Structure and Construction Engineering, Transaction of Archcitectural Instistue of Japan,* 76 (666) (2011) 1367-1374.

[29] J. E. Wallevik, Rheology of Particle Suspensions-Fresh Concrete, *Ph. D Thesis of Norwegian University of Science and Technology,* (2003) 11-47.

[30] A. Papo, Rheological models for cement pastes, *Materials and Structures,* 21 (1) (1988) 41-46.

[31] F. de Larrard, C. F. Ferraris, T. Sedran, Fresh concrete: a Herschel-Bulkley material, *Materials and Structures,* 31 (7) (1998) 494-498.

[32] D. Feys, R. Verhoeven, G. De Schutter, Steady-state rheological properties of fresh Self Compacting Concrete and their evolution in time, *Annual Transactions the Nordic Rheology Society,* (2007) 35-41.

[33] Z. Li, Theoretical investigation on rheological properties of fresh concrete, *Journal of Structural and Construction Engineering, Transaction of Archcitectural Instistue of Japan,* 78 (687) (2013) 895-904.

[34] Z. Li, K. kajiwara, M. Iidaka, Investigation on particle contact angle of fresh concrete using X-ray CT imaging, *Journal of the Society of Matarials Science,* 62 (9) (2013) 585-591.

[35] Z. Li, Y. Tanigawa, Investigation on granular characteristics of fresh concrete based on visualized

experiment using alternative materials, *Journal of Structural and Construction Engineering, Transaction of Archcitectural Instistue of Japan,* 77 (678) (2012) 1175-1184.

[36] Z. Li, Rheological model and rheometer of fresh concrete *Journal of Structural and Construction Engineering, Transaction of Archcitectural Instistue of Japan,* 80 (710) (2015) 527-537.

[37] Z. Li, J. Li, Exterimental investigation on shear defromation of fresh concrete, *Journal of Structural and Construction Engineering, Transaction of Archcitectural Instistue of Japan,* 75 (653) (2010) 1173-1180.

[38] A. Sadrekarimi, S. M. Olson, A new ring shear device to measure the large displacement shearing behavior of sands, (2009).

[39] N. R. Iverson, R. W. Baker, T. S. Hooyer, A ring-shear device for the study of till deformation: tests on tills with contrasting clay contents, *Quaternary Science Reviews,* 16 (9) (1997) 1057-1066.

[40] H. Mori, Y. Tanigawa, Simulation methods for fluidity of fresh Concrete, *Memoirs of the school of Engineering, Nagoya University,* 44 (1992) 71-133.

[41] M. A. Dhaheer, S. Kulasegaram, B. Karihaloo, Simulation of self-compacting concrete flow in the J-ring test using smoothed particle hydrodynamics (SPH), *Cement and Concrete Research,* 89 (2016) 27-34.

[42] W. Alyhya, S. Kulasegaram, B. Karihaloo, Simulation of the flow of self-compacting concrete in the V-funnel by SPH, *Cement and Concrete Research,* 100 (2017) 47-59.

[43] X. Xiao, Y. Tan, H. Zhang, et al., Experimental and DEM studies on the particle mixing performance in rotating drums: Effect of area ratio, *Powder Technology,* 314 (2017) 182-194.

[44] R. Deng, Y. Tan, H. Zhang, et al., Experimental and DEM studies on the transition of axial segregation in a truck mixer, *Powder Technology,* 314 (2017) 148-163.

[45] Y. Tan, H. Zhang, D. Yang, et al., Numerical simulation of concrete pumping process and investigation of wear mechanism of the piping wall, *Tribology International,* 46 (1) (2012) 137-144.

[46] H. KITAOJI, Y. TANIGAWA, H. MORI, et al., Flow simulation of fresh concrete cast into wall structure by viscoplastic divided space element method, *Transactions of the Japan Concrete Institute,* 18 (1997) 45-52.

[47] Y. Tanigawa, H. Mori, Analytical study on deformation of fresh concrete, *Journal of Engineering Mechanics,* 115 (3) (1989) 493-508.

[48] Y. Kurokawa, Y. Tanigawa, H. Mori, et al., Analytical study on effect of volume friction of coarse aggregate on bingham's constants of fresh concrete, *Transactions of the Japan Concrete Institute,* 18 (1997) 37-44.

[49] L. N. Thrane, P. Szabo, M. Geiker, et al., Simulation of the test method "L-Box" for self-compacting concrete, *Annual Transactions of the NORDIC rheology society,* 12 (1) (2004) 47-54.

[50] N. Roussel, A. Gram, M. Cremonesi, et al., Numerical simulations of concrete flow: a benchmark comparison, *Cement and Concrete Research,* 79 (2016) 265-271.

[51] N. Roussel, Correlation between yield stress and slump: comparison between numerical simulations and concrete rheometers results, *Materials and Structures,* 39 (4) (2006) 501-509.

[52] J. Oldroyd, A rational formulation of the equations of plastic flow for a Bingham solid, in: Mathematical Proceedings of the Cambridge Philosophical Society, Cambridge University Press, 1947, pp. 100-105.

[53] G. H. Tattersall, P. Banfill, The rheology of fresh concrete, Pitman London, 1983.

[54] S. Chen, G. D. Doolen, Lattice Boltzmann method for fluid flows, *Annual review of fluid mechanics,* 30 (1) (1998) 329-364.

[55] J. Latt, Hydrodynamic limit of lattice Boltzmann equations, in, University of Geneva, 2007.

[56] O. Svec, J. Skocek, H. Stang, et al., Flow simulation of fiber reinforced self compacting concrete using Lattice Boltzmann method, in: 8th International Congress on the Chemistry of Cement, 2011.

[57] Z.-G. Feng, E. E. Michaelides, Proteus: a direct forcing method in the simulations of particulate flows, *Journal of Computational Physics,* 202 (1) (2005) 20-51.

[58] S. Shyshko, V. Mechtcherine, Developing a Discrete Element Model for simulating fresh concrete: Experimental investigation and modelling of interactions between discrete aggregate particles with fine mortar between them, *Construction and Building Materials,* 47 (2013) 601-615.

[59] R. Pieralisi, S. Cavalaro, A. Aguado, Discrete element modelling of the fresh state behavior of pervious concrete, *Cement and Concrete Research,* 90 (2016) 6-18.

[60] V. Mechtcherine, S. Shyshko, Simulating the behaviour of fresh concrete with the Distinct Element Method–Deriving model parameters related to the yield stress, *Cement and Concrete Composites,* 55 (2015) 81-90.

[61] H. Chu, A. Machida, Numerical simulation of fluidity behavior of fresh concrete by 2d distinct element method, *Transactions of the Japan Concrete Institute,* 18 (1997) 1-8.

[62] M. A. Noor, T. Uomoto, Three-dimensional discrete element simulation of rheology tests of self-compacting concrete, in: Proc. of the 1rd Int. RILEM Symp. on SCC, 1999, pp. 35-46.

[63] Ö. Petersson, H. Hakami, Simulation of SCC—laboratory experiments and numerical modeling of slump flow and L-box tests, in: Proc. of the 2nd Int. RILEM Symp. on SCC, 2001, pp. 79-88.

[64] Ö. Petersson, Simulation of self-compacting concrete—laboratory experiments and numerical modelling of testing methods, j-ring and l-box tests, in: Proceedings of the 3rd international RILEM Symposium on Self-Compacting Concrete, RILEM PRO33 Reykjavik, Iceland, 2003, pp. 202-207.

[65] Y. Tan, R. Deng, Y. Feng, et al., Numerical study of concrete mixing transport process and mixing mechanism of truck mixer, *Engineering Computations,* 32 (4) (2015) 1041-1065.

[66] L. B. Lucy, A numerical approach to the testing of the fission hypothesis, *The astronomical journal,* 82 (1977) 1013-1024.

[67] R. A. Gingold, J. J. Monaghan, Smoothed particle hydrodynamics: theory and application to non-spherical stars, *Monthly notices of the royal astronomical society,* 181 (3) (1977) 375-389.

[68] G.-R. Liu, M. B. Liu, Smoothed particle hydrodynamics: a meshfree particle method, World Scientific, 2003.

[69] S. Kulasegaram, B. L. Karihaloo, Fibre-reinforced, self-compacting concrete flow modelled by smooth particle hydrodynamics, *Proceedings of the Institution of Civil Engineers-Engineering and Computational Mechanics,* 166 (1) (2013) 22-31.

[70] R. Deeb, S. Kulasegaram, B. L. Karihaloo, 3D modelling of the flow of self-compacting concrete with or without steel fibres. Part II: L-box test and the assessment of fibre reorientation during the flow, *Computational Particle Mechanics,* 1 (4) (2014) 391-408.

[71] Y. Sakihara, S. Iraha, J. Matsubara, Application of particle method in flow simulation of fresh concrete, *Summaries of Technical Papers of Annual Meeting, Japan of Society of Civil Engineerings, ,* 59 (439-440) (2004).

[72] S. Koshizuka, Y. Oka, Moving-particle semi-implicit method for fragmentation of incompressible fluid, *Nuclear science and engineering,* 123 (3) (1996) 421-434.

[73] C.-G. Cho, W.-J. Kim, Y. Choi, Model for Flow Analysis of Fresh Concrete using Particle Method with Visco-Plastic Flow Formulation, *Journal of the Korea Concrete Institute,* 20 (3) (2008) 317-323.

[74] Y. Yamada, Y. Uehara, K. Sakihara, et al., The flow analysis by MPS method of fresh concrete applying the new material segregation model, Part 1. Proposal of material segregation model and distribution measurement test of coarse aggregate, *Summaries of Technical Papers of Annual Meeting, Architectural Institute of Japan (AIJ),* 39 (2015) 1-2.

[75] Y. Uehara, Y. Yamada, K. Sakihara, et al., The flow analysis by MPS method of fresh concrete applying the new material segregation model, Part 2. Material segregation factor decision and flow analysis by MPS method of applying the material segregation model, *Summaries of Technical Papers of Annual Meeting, Architectural Institute of Japan (AIJ),* 39 (2015) 3-4.

[76] L. Moresi, F. Dufour, H.-B. Mühlhaus, A Lagrangian integration point finite element method for large deformation modeling of viscoelastic geomaterials, *Journal of Computational Physics,* 184 (2) (2003) 476-497.

[77] F. Dufour, G. Pijaudier‑Cabot, Numerical modelling of concrete flow: homogeneous approach, *International Journal for Numerical and Analytical Methods in Geomechanics,* 29 (4) (2005) 395-416.

[78] N. Roussel, Steady and transient flow behaviour of fresh cement pastes, *Cement and concrete research,* 35 (9) (2005) 1656-1664.

[79] J. E. Wallevik, Rheological properties of cement paste: thixotropic behavior and structural breakdown, *Cement and Concrete Research,* 39 (1) (2009) 14-29.

[80] J. E. Wallevik, Thixotropic investigation on cement paste: Experimental and numerical approach, *Journal of non-newtonian fluid mechanics,* 132 (1) (2005) 86-99.

Chapter 3
Experiments

3.1 Introduction

For investigating the time-dependent flow behavior of fresh concrete using the numerical approach, we have to compare the numerical and experimental results to verify and evaluate the accuracy of numerical simulation. Though the size distribution of aggregate particles in fresh mortar is different from fresh concrete, both of them are viscous granular material, and have similar internal structure and time-dependences. Also, since the scale of fresh concrete in dimension is larger than that of fresh mortar, the numerical analysis of concrete experiment should divide the larger specimen in a lot of elements (particles and walls), thus needs a longer computation time. Moreover, if using fresh concrete, the precision and repeatability of experimental results decrease due to the random distribution of coarse aggregate particles, and the effect of coarser particles' segregation. In order to decrease the effect of the segregation, reduce the computation time, and ensure the precisions of experimental measurement and numerical calculation, we used fresh mortar.

To study the standing time-dependent flow behavior of fresh concrete using the td-DEM model, the input parameters of td-DEM model needed to be calibrated. The flow table test is often used to measure the flow ability of fresh mortar and it was used as calibration test in this paper.

A usual thixotropic phenomenon in laboratory is that the up-curve and down-curve of torque-angular rotation velocity relationship are not coincident [1]. The area of the hysteresis loop formed by the up and down curves (as shown in Fig. 3.1) is usually employed to quantify thixotropic degree [1, 2]. However, the area depended on the test conditions such as the shear history, the maximum rotation velocity, and the increasing and decreasing rates of rotation velocity [3]. Another approach is monitoring the decay of measured torque from the beginning to the equilibrium state
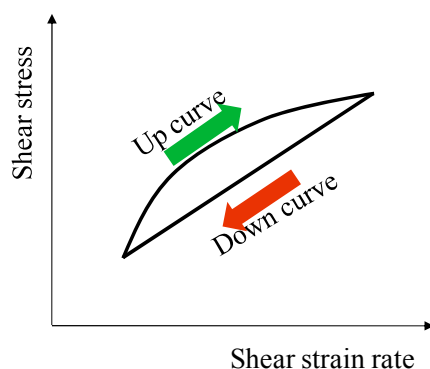
Fig. 3.1 Hysteresis loop

under a constant rotation velocity [2]. However, all these experimental methods more or less destroyed flocculent structure, it is almost impossible to use these test results to predict the change of fresh concrete' s consistency with time. For decreasing the effect of external force on standing time-dependent flow behavior, the funnel flow under self-gravity was conducted to evaluate the accuracy of td-DEM model.

In order to study the shearing time-dependent flow behavior of fresh concrete using SPH approach, the L-flow test is used to describe the flow ability of fresh concrete and it was performed to evaluate the accuracy of SPH simulation approach of fresh concrete. The VGM model, which can describe the non-linear flow behavior, and pressure (σ_n)-dependence of the rheological behaviors of fresh concrete besides the shearing time (t)-dependence, was employed as constitutive model. In order to contrast, the SPH simulation with Bingham model was also conducted for the same mortar. The RSNS rheometer tests were carried out to measure the input parameters of VGM and Bingham models.

In this chapter, the materials and mix proportions used in this paper were firstly introduced. Then the flow table test, funnel flow, L-flow test and RSNS rheometer test were presented, respectively. The experimental results of these tests were provided.

3.2 Raw Materials and Mix Proportions

Mix proportions of seven series of fresh mortars are presented in Table 3.1. In this paper, we firstly used series No. 1 mortar to validate the td-DEM model. Then in order to investigate the effect of mineral admixture on time-dependent flow behavior using the DEM, we used the series No. 2-4 mortars .

Table 3.1 Mix proportions of mortars and results of the flow table test

No.	W/B	S/B	FA/B	BFS/B	WR1/B (%)	WR2/B (%)	Spread diameter (mm)
1	0.48	1.5	0.0	0.0	0.3*	0.4	210
2	0.50	1.5	0.0	0.0	0.5	0.7	265
3	0.50	1.5	0.2	0.0	0.5	0.7	295
4	0.50	1.5	0.0	0.5	0.5	0.7	305
5	0.40	2.0	0.0	0.0	0.5*	0.0	168
6	0.45	2.0	0.0	0.0	0.5*	0.0	205
7	0.55	2.0	0.0	0.0	0.5*	0.0	208

Unit mass (kg/m^3)

No.	W	C	S	FA	BFS	WR1	WR2
1	335.4	698.7	1048.1	0	0	2.1	3.5
2	356.0	688.0	1020.0	0	0	3.4	4.8
3	356.0	551.0	1020.0	138	0	3.4	4.8
4	356.0	344.0	1020.0	0	344	3.4	4.8
5	258.6	646.6	1293.2*	0	0	3.2	0
6	281.5	625.4	1250.9*	0	0	3.1	0
7	322.9	587.0	1174.0*	0	0	2.9	0

[Notes] *W*: water, *C*: ordinary portland cement, *S*: Toyoura sand, *: sea sand, *W/B*: water-binder ratio by mass, *S/B*: sand-binder ratio by mass, WR1: standard type water-reducing agent, *: high range water reducing and retarding admixture, WR2: retarding type water-reducing agent. FA: fly ash, BFS: ground blast furnace slag.

Table 3.2 Physical properties and compositions of portland cement and mineral admixtures

	Physical properties		Chemical compositions						
	Density (g/cm^3)	Blaine fineness (cm^2/g)	SiO$_2$	Al$_2$O$_3$	Fe$_2$O$_3$	CaO	MgO	SO$_3$	Others
C	3.16	3110	22.3	5.6	3.0	63.7	2.4	2.2	0.8
FA	2.24	3550	55.0	27.0	5.0	4.0	3.0	4.5	1.5
BFS	2.90	7980	34.5	15.3	0.5	42.5	5.9	0.0	1.8
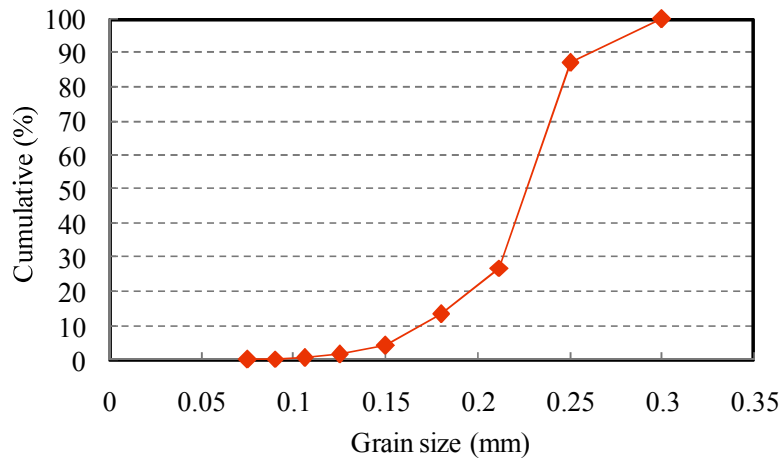
Fig. 3.2 Particle size distribution of Toyoura sand

Series No. 1-4 mortars were used in flow table test to calibrate the input parameters of td-DEM model and in the funnel flow to validate the td-DEM model. The others were used to in RSNS rheometer test to measure the parameters of VGM and Bingham model and in L-flow test to evaluate the accuracy of SPH approach.

Ordinary portland cement and Toyoura or sea sand were used. The composition of cement, fly ash (FA) and ground blast furnace slag (BFS) are shown in Table 3.2, and the particle size distribution of the Toyoura sand is shown in Fig. 3.2. The densities of cement, FA, BFS and sand are 3.16, 2.24, 2.90 and 2.64 g/cm^3, respectively.

Standard type water-reducing agent (WR1) was added to reduce the bleeding of mortar to the utmost. For series No. 1-4 mortars, the addition of (WR2) at an adequate dosage would delay the hydration rate of cement to guarantee that fresh mortar can still flow under itself gravity in the funnel after a rest time, simultaneously not greatly weakening the effect of cement hydration on the time-dependence of fresh concrete. It is considered that even if two types of water reducing agents were used, the physical flocculation and the hydration of cement were not completely inhibited. And the effect of water-reducing agent on the time-dependence of fresh mortar was reflected in the calibration of the parameters.

Series No. 2-4 of same water-binder ratio (*W/B*) by mass were used to study the effect of mineral admixture on the time-dependent flow behavior of fresh mortar. Series No. 2 mortar only contained cement without the addition of any mineral admixture, but part of cement was replaced by FA or BFS in series No. 2 and No. 3 mortars. There were the same water-binder ratio of 0.5 and the sand-binder ratio of 1.5 by mass in series No. 2-4 mortars.

Because the temperature has important effect on the velocity of cement hydration. Hence, the temperature of the laboratory room was kept at 22°C by air conditioner. The used raw materials, were moved in the laboratory room on the day before the experiment. Because the mortar sample of each measurement had a small volume (0.23 liter), its temperature was almost the same to the room temperature.

48

3.3 Flow Table Test

The flow table test is mostly used to evaluate the flow ability of fresh mortar. The geometry of the flow table test's cone is shown in Fig. 3.3. The flow table is 50 cm in diameter. A Hobart mixer was used to mix the mortar mixture. The cement and sand were first placed into the bowl and mixed at 64 rpm for 1 minute, then the water and admixtures were added and further mixed at 192 rpm for 3 minutes. Immediately after the mixing, the flow table test was performed without vibration. The cone was poured with the mortar sample and then lifted up within three seconds, the mortar flowed under itself gravity. After the mortar sample stopped to flow, its final diameter on the table was measured (see Fig. 3.4). Mean flow value of the mortar for three tests were shown in Table 3.1.
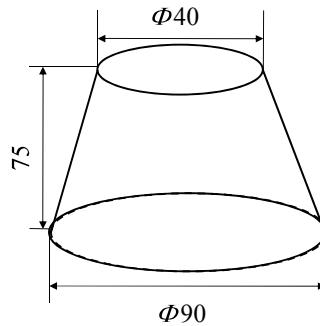
Fig. 3.3 Dimensions of cone (unit: mm)

Fig. 3.4 The final shape of the series No. 1-4 fresh mortar on the flow table

3.4 Funnel Flow

The funnel flow test is usually used to measure the apparent viscosity of paste and grout. The geometry of used funnel is shown in Fig. 3.5. The volume of the funnel was 0.23 liter. During the process that sample flows out the funnel, it is almost not agitated by external force except self-gravity, thus the test result doesn't change with the lasting time of measurement. Also, the specimen becomes stiff with time, and thus the measurement of yield stress and viscosity by rheometer becomes difficult. Therefore, a series of the gravity-induced funnel flow tests rather than rheological tests using rheometer, were carried out to evaluate the time-dependence of fresh mortar's consistency in this paper. And the table flow test's results were employed to calibrate the material parameters of the mortar for the numerical analysis of DEM.

As stated above, we filled the mortar samples, mixed in a patch, enclosed into several funnels right after mixing. The outlets were shut with a plastic plug at the beginning and during the rest period. At the time point of measurement, the plug was taken out by hand, the outlet of the funnel was opened. The sample then flowed down into a container located on the digital balance, which can recorded the outflow mass and the standing time. From cement was mixed with water to first measurement, it cost 6 min. Series No.1 mortar used the high range water reducing and retarding admixture and retarding type water-reducing agent, and obviously compared the experimental results of different moment, so a long time interval was selected. Because series No. 4 mortar contained 50% BFS is of high fluidity, series No. 2-4 mortars used the standard type water-reducing agent rather than high range water reducing and retarding admixture. The time intervals was 20, 5, 5 and 10 min. for series No. 1-4 mortars. The relationship between the mass flowing from the funnel and the standing time of series No .1 mortar is shown in Fig. 3.6. Fig 3.7 shows the experimental results of the first two funnel tests of fresh mortar with or without mineral admixture (series No. 2 and 3 mortars at 6 and 11min., series No. 4 mortar at 6 and 16min.).

In the first test at the standing time of 6 min, some samples adhered to the inner walls of the funnel, but for the measurements at 26min and 46min, because the bleeding occurred slightly and the
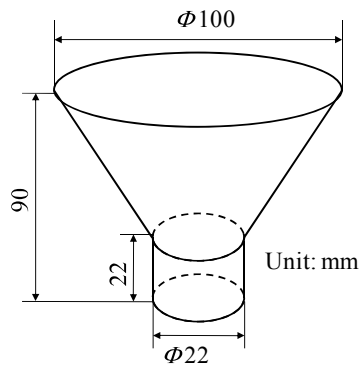
Fig. 3.5 Dimensions of funnel (unit: mm)

50
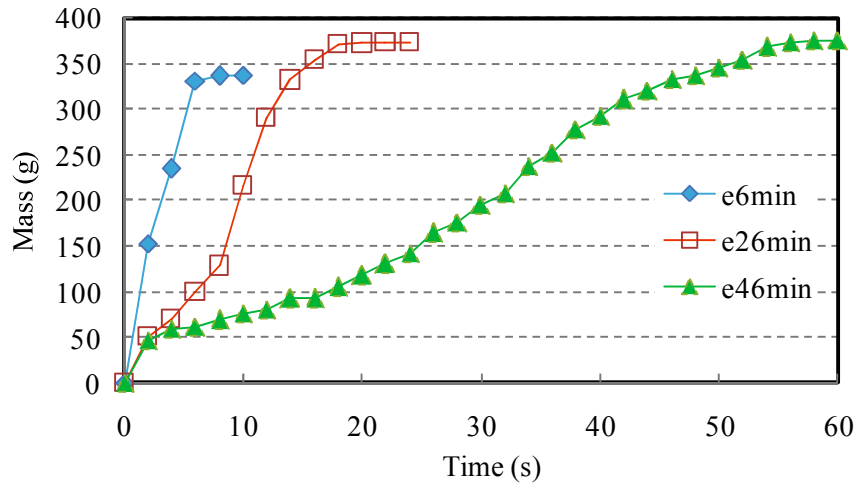
Fig. 3.6 Variation of the outflow mass with the standing time of series No. 1 at different moments in the experiment
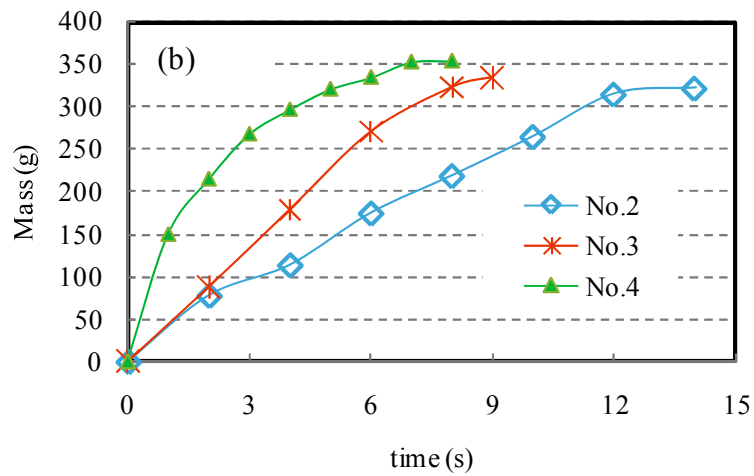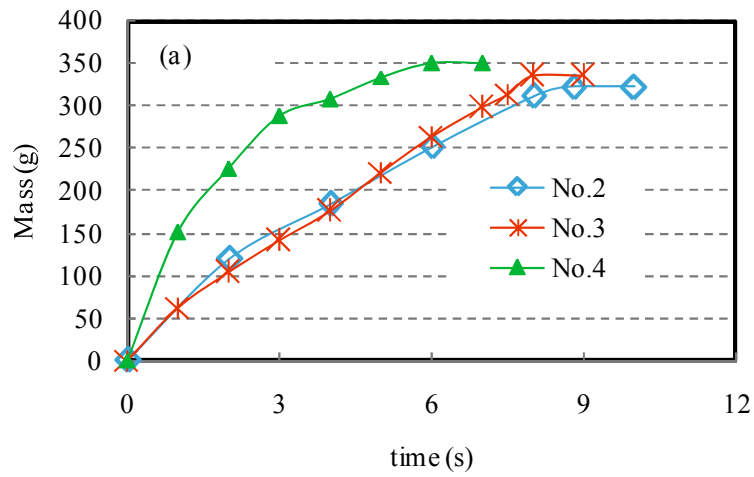
Fig. 3.7 Experimental results of funnel flow of first two measurements ((a) 6 min. (b) series No.2, No.3 at 11min., series No. 4 at 16min.)

bleeding water washed out the inner walls, no sample adhered to the inner walls of the funnel. Hence, , the final outflow mass at 6 min. was less than that at 26 and 46 min.. (see Fig 3.6). Due to the particle flocculation and hydration of cement, the apparent viscosity increases with time, the slopes of the outflow mass-time relational curves were in order of e6min > e26min > e46min.

Fig. 3.7 shows the results of funnel of fresh mortar with or without mineral admixture. Right after mixing (Fig. 3.7(a)), the funnel flow time of series No. 3 mortar was almost the same to series No. 2 mortar, but series No.4 mortar had the shortest funnel flow time. This is because fresh mortar containing BFS exhibits a lower viscosity than the reference mixture containing only Portland cement [4]. After a rest of the same time (Fig. 3.7(b).), series No.3 mortar needed less time to flow out than series No.2 mortar. The FA has a lower activity than cement in the surrounding of room temperature [5], and the contact force resulted from cement hydrates depends on cement content, Therefore, the fluidity of fresh mortar series No. 3 mortar containing FA can be easily kept.

As shown in Fig. 3.7(b), after 5 or 10 min. rest, the funnel flow time of series No.4 mortar was shorter than that of the others. The replacement ratio of BFS (50%) was higher than that of FA in series No.2 mortar, and BFS has a lower hydration ability than Portland cement [6]. For these reasons, the fluidity of fresh mortar containing BFS becomes easy to be kept up.

The funnel flow test's results were compared to the numerical predictions to verify the new DEM in chapter 4.

3.5 L-flow Test

The L-flow tests is for assessing the passing ability of SCC [7]. A closed vertical chamber is filled with the concrete to be tested so that a hydrostatic pressure head is produced. After a sliding door is opened the concrete has to level out through horizontal (L-box) flow obstacles. The difference in levels determines the tendency to blocking.

In this paper, the L-flow test was used to verify our SPH simulation, so the effect of reinforcing steel bars on the flow behavior is not taken into account. That is to say, the L-box without reinforcing steel bars was used. The geometry of L-shaped box is shown in Fig. 3.8. A tapeline is stuck by instant glue on the inside of the L-box's bottom to measure the flowing distance of fresh mortar. The tapeline is 5 mm width and 1 mm thickness, and the scale interval is 0.5 mm. The vertical section of L-box has a capacity of 2.5 liters. The sliding door was lifted up quickly within 2~3 seconds. After the door was opened, the flowing distances of the mortar sample were recorded at a certain time interval. The mortar of series No. 4 - 7 were used in L-flow test. The L-flow test was repeated three times for each mortar sample.

Final flow shapes of the mortars in the L-flow box are shown in Fig. 3.9. The final flow distance of series No. 5 mortar was shortest. This is because series No. 5 mortar had the lowest W/C (0.40), and accordingly had the lowest fluidity (the spread diameter of the flow table test was only 168 mm). However, in case of series No. 7 mortar, it had the largest W/C (0.55) and the largest spread diameter (208 mm), almost all the samples flowed out the vertical section of the L-flow box, and the final shape was nearly horizontal. Variation of the L-flow distance with the standing time is shown in Fig. 3.10. The data in Fig. 3.10 were mean values of three times measurements for mortar
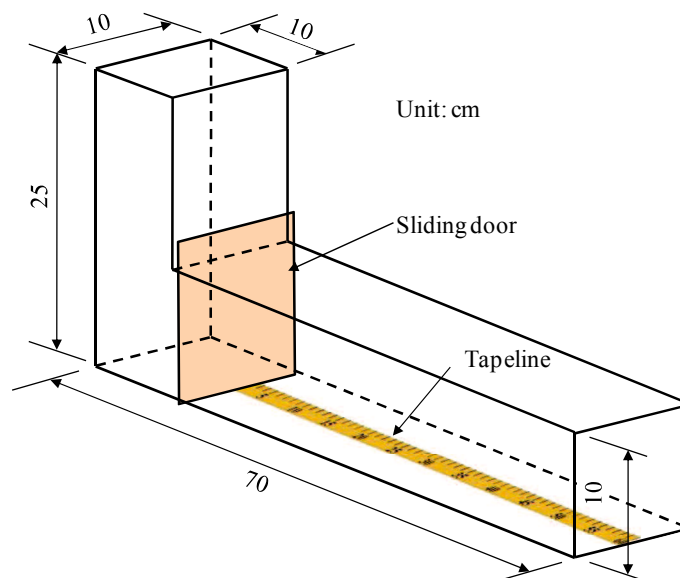
Fig. 3.8 Geometry of L-shaped box used in the L-flow test
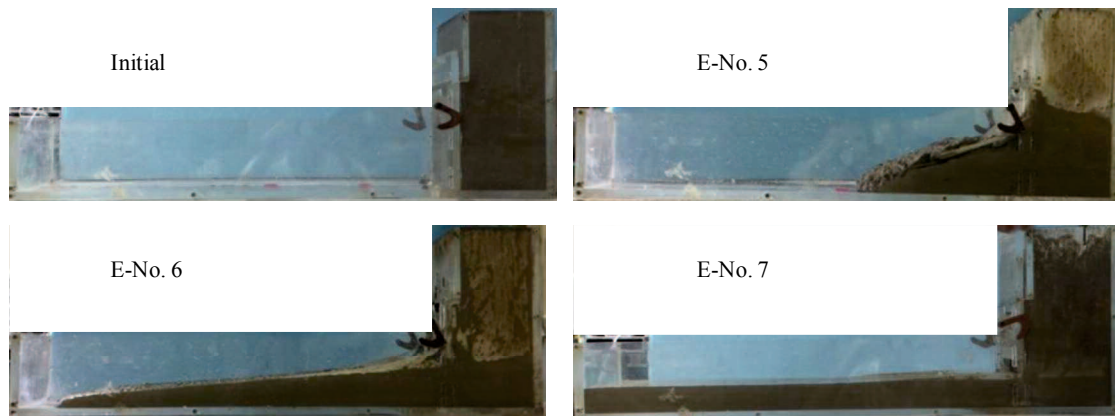
Fig. 3.9 Final shapes of fresh mortars in the L-flow box (E-No. n represents the experimental
results of series No. n)
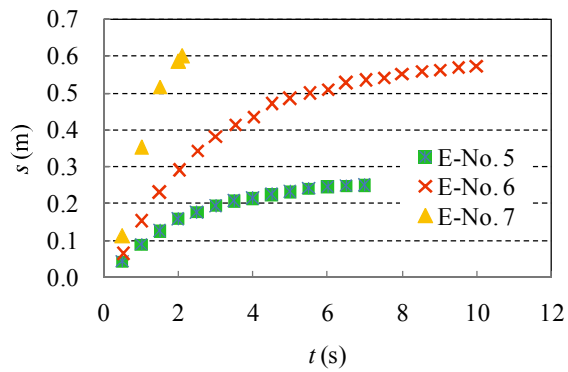
Fig. 3.10 Experimental results of the L-flow distance changing over time

mixtures. The flow speed of No. 7 mortar was the fastest, compared to other two series. Although the
final flow distances of series No. 6 and No. 7 mortars were near (about 6 cm), but the former had a
lower flow speed so that it spent more time till the flow stopped, and the final shape was different.

3.6 RSNS Rheometer Test

As stated in Section 2.3.3. The RSNS rheometer, recently developed by Li for measuring the parameters of VGM model [8] was used in this paper.

After mixing the mortars, we used the RSNS rheometer to measure the parameters in VGM model. About 18 liter samples was used at every measurement. The thickness of sample was 100 mm, and the measurement was repeated three times for each mixture. The measurement is divided into two parts: torque control or rotation speed sweep control. The detailed measurement and calculation are given as follows [8].

3.6.1 Measurement Before Yield

If the shear stress is increased from 0, the increment of shear stress is very small, the shear deformation is not dependent on the shear history, Eq. (2-13) is approximately expressed by

$$\frac{\tau/(\sigma_n + C_{w2})}{\gamma} = \frac{c_2 + c_3\tau}{c_6} \qquad (3\text{-}1)$$

Compared to normal stress σ_n, the adhesive force caused by the surface tension and suction of mixing water C_{w2} is very small. So it is negligible. The Eq. (3-1) is expressed by

$$\frac{\tau/\sigma_n}{\gamma} = \frac{c_2}{c_6} + \frac{c_3}{c_6}\tau \qquad (3\text{-}2)$$

When the shear stress is steady, and C_{w2} is negligible. And when $x < 1$, $\ln(1+x) \doteq x$. Eq. (2-13) is approximately given by

$$\ln(-\ln\frac{\gamma}{\gamma_\infty}) = -qt \qquad (3\text{-}3)$$

The measurement before yield consist of two stages: steady torque stage and torque's increasing stage.

1) Steady torque stage

The torque exerted on mortar is trail and error adjusted until the lower blade starts to move. Then the torque is fixed. The relationship in Eq. (3-3) is shown in Fig. 3.11. q is equal to the absolute of slope of linear regressive line.

2) Torque's increasing stage

Yield stress is the maximum shear stress before shear deformation, i.e. the shear stress at yield point, as shown in Fig. 3.12. The shear strain rate is closer to 0, that is to say, the shear strain do not
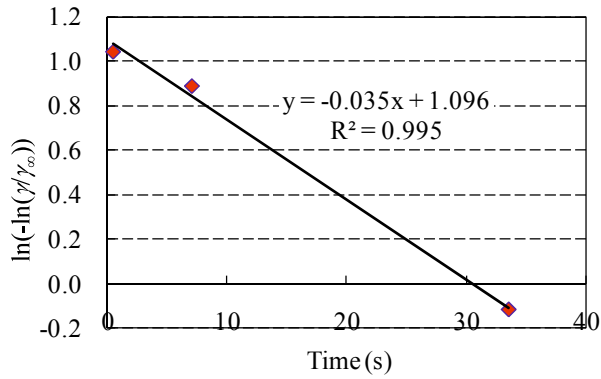
Fig. 3.11 The relationship of ln(-ln($\gamma/\gamma\infty$)) at steady stage
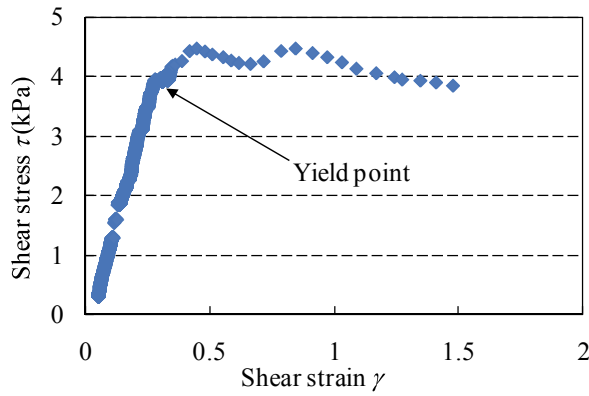
Fig. 3.12 The relationship of shear stress τ and shear strain γ at torque's increasing stage
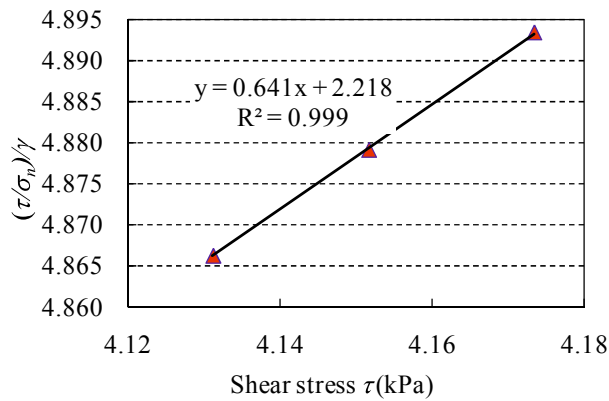
Fig. 3.13 The relationship of (τ/σ_n)/γ and shear stress at torque's increasing stage

change. The shear stress and shear strain at yield point are shear failure limit stress τ_f and shear failure limit shear strain γ_f.

Fig. 3.13 shows the relationship of (τ/σ_n)/γ and shear stress in Eq. (3-3). c_2/c_6, c_3/c_6 are equal to the slope and intercept of the linear regressive line, respectively.

3.6.2 Measurement After Yield

By combining Eq.(2-14) and Eq.(2-16), Eq.(3-4) is obtained.

$$\tau - \tau_f = \sigma_n \tan\{[\theta_f e^{-\kappa \cdot \dot{\gamma} \cdot (t-t_f)} + \phi] - \tan(\theta_f + \phi) + \frac{\eta}{\cos(\theta_f e^{-\kappa \cdot \dot{\gamma} \cdot (t-t_f)})} \dot{\gamma} \qquad (3\text{-}4)$$

When $x \doteq 0$, $\tan x \doteq x$. And viscous resistance (the second term of right of Eq. (3.4)) is negligible when the shear strain is very small. Hence, the Eq. (3-4) is simplified into

$$\tau_f - \tau = \sigma_n \theta_f [1 - e^{-\kappa \cdot \dot{\gamma} \cdot (t-t_f)}] \qquad (3\text{-}5)$$

Also, when $x < 1$, $\ln(1+x) \doteq x$. Eq. (3-5) is approximately expressed by

$$\ln(-\ln\frac{\tau_f - \tau}{\sigma_n \theta_f}) = -\kappa \dot{\gamma}(t - t_f) \qquad (3\text{-}6)$$

When shear deformation is large, the average particle contact angle is closer to 0. Eq.(2-14) can be simplified into

$$\tau = \sigma_n \tan\phi + (C_{w1} + \eta\dot{\gamma}) \qquad (3\text{-}7)$$

The measurement after yield consists of four stages.

1) Steady rotational velocity's stage

Motor rotates at a steady and small angular velocity. Because that the contact between particles is destroyed under shear stress, the torque of motor decreases until to a certain value, it goes to next stage.

2) Rotational velocity's increasing stage

The angular velocity of motor increases from 5 to 45 deg./s at a certain angular acceleration. It goes to third stage.

3) Rotational velocity's decreasing stage

The angular velocity of motor decreases from 45 to 5 deg./s at a certain angular acceleration. It goes to last stage.

4) Normal stress' increasing stage

The motors rotates at 5 deg./s, the normal stress exerted on the sample by the air cylinder is seriatim adjusted within four different air pressure (0, 0.3, 0.5, 0.7 Mpa).

The average shear stress, average shear strain rate and average normal stress is used, the parameters of VGM model is calculated.

Fig 3.14 shows shear strain rate $\dot{\gamma}$ and shear stress τ at rotational velocity's decreasing stage.
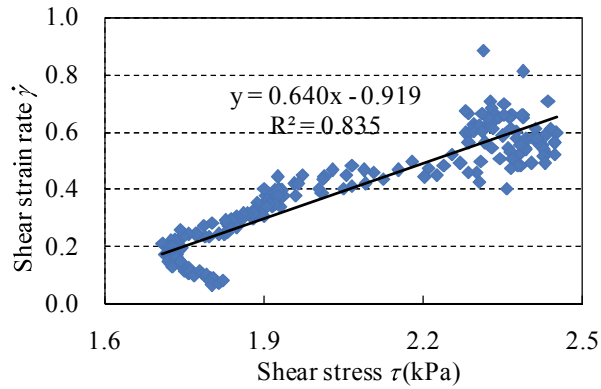
Fig. 3.14 The relationship of shear strain rate $\dot{\gamma}$ and shear stress τ at rotational velocity's decreasing stage
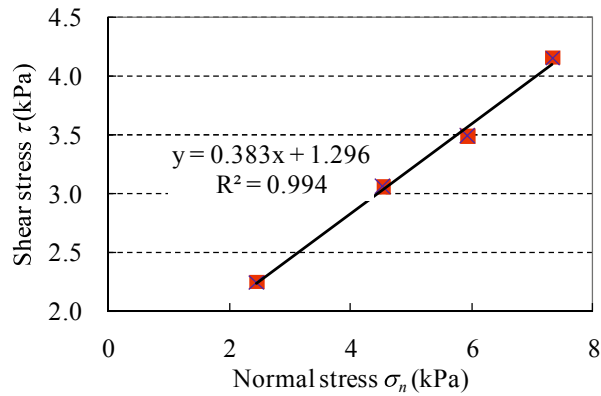
Fig. 3.15 The relationship of shear stress τ and normal stress σ_n at normal stress' increasing stage
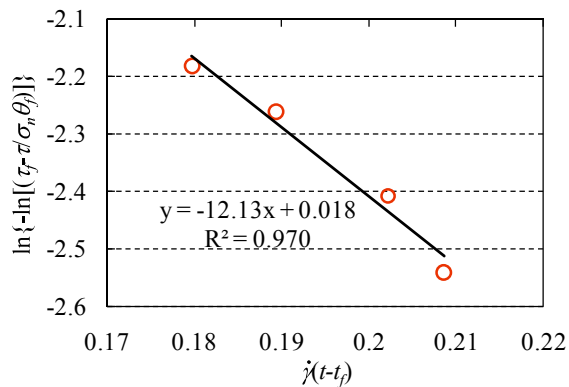
Fig. 3.16 The relationship of $\ln\{-\ln[(\tau_f-\tau)/\sigma_n\theta_f]\}$ and $\dot{\gamma}(t-t_f)$ at steady rotational velocity's stage

The essential viscosity η is equal to the slope of the linear regressive line. The relationship of shear stress τ and normal stress σ_n at normal stress' increasing stage is shown in Fig. 3.15. According to Eq.(3-7), the average inter-particle frictional angle ϕ is equal to the arctangent value of slope of the linear regressive line. And the shear resistance caused by the surface tension and suction of mixing

58

Table 3.3 Experimental results of VGM and Bingham model

Series No.	Parameters in VGM model								Bingham model parameters	
	τ_f (Pa)	γ_f (s-1)	η (Pa.s)	C_{wl} (Pa)	ϕ (rad)	θ_f (rad)	κ	σ_n (Pa)	τ_0 (Pa)	η_b (Pa.s)
1	1538	0.20	772	400	0.157	0.284	2.2	2412	1254	833
2	569	0.18	558	150	0.054	0.121	1.5	2372	379	560
3	302	0.16	455	90	0.030	0.062	0.7	2300	111	457

water C_{wl} is calculated by combining the intercept of the linear regressive line, the essential viscosity η and shear strain rate $\dot{\gamma}$. According to Eq. (2-16), the average particle contact angle can be obtained. Fig. 3.15 shows the relationship of $\ln\{-\ln[(\tau_f-\tau)/\sigma_n\theta_f]\}$ and $\dot{\gamma}(t-t_f)$ at steady rotational velocity's stage. According to Eq. (3-6). The absolute value of the slope in Fig. 3.16 is κ.

We also measured the Bingham model parameters (yield stress τ_0 and plastic viscosity η_b) of three series of mortars with the RSNS rheometer at Rotational velocity's decreasing stage. The average of three measuring results of each parameter was shown in Table 3.3. The standard deviation of three measuring results of every parameter was less than 10%.

As shown in Eq. (2-14), the shear failure limit stress τ_f is dependent on the normal stress σ_n, thus it should be noted that the τ_f shown in Table 3.3 was only a specific measuring value under the σ_n that was also shown in Table 3.3. For different σ_n, τ_f can be calculated by Eq. (2-14).

3.7 Summary

In this chapter, the materials and mix proportions of used fresh mortar were presented. Then the flow table test, funnel flow, L-flow and RSNS rheometer test were conducted, respectively. Main summary is concluded as follows:

1) Fresh mortars with same W/C (series No. 2, 3 and 4), the spread diameter increased with the decrease of cement content. Fresh mortars with different W/C (series No. 5, 6 and 7), the spread diameter increased with the increase of W/C.

2) For the same series, the flow time of funnel flow increased with the standing time. For different series, the flow time of funnel flow decreased with the increase of W/C and the decrease of cement content.

3) The flow time of L-flow test decreased with the increase of W/C.

4) τ_f, η in VGM model and τ_0, η_b increased with the decrease of W/C.

References

[1] H. A. Barnes, Thixotropy—a review, *Journal of Non-Newtonian fluid mechanics,* 70 (1-2) (1997) 1-33.

[2] G. H. Tattersall, P. Banfill, The rheology of fresh concrete, Pitman London, 1983.

[3] R. Shaughnessy, P. E. Clark, The rheological behavior of fresh cement pastes, *Cement and Concrete Research,* 18 (3) (1988) 327-341.

[4] O. Boukendakdji, E.-H. Kadri, S. Kenai, Effects of granulated blast furnace slag and superplasticizer type on the fresh properties and compressive strength of self-compacting concrete, *Cement and Concrete Composites,* 34 (4) (2012) 583-590.

[5] J. Linhua, The study of hydration properties of high content fly ash cement, *The Journal of the Chinese Ceramic Society,* 26 (1998) 695-701.

[6] R. S. Ahari, T. K. Erdem, K. Ramyar, Thixotropy and structural breakdown properties of self consolidating concrete containing various supplementary cementitious materials, *Cement and Concrete Composites,* 59 (2015) 26-37.

[7] A. U. Elinwa, S. P. Ejeh, A. M. Mamuda, Assessing of the fresh concrete properties of self-compacting concrete containing sawdust ash, *Construction and building materials,* 22 (6) (2008) 1178-1182.

[8] Z. Li, Rheological model and rheometer of fresh concrete *Journal of Structural and Construction Engineering, Transaction of Archcitectural Instistue of Japan,* 80 (710) (2015) 527-537.

Chapter 4
Standing time-dependent DEM

4.1 Introduction

Concrete is the most widely used construction materials. The quality of concrete structure is importantly affect by the rheological behaviors of fresh concrete. Factors affecting the rheological properties of freshly mixed cement-based material include environmental conditions (such as temperature and humidity), mix proportion, and constituents' flow behaviors. Furthermore, the mixing process, including mixer type, mixing sequence, and duration, also influences the rheological parameters [1].

The deformability of cement particles is minor, but their flocculation affects the rheological behavior of the cement paste [2]. Physical flocculation is a reversible process. But the cement hydration is a irreversible process. Concrete with a high bulid-up rate at rest can improve the segregation resistance and decrease later pressure exerted on the formwork during the casting process [3, 4]. During the transportation process of fresh concrete in a truck, the internal structure built-up by cement hydration may not be broken, this is why slump loss occurs at construction sites, especially in the seasons of high temperature [5]. In fact, if the material builds-up its internal structure too fast and apparent yield stress exceeds a critical value, any stoppage (such as due to the replenishment of buckets) may cause a blockage of pipes and eventually abuse the equipment ultimate pressure capacity in order to resume placement [6]. Predicting the change of fresh concrete's property or slump loss during waiting is important for suitable concrete construction[7].

Usage of supplementary cementitious materials, e.g. fly ash (FA) and ground granulated blast furnace slag (BFS), etc., can recycle industrial wastes or by-products to save Portland cement. The requirement of reducing the environmental burden of concrete has been moving on the use of mineral admixtures. The decrease of cement content can reduce CO_2 emission in cement manufacture, and the use of industrial wastes or by-products will reduce the needs of landfill and waste disposal.

The use of mineral admixture also can improve the properties of concrete [8-10]. The concrete containing BFS has small slump loss, high strength, and good durability. It is well known that using FA can improve the workability of fresh concrete. Although the effects of mineral admixture on the rheological behaviors of fresh concrete and the properties of harden concrete are often studied [11-14], and there are a few literatures about the thixotropic behavior of fresh concrete containing mineral admixtures [15, 16], the prediction of the fluidity's change of fresh concrete with the

standing time is still a problem awaiting solution.

Discrete Element Method (DEM) is a traditional numerical approach to the mechanical behaviors of granular materials, which treats a material with discrete particles. DEM has also been recently applied to the flow simulation of fresh concrete during mixing, transport, placement, and compaction [17]. In the traditional DEM, the physical contact and separation of discrete particles can be described by a parallel bond model, as explained later. The parameters in the parallel bond model, such as stiffness and bond strength, are constants for a given material, not changing with time.

In this chapter, the general DEM was introduced. The mechanism of the time-dependence was discussed, followed by proposing a new numerical approach to predict the standing time-dependent flow behavior on the basis of the Discrete Element Method (DEM). In the proposed standing td-DEM model, both the effects of hydration and physical flocculation were taken into account. The input parameters of standing td-DEM model was calibrated by flow table test. Using these input parameters, the numerical calculation of the gravity-induced funnel flow of fresh mortar were performed and compared to the experimental results at different times after mixing to validate the numerical method.

4.2 DEM

4.2.1 General Formulation

The DEM was introduced by Cundall for the analysis of rock-mechanics problems [18] and then applied to soils by Cundall and Strack [19]. The DEM is a particle approach, of which a fundamental assumption is that the analyzed material consists of separate discrete particles: circular particles (2D) or spherical particles (3D). The particles themselves are defined to be rigid, and each particle has mass, density, and dimension. Their interaction is treated as a dynamic process with a developing state of equilibrium whenever the internal forces are in balance. A contact between two neighbour particles is only at one point. The particles move according to the Newton's Second Law, and the contacts between the elements (particles or walls) follow the force-displacement law. That is to say, the Newton's Second Law determines the motion of each particle subjected the inter-particle contact forces, while the force-displacement law is used to calculate the contact forces arising from the relative motion at each contact, as shown in Fig. 2.1.

The displacements and rotations of the particles follow the governing Eqs. (4-1) and (4-2).

$$F_i = m \cdot (x_i'' - g) \tag{4-1}$$

$$M_i = I \cdot \omega_i' \tag{4-2}$$

where, F_i is the contact force vector acting on particle i, m is the mass of the particle i, x_i'' is the translational acceleration, g is the acceleration of gravity, M_i is the resultant moment acting on the particle i, I is the moment of inertia, and ω_i' is the angular acceleration.

The translational motion of the centre of mass of particle i is described in terms of position x_i, velocity x_i', and acceleration x_i''. The rotational motion of particle i is described in terms of its angular

Update positions of particle and wall, set of contacts

| Law of motion (Applied to each particle) Resultant force, Moment | Force-displacement law (Applied to each contact) Relative motion, constitutive law |
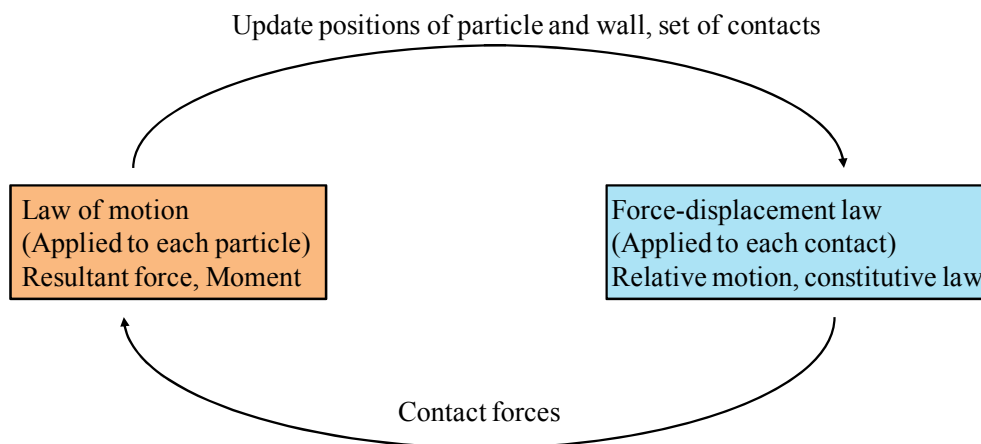
Contact forces

Fig. 4.1 Calculation cycle

velocity ω_i and its angular acceleration $\omega_i{}'$. The contact force vector F_i, means the action of particle j on particle i in particle-to-particle contact, or represents the action of wall element on particle i in wall-to-particle contact.

In DEM, inner wall of specimen's container, and rotating parts of rheometer, are treated with wall elements. The wall's position is updated according to the wall motion velocity specified by the calculator, not changing according to the Newton's Second Law.

4.2.2 Contact Model of Elements

Fresh concrete is generally considered to be a two-phase system, i.e., aggregate and mortar or cement paste. Each of the phases is simulated at its lowest level by circular or spherical particles with specific properties according to the modeled phase. Two basic elements are used in our DEM: spherical (3D) particle and wall. The former is used to render the concrete meso-structure discrete, i.e., as coarse aggregates and matrix mortar, the latter is used to represent the boundaries. The particles, connected by the hydrates (CSH gel, and $Ca(OH)_2$, etc.) are called clumped particles, and the particles, linked by physical flocculation are called flocculated particles. The others are dispersed particles. Hence, three types of particles exist in fresh concrete: dispersed particles, chemically clumped particles, and physically flocculated particles.

Except for the clumped particles, the contact forces between particles can be resolved by elastic
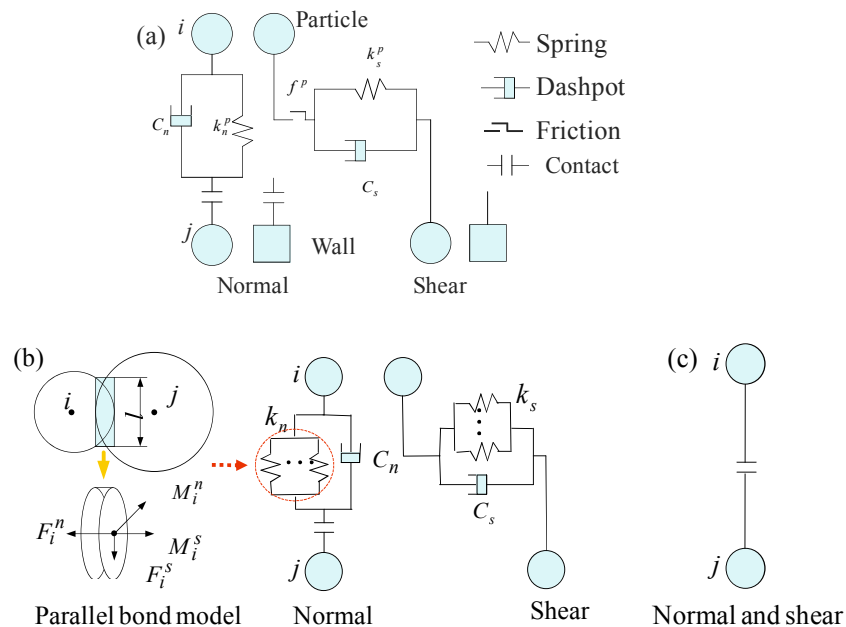
Fig. 4.2 Interaction model between (a) two dispersed particles, or dispersed particle and clumped particle or flocculated particle or wall, (b) two flocculated particles, (c) two clumped particles.

and viscous components. The interaction model between dispersed particle and dispersed particle or clumped particle or flocculated particle or wall is shown in Fig. 1(a). For dispersed particles, slip is an intrinsic property and is described by a slip component.

Obviously, the contact intensity of the flocculated discrete particles is greater than the dispersed particles and the contact between flocculated particles can be broken by an agitation. Hence, the parallel bond model is used to reflect the effect of physical flocculation, as shown in Fig. 1(b).

The parallel bond model describes the interaction of reversible flocculated particles' contact by the springs in normal and tangential directions, which has five parameters: normal and shear stiffness k_n and k_s, normal and shear strength σ_c and τ_c, and bond-radius coefficient l. The bond radius is equal to the minimum value of the radius r_i, r_j of the bonded particle i and j, multiplied by l. In general DEM for non-suspension body, the normal and shear stiffnesses are constants. But for fresh concrete, due to the flocculation and the hydration, the stiffness k_n, k_s or the strength σ_c, τ_c are not constants. The challenge is how to appropriately set these parameters.

Once a bond is formed between the particles, the contact force F_i and the moment M_i occur at the contact point. Relative motion over a time Δt between the two bonded particles results in the increments ΔF_i, ΔM_i of F_i and M_i. These increments in normal and shear directions are expressed by Eqs. (4-3)~(4-6).

$$\Delta F_i^n = -k_n A \Delta U_i^n \tag{4-3}$$

$$\Delta F_i^s = -k_s A \Delta U_i^s \tag{4-4}$$

$$\Delta M_i^n = -k_s J \Delta \theta_i^n \tag{4-5}$$

$$\Delta M_i^s = -k_n I \Delta \theta_i^s \tag{4-6}$$

where, ΔF_i^n, ΔF_i^s, ΔM_i^n, ΔM_i^s are the increments of contact force F_i, and moment M_i in normal and shear directions, respectively. ΔU_i^n, ΔU_i^s are the increments of relative displacement U_i in the normal and shear directions. $\Delta \theta_i^n$, $\Delta \theta_i^s$ are the increments of relative rotation θ_i in the normal and shear directions. A is cross-section area of parallel bond. A parallel bond is imaged as a set of springs with normal and shear stiffnesses, uniformly distributed over a circular area on the contact plane and centered at the contact point. k_n, k_s are thus normal and shear stiffness (N/m·m^2) at per unit contact area, respectively. J is the polar moment of inertia. I is the moment of inertia. A, J and I are calculated by Eqs. (7), (8) and (9).

$$A = \pi r^2 \tag{4-7}$$

$$J = \frac{1}{2} \pi r^4 \tag{4-8}$$

$$I = \frac{1}{4}\pi r^4 \qquad (4\text{-}9)$$

The maximum tensile stress σ and shear stress τ acting on the bond are calculated by Eqs. (4-10) and (4-11) (via beam theory). When $\sigma \geq \sigma_c$ or $\tau \geq \tau_c$, the bond breaks, and the contact forces disappear.

$$\sigma = \frac{F_i^n}{A} + \frac{\left| M_i^s \right|}{I} r \qquad (4\text{-}10)$$

$$\tau = \frac{F_i^s}{A} + \frac{\left| M_i^n \right|}{J} r \qquad (4\text{-}11)$$

On the other hand, in this study, we used clumps of particles to characterize the irreversible contacts caused by the cement hydrates. The particle contacts in the clumps can't be broken and behave as a rigid body. The mass of a clump is the total mass of the particles clumped. The motion of the particle clump is described in terms of the translational movement of its central point and the rotation of the entire clump. The motion of the clump follows the governing Eqs. (4-1) and (4-2).

Moreover, for fresh concrete the energy dissipation needs time due to the viscosity. Therefore, the dashpots are necessary besides the springs to form the viscous damping model. The dashpots are usually described by the normal and shear damping coefficients: C_n, C_s. Damping forces D_n and D_s, reacting to the contact bond of particle i and particle or wall j, are given by Eq. (4-12).

$$D_n = C_n \left| V_n \right|, \quad D_s = C_s \left| V_s \right| \qquad (4\text{-}12)$$

where, V_n, V_s are the relative movement velocities at the contact in the normal and shear directions, respectively.

4.3 Standing Time-dependent DEM

After cement is mixed with water, the physical flocculation and the hydration occur, thus some cement particles become in bonds even though water-reducer is added. With the advance of the physical flocculation and the hydration, dispersed particles decrease, and physically flocculated particles (reversible contacts) and chemically clumped particles (called as clumped particles, irreversible contacts) increase with the standing time. Time-dependent contact state of particles is imaginarily shown in Fig. 4.3. Because of water surface tension, smaller aggregate particles would be flocculated, and the hydrates would connect aggregate particles. Thus, The flocculated particles and the clumped particles consist of not only cement particles but also aggregate particles.

From mixing water with cement and aggregates to initial setting of concrete, the numbers of three types of particles: dispersed, flocculation and clumped particles, change with time, as described in Fig. 4.3. At the initial state, the particles are mostly dispersed (see Fig. 4.3(a)). With the increase of the standing time, the physically flocculated particles and chemically clumped particles become more and more (see Fig. 4.3(b) and (c)). At last, the concrete sets, all the particles are connected by the hydrates to become clumped particles (see Fig. 4.3(d)).

4.3.1 Number of Clumped Particles N_h

After cement is mixed with water, the hydration starts at once, ettringite accordingly generates. This kind of hydrate may at first connect cement particles. However, since the ettringite crystals are few and weak, the ettringite crystal bonds would be easily broken by agitation [20]. Therefore, as
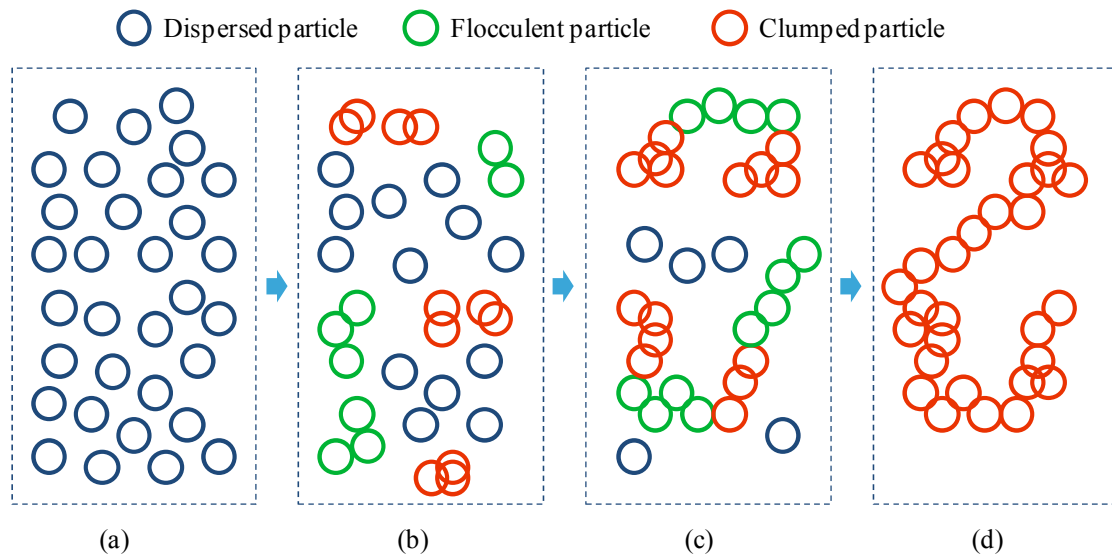
Fig. 4.3 Summary of different types of particles in fresh concrete

initial state (just after mixing), it is assumed that the number N_h of irreversible contacts or bonds due to the hydrates is zero. With the evolution of cement hydration, N_h increases.

The hydration process of portland cement is generally divided into three periods: dormant period, setting and hardening periods, as shown in Fig. 4.4. The degree of hydration $\alpha(t)$ is given by Eq. (4-13) [21].

$$\alpha(t) = \alpha_\infty \cdot \exp(-\left[\frac{a}{t_e}\right]^b)$$ (4-13)

where t_e is equivalent age when the environment temperature is different from the standard value (generally 20℃). α_∞ is the maximum hydration degree at the standard temperature. b is a parameter for describing the hydration degree changing over time. a is a constant relating to the hydration rate.

The hydration rate is dependent on the environmental temperature, if the standard temperature is 20 °C, the equivalent age under temperature T is calculated by Eq. (4-14) [21]

$$t_e = t \cdot \exp\left[\frac{E}{R}(\frac{1}{293} - \frac{1}{273+T})\right]$$ (4-14)

where T is environmental temperature (°C), E is the activation energy of binder (J/mol), R is the constant of gas (8.3144J/mol/K), and t is actual age under temperature T. The effect of temperature on the standing time-dependence is taken into account.

In the dormant period, the activation energy E is dependent on the specific surface area of binder, the chemical constituents of cement, the types of mineral and chemical admixtures, etc. E is expressed by
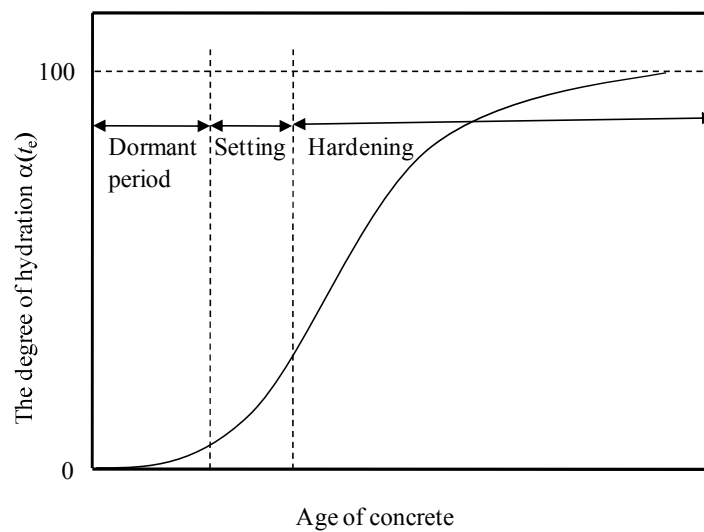
Fig. 4.4 The growth of hydration degree with time

$$E = 22100 \cdot f_e \cdot P_{C_3A}^{0.30} \cdot P_{C_4AF}^{0.25} \cdot B^{0.35} \tag{4-15}$$

where $P_{C_3A}^{0.30}$, $P_{C_4AF}^{0.25}$ are the contents of C_3A and C_4AF in cement by mass, respectively. B is the specific surface area (m²/kg) of binder. f_e is a correction factor when mineral admixture (e.g. fly ash) is used, which is calculated by

$$f_e = 1 - 1.05 \cdot P_{FA} \cdot \frac{P_{FACaO}}{0.40} + 0.40 \cdot P_{Slag} \tag{4-16}$$

where P_{FA}, P_{Slag} are the replacing ratios of fly ash and ground blast furnace slag by mass, respectively. P_{FACaO} is CaO content in fly ash by mass.

A linear relationship shown in Eq. (17) would be used to describe approximately the evolution of hydration degree with the standing time in the dormant period [22].

$$\alpha(t) = \omega \cdot t_e \tag{4-17}$$

where ω is constant.

Reference [21] shows that the degree α_i of hydration at initial setting depends on the water-binder ratio. When the environmental temperature is about 20 °C, α_i is given by

$$\alpha_i = 0.15 \frac{W}{CM} \tag{4-18}$$

By combining Eq. (4-17) and Eq. (18), the ω at 20 °C is obtained by Eq. (4-19).

$$\omega = \frac{0.15}{t_i} \frac{W}{CM} \tag{4-19}$$

where t_i is initial setting time at 20 °C.

Therefore, based on Eqs. (4-17) and (4-19), the hydration degree at time t under temperature T is expressed by

$$\alpha(t) = 0.15 \frac{t}{t_i} \cdot \frac{W}{CM} \cdot \exp\left[\frac{E}{R}\left(\frac{1}{293} - \frac{1}{273+T}\right)\right] \tag{4-20}$$

If it is assumed that the number N_h of clumped particles is in proportion to the hydration degree $\alpha(t)$, N_h is given by Eq. (4-21).

$$N_h = c \cdot N \cdot \alpha(t) \tag{4-21}$$

where c is a constant, N is number of total particles in fresh concrete.

At the time point of initial setting, it is considered that all the particles become the clumped

particles, i.e. $N_h=N$. At this time, the hydration degree is given by Eq. (4-18).Therefore, the constant c in Eq. (4-21) can be obtained by Eq.(4-22)

$$c = \frac{1}{0.15}\frac{B}{W}$$

(4-22)

By combining Eqs. (4-20) and (4-22), the number of clumped particles N_h is expressed by Eq. (4-23)

$$N_h = N \cdot \frac{t}{t_i} \cdot \exp\left[\frac{E}{R}(\frac{1}{293} - \frac{1}{273+T})\right]$$

(4-23)

As the number of clumped particles increases with time, the dispersed particles decrease with time, which flocculate at rest and can be dispersed again when shaken or agitated.

4.3.2 Number of Flocculation Particle N_f

Right after concrete is mixed, almost particles are in dispersed state (see Fig. 4.3(a)). The physical flocculation of particles increases with the standing time due to the Brownian motion and van der Waals attraction [20], [23, 24]. The contacts resulted from physical flocculation can be separated under an external force, such as agitation, and they would be renewed at stationary state due to re-flocculation after an agitation, so called reversible contacts. The number of physically flocculated particles is noted by N_f.

The decrease rate of dispersed particles due to the physical flocculation is given by [25]

$$\frac{dN_d}{dt} = -\frac{8kTN_d^2}{3\eta}$$

(4-24)

where, N_d is number of dispersed particles, t is the standing time after mixing. k is the Boltzmann constant, and η is the viscosity of mixing water.

Integrating Eq. (4-24) over time t, the number of dispersed particles at time t is obtained as

$$N_d = \frac{3\eta N_{d0}}{8kTtN_{d0} + 3\eta}$$

(4-25)

where N_{d0} is the number of dispersed particles at the initial state, and is equal to the number of total particles N in concrete. Based on Eqs. (4-12), (4-21) and (4-25), the number of flocculation particles N_f is obtained as

$$N_f = N \cdot \left[1 - c \cdot \alpha(t) - \frac{3\eta}{8kTNt + 3\eta} \right] \qquad (4\text{-}26)$$

With the increase of the flocculation particles and the clumped particles, the linkages of the particles becomes strong, thus the movement of particles becomes hard for a given external force. That is to say, the contact bonds between the particles become uneasy to be broken. In this calculation, firstly, we increased the number of clumped particles (see Eq. (4-21)) to describe the effect of hydration, then we treated the increase in the bond intensity with the growths of the normal and shear stiffness k_n, k_s with the standing time based on Eq. (4-26), as shown in Eqs. (4-27) and (4-28).

$$k_{nt} = \left[1 - c \cdot \alpha(t) - \frac{3\eta}{8kTNt + 3\eta} \right] \cdot \Delta k_n^{pb} + k_{n0} \qquad (4\text{-}27)$$

$$k_{st} = \left[1 - c \cdot \alpha(t) - \frac{3\eta}{8kTNt + 3\eta} \right] \cdot \Delta k_s^{pb} + k_{s0} \qquad (4\text{-}28)$$

where k_{nt}, k_{st} are normal and shear stiffnesses at time t, respectively. k_{n0}, k_{s0} are normal and shear stiffnesses at the time of t=0, respectively.

Therefore, our standing td-DEM model is different from general DEM at two aspects: one is that the clumped particles with irreversible bonds were introduced to reflect the effect of hydration, which grow in quantity with time. The second is to permit the normal and shear stiffness (k_n, k_s) to change with standing time due to the hydrates' formation and particle flocculation, whereas in general DEM model the normal and shear stiffness are constants.

The accuracy of the our DEM model is calibrated by comparing the numerical and experimental results of funnel flow. After long standing time, the sample can't flow under self-gravity, it is difficult to calibrate the accuracy of our DEM model by the flow test under self-gravity. Hence, the flow exerted by external force (such as shear in the rheometer) will be performed. The effect of external force on the numbers of flocculated and dispersed particles is had to be considered in Eqs.(4-27 and 28). This work will be done in the future work.

4.4 Calibration of Input Parameters

There are two kinds of primary particles in the mortar mixture: sand and cement particle. Since cement particles are a lot, if all the particles in the mortar are treated with discrete elements, the number of the elements will be numerous so that the calculation becomes difficult and time-consuming. As a compromise between modeling aggregate movement and limiting computation time, the mortar was divided into cement paste and fine aggregate phases. The cement paste exists in the form of imaginary particles with the diameter of 1~2 mm that is the same to that of the aggregate particles.

Through simulating the flow table test, we determined the input parameters of the td-DEM for the mortar by "trail and error". That is to say, all the input parameters were iteratively adjusted until the numerical results of the table flow test agreed with the experimental results on the shape of flow and the mean flow value, as shown in Fig 4.5. In the flow table test simulation, the number of the modeling particles was 14777, which were included within the cone.

The porosity is a ratio of the void volume to the total volume of a given volumetric region of a model. In the case of fresh concrete or mortar, air and free mixing water form voids between solid particles. The water content of the mortar of series No. 1 was 335kg/m^3, as shown in Table 3.1. Because part of mixing water is absorbed tightly by cement and aggregate particles on their surfaces, the absorbed or bonded water can be considered as a part of the solid particles. Hence, the free mixing water of the mortar is less than 335kg/m^3, i.e. the void is smaller than 0.335m^3/m^3. Base on the assumption that 140kg/m^3 of water (corresponding to 20% of water-cement ratio) was tightly bonded to the cement and aggregate particles, we set up the porosity to be 0.2 ($\doteqdot$ (0.335-0.140)m^3/m^3).

The inter-frictional force of the mortar depends on the vertical pressure applied. In order to

(a)   (b)

Fig. 4.5 The final shape of the series No. 1 fresh mortar on the flow table: (a) experiment (mean flow value: 210 mm), and (b) numerical simulation (mean flow value: 212 mm)

Table 4.1 Setup of the input parameters for the mortar's particles and walls

	ρ (kg/m^3)	r (mm)	k_n^p, k_n^w (N/m^3)	k_s^p, k_s^w (N/m^3)	f^p, f^w
Particles	2088	1~2	500	200	0.2
Walls	---	---	2×E+06	2×E+06	0.4

Table 4.2 The input parameter values of the parallel model and viscous damping model

	l	k_{n0} (N/m^3)	k_{s0} (N/m^3)	σ_c (N/m^2)	τ_c (N/m^2)	C_n	C_s
P_C	0.5	5500	600	550	22	---	---
Vd_C	---	---	---	---	---	0.3	0.1

Notes: P_C: parallel bond contact, Vd_C: viscous damping contact

keep the vertical pressure is the same as the experiment, the gravitational acceleration was set to be 12.25 m/s^2. The density of the mortar was 2088 kg/m^3. Based on this calibration simulation, the input parameters of the mortar were obtained. The input parameters for the modeling particles and walls are shown in Table 4.1, while the input parameters for the parallel contact and viscous damping are shown in Table 4.2.

4.5 Comparison Between Experimental and Numerical Results of the Funnel Flow

As stated above, we first performed the numerical simulation of the series No. 1 fresh mortar and compared to the corresponding experimental results to validate the standing td-DEM model. Then based on the td-DEM model, the effects of mineral admixture on standing time-dependent flow behavior were numerically analyzed.

4.5.1 Fresh Mortar without Mineral Admixture

The numerical calculations were carried out for the funnel flow test using the td-DEM proposed by us. The mortar sample, filled into the funnel, was modeled by 12777 particles. The other input parameters used are shown in Table 4.3.

In this study, the clumps were employed to describe the particles bonded by the hydrates. We fixed the size of the clump particles, but permitted the number of clumps to increase with the standing time due to hydration evolution. The total number of clumped particles at time t_i is calculated by Eq. (4-21).

Table 4.3 The input parameters values about the mortar mixture

No.	T (°C)	E (J/mol)	t_i (min.)	f_e	P_{C3A}	P_{C4AF}	B (m²/kg)	N	c	Δt (min.)	Δk_n^{pb}	Δk_s^{pb}	η (Pa·s)
1		44977	360	1.0					12.3	20	2000	800	
2	22	44977	360	1.0	0.09	0.09	335	6E+13	12.3	5			0.001
3		36593	420	0.8					12.6	5	3000	500	
4		53972	480	1.2					12.3	10			
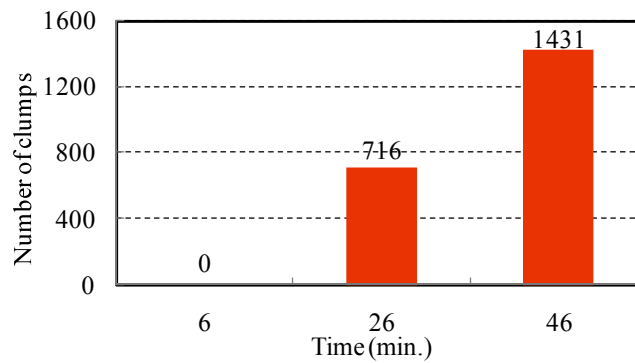
Fig. 4.6 The number of particle clumps at different moments

The dimensions of funnel outlet are limited, and the size of the clump particle has great effect on the flow behaviors of the mortar. Under the conditions that the clump particles can flow through the outlet and the effect of the clump particle's size on the flow behaviors is minimized, after several trial calculations, we found that it is appropriate to form a clump particle with ten imaginary particles. The numbers of clumps at different moment are shown in Fig. 4.6. As mentioned before, almost particles are in dispersed state right after concrete is mixed, so the number of the clumps is

(a) 6min.   (b) 26 min.   (c) 46min.
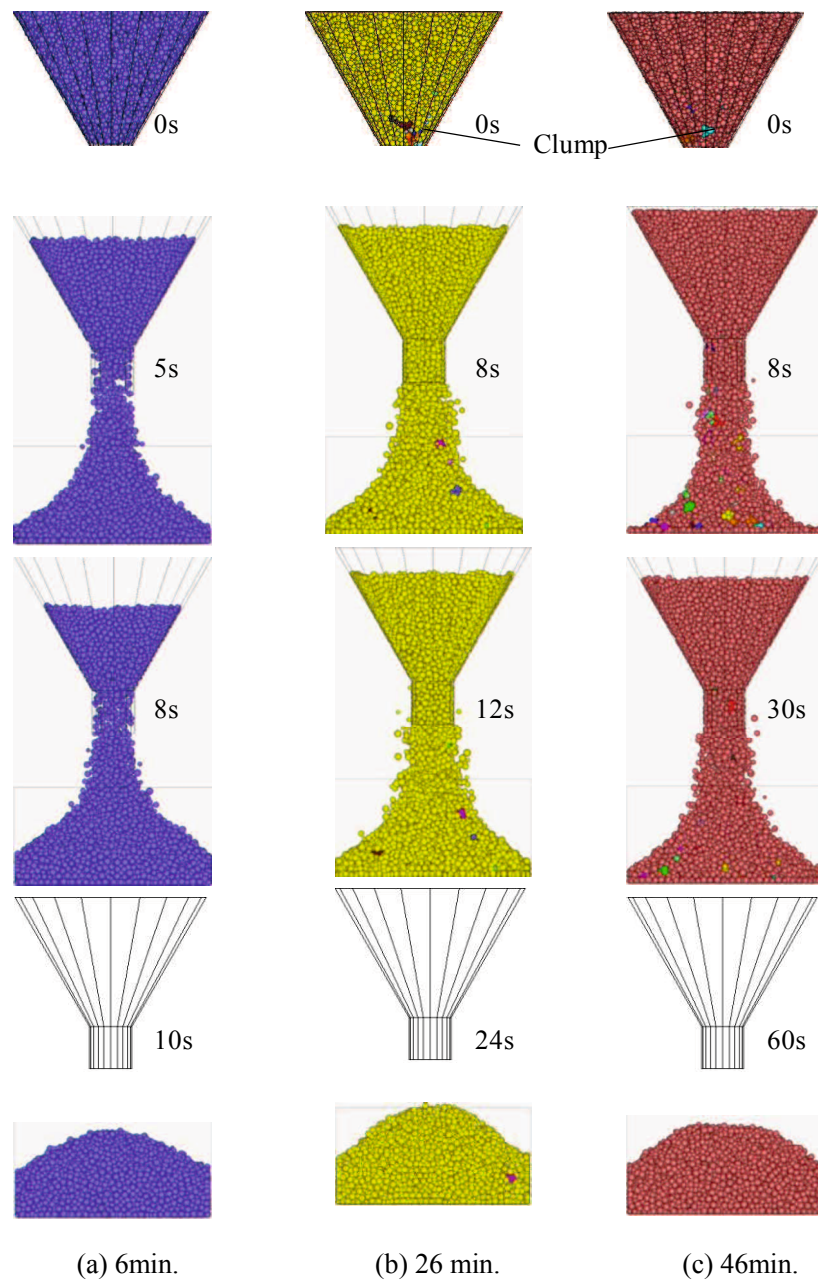
Fig .4.7 Funnel flow simulations of the series No. 1 mortar at different rest moments: (a) 26min. (b) 26min., and (c) 46min

zero at 6 min. The discrete particles were generated in the funnels, and the clump particles were randomly created, as shown in Fig. 4.7(a), (b), and (c): 0 second. After the funnel outlet was opened, the particles flow down (see Fig. 4.7(a), (b), and (c)). When all the particles flow out funnel, the calculation is over. At the same flowing moment (8s), from the distributions of the particles shown in Fig. 4.7(a), (b), and (c): 8 seconds, we can see that with the increase of rest time, the remained sample in the funnel increased, i.e. the funnel flow of the mortar became difficult.

Fig. 4.8 shows the numerical results (s6min, s26min, s46min) of the funnel flow test together with experimental values and the error of simulation (=(s-e)/e×100%). Each numerical data is an average of three repeated numerical analyses. There is a good consistency between the final
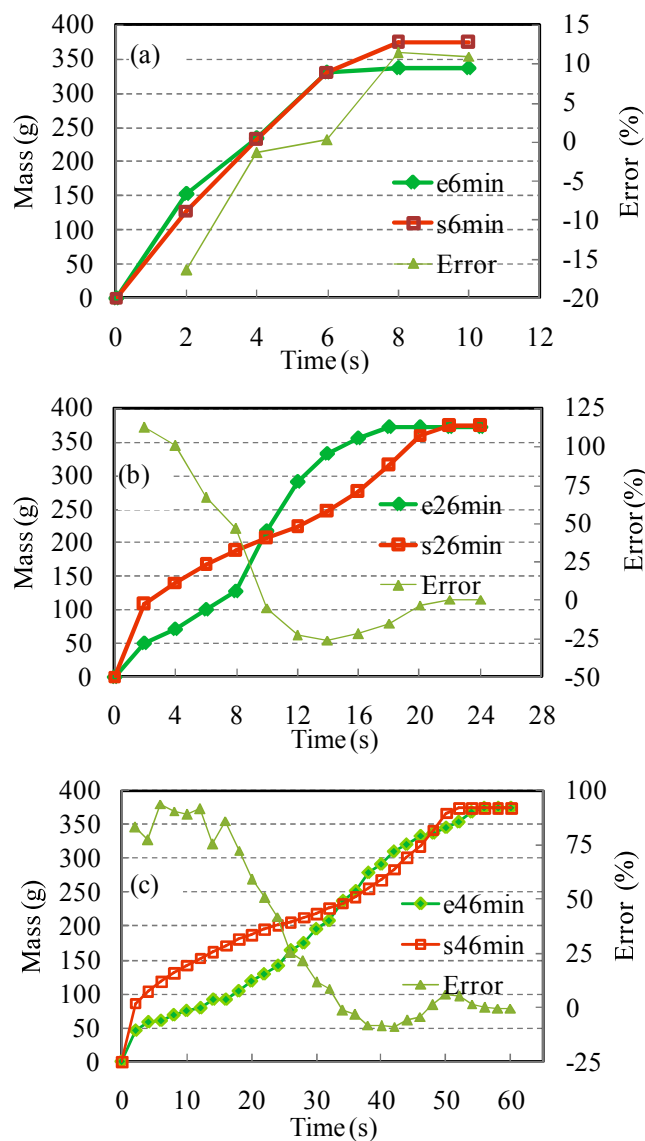
Fig. 4.8 Variation of the outflow mass over the flowing time at different moments: (a) 6 min., (b) 26 min., and (c) 46 min. "e" and "s" represent experimental and numerical result, respectively.
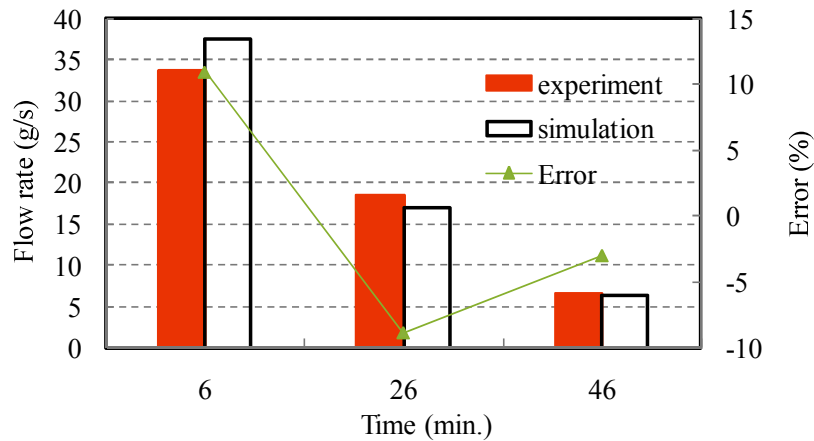
Fig. 4.9 The average outflow rates at different moments after mixing

experimental and numerical results. The final flow masses after 8 second were slightly smaller than the numerical values in the case of 6 min. standstill (see Fig. 4.8(a)). This is because some sample adhered to the funnel's inner wall, and thus didn't flow down in the experiment.

With the increase of standstill time, the bleeding and particle precipitation occurred slightly in the samples, the flow ability of the lower part of mortar sample in the funnel became worse. Thus, in the early stage the funnel flow in the experiment was slower than in the simulation, as shown in Fig. 4.8(b) and (c). But in the latter time, the upper part of mortar sample, which had greater water-cement ratio and smaller sand content, flowed down faster in the experiment than in the simulation. However, as stated above, total outflow masses in the experiments and in the simulations were almost the same.

The experimental and numerical results of the mean funnel flow rates at different moments are shown in Fig. 4.9. The mean flow rate is a ratio of the total outflow mass to the total flowing time. As shown in this figure, the mean flow rate decreased with the increase of standstill time. And the numerical results agreed well with the experimental ones within an error of $\pm 10\%$ for final outlet masses. Hence, the new td-DEM would be applied to the numerical prediction of the standing time-dependent behaviors of fresh concrete.

4.5.2 Effect of Mineral Admixture on Standing Time-dependent Flow behavior

The input parameter values used in numerical simulation of funnel flow are shown in Table 4.3. Because the contents of mineral admixtures were different, the correction factor f_e varies with the series. The mortar sample, filled into the funnel, was also represented by 12777 particles. The other input parameters used are shown in Table 4.1 and 4.2. The numerical simulations of three series at 6s after 5 min. or 10 min. rest time were shown in Fig. 4.10. The height of fresh mortar in the funnel decrease with the advance of content of mineral admixture. This is because that the use of mineral

<div align="center">

(a) No.1   (b) No.2   (c) No.3
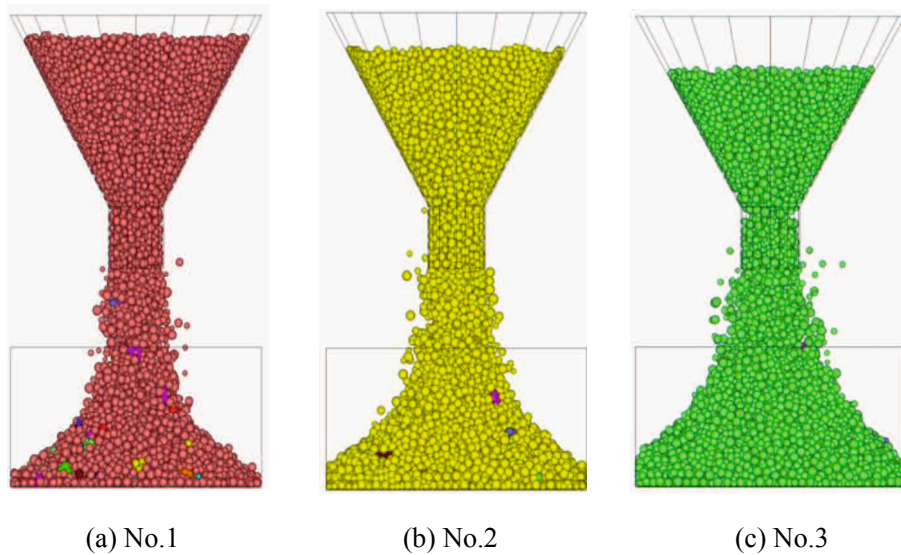
Fig. 4.10 The numerical results of three series at 6s after (a) (b) 5 min. and (c) 10 min. rest time.

</div>

admixture raised the fluidity of fresh mortar, and then the outflow mass increased.

The numerical and experimental results of series No. 2 mortar are shown in Fig. 4.11. The numerical results are close to the experimental results. The total funnel flow time was about 9s in the first measurement. With the advance of cement hydration and physical flocculation, the interaction between the particles increases, the total flow time after 11 min. rest thus became longer than after 6 min. After 16 min. rest, the fresh mortar couldn't flow out by its gravity so that only the results at 6 min. and 11 min. are given in Fig. 4.11.

The flow ability of fresh mortar containing FA is shown in Fig. 4.12. The interval of two measurements was 5 min. Like series No. 3 mortar, the longer the rest time, the longer the funnel flow time. After 21min. rest, the mortar couldn't flow out of the funnel. The numerical and experimental results of series No. 4 mortar are shown in Fig. 4.13. The interval of two measurements is 10 min. Even after 46 min. rest, the funnel flow test could still be conducted. As shown in Fig.

<div align="center">
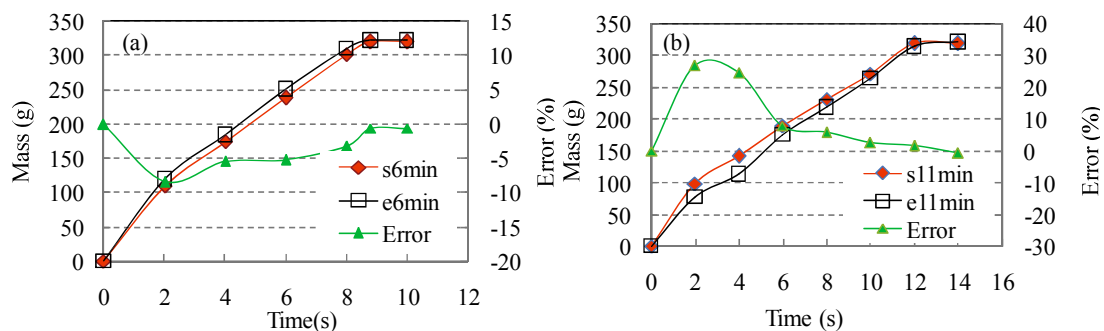
Fig. 4.11 Numerical and experimental results of series No.2 ((a) 6 min. (b) 11min.)

</div>
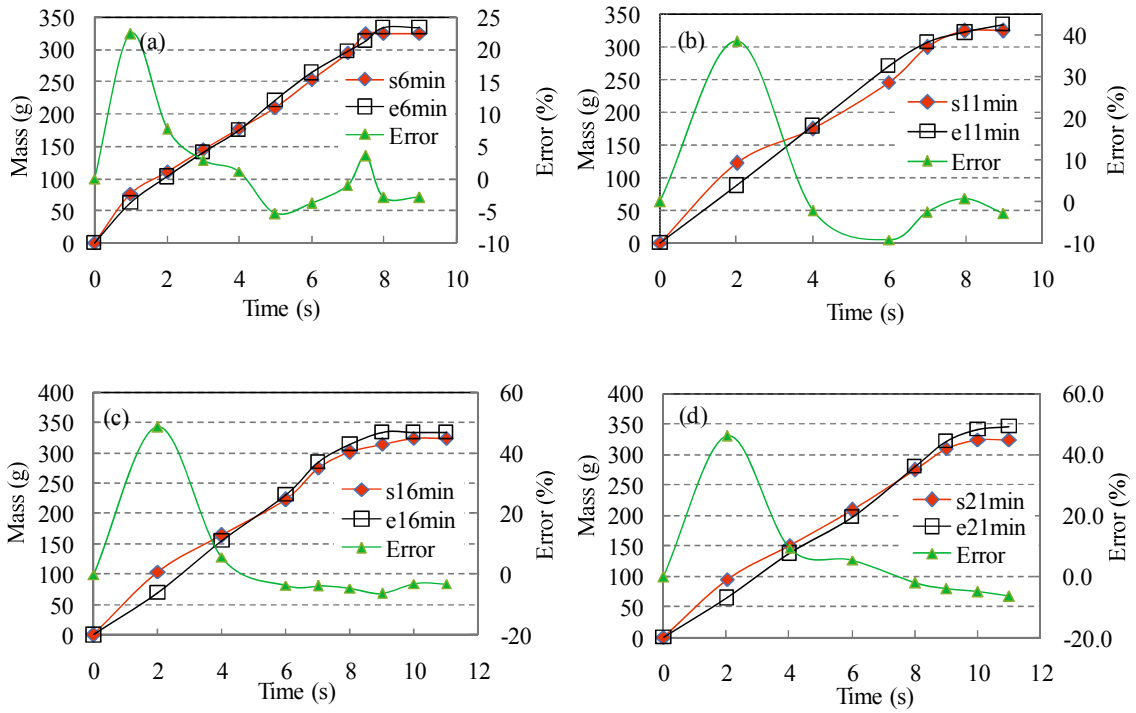
Fig. 4.12 Numerical and experimental results of series No.3 ((a) 6 min. (b) 11min. (c) 16 min. (d) 21min.)

4.11 and 4.12, The numerical and experimental results of the funnel flow tests of series No.2 and 3 mortars are very near.
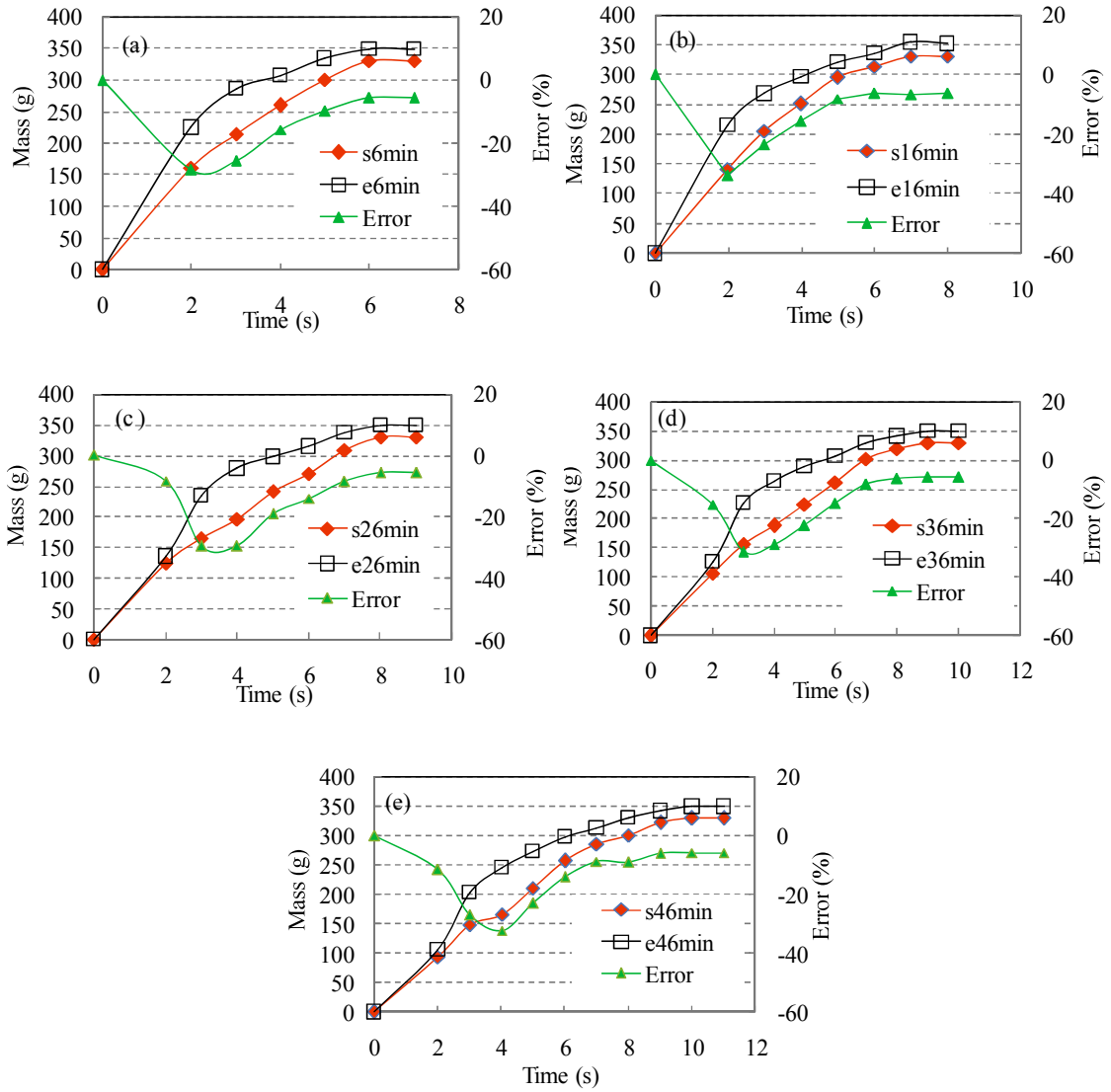
Fig. 4.13 Numerical and experimental results of series No.4 ((a) 6 min. (b) 16min. (c) 26 min. (d) 36min. (e) 46 min.)

4.6 Conclusions

In this chapter, we used the parallel bond model to express the contact between the particles, and introduce particle clumps to reflect the effect of hydration. A viscous damping model was used for the energy dissipation of particle. Based on these model, a numerical approach was proposed to predict the standing time-dependent flow behavior of fresh concrete. The contact described by the parallel bond model may be broken when maximum tensile stress σ or shear stress τ acting on the bond lager than the certain value. The particles in the particle clumps are linked by the hydrates to form irreversible bonds, and the numbers of the clumps increase with the standing time. The changes of the numbers of the clumped particles and the flocculation particles with the standing time were investigated theoretically. Based on these investigations, the time-dependent stiffness of the parallel bond model were proposed. The parameters used in the numerical simulation was calibrated by the flow table test.

In order to verify that this newly proposed td-DEM is applied to the prediction of the variation of flow performance of fresh concrete with standing time, gravity-induced funnel flow rates of fresh mortar at different moments after mixing were measured and compared to the results of the DEM simulation.

The td-DEM can accurately predict the standing time-dependent behavior of fresh concrete containing mineral admixture or not.

References

[1] C. Ferraris, F. De Larrard, N. Martys, Fresh concrete rheology: recent developments, *Materials Science of Concrete VI, Amer. Cer. Soc. Ed. S. Mindess, J. Skalny,* (2001) 215-241.

[2] H. J. Yim, J. H. Kim, S. P. Shah, Cement particle flocculation and breakage monitoring under Couette flow, *Cement and Concrete Research,* 53 (2013) 36-43.

[3] K. Khayat, D. Mitchell, Self-consolidating concrete for precast, prestressed concrete bridge elements, Transportation Research Board, 2009.

[4] N. Roussel, A thixotropy model for fresh fluid concretes: theory, validation and applications, *Cement and Concrete Research,* 36 (10) (2006) 1797-1806.

[5] S. Karasuda, Transport planning and management of ready mixed concrete for concreteconstruction, *Summaries of Cement and Concrete, Japan Cement Association (JCA),* 277 (1970) 28-34.

[6] R. T. Committe, Final report of RILEM TC 188-CSC 'Casting of self compacting concrete', *Materials and Structures,* 39 (2006) 937-954.

[7] T. Ota, Y. Nakata, R. Chikamatsu, et al., Survey on actual condition of pumping in concrete pumping method, *Proceedings of the Japan Concrete Institute,* 30 (2) (2008) 259-264.

[8] C. F. Ferraris, K. H. Obla, R. Hill, The influence of mineral admixtures on the rheology of cement paste and concrete, *Cement and Concrete Research,* 31 (2) (2001) 245-255.

[9] F. Collins, J. Sanjayan, Effects of ultra-fine materials on workability and strength of concrete containing alkali-activated slag as the binder, *Cement and Concrete Research,* 29 (3) (1999) 459-462.

[10] E. Güneyisi, M. Gesoglu, E. Özbay, Permeation Properties of Self-Consolidating Concretes with Mineral Admixtures, *ACI Materials Journal,* 108 (2) (2011).

[11] M. Uysal, V. Akyuncu, Durability performance of concrete incorporating Class F and Class C fly ashes, *Construction and Building Materials,* 34 (2012) 170-178.

[12] M. Şahmaran, İ. Ö. Yaman, M. Tokyay, Transport and mechanical properties of self consolidating concrete with high volume fly ash, *Cement and Concrete Composites,* 31 (2) (2009) 99-106.

[13] F. Cassagnabère, P. Diederich, M. Mouret, et al., Impact of metakaolin characteristics on the rheological properties of mortar in the fresh state, *Cement and Concrete Composites,* 37 (2013) 95-107.

[14] Y. Fan, S. Yin, Z. Wen, et al., Activation of fly ash and its effects on cement properties, *Cement and Concrete Research,* 29 (4) (1999) 467-472.

[15] J. Assaad, K. H. Khayat, Assessment of thixotropy of self-consolidating concrete and concrete-equivalent-mortar-effect of binder composition and content, *ACI Materials Journal,* 101 (5) (2004) 400-408.

[16] M. Rahman, M. Baluch, M. Malik, Thixotropic behavior of self compacting concrete with different mineral admixtures, *Construction and Building Materials,* 50 (2014) 710-717.

[17] H. Chu, A. Machida, H. Kobayashi, Verification of application of dem to fresh concrete by sphere

dragging viscometer, *Transactions of the Japan Concrete Institute,* 19 (1998) 1-8.

[18] P. A. Cundall, A computer model for simulating progressive, large scale movement in blocky rock systems, in: Symp. ISRM, Nancy, France, Proc., 1971, pp. 129-136.

[19] P. A. Cundall, O. D. Strack, A discrete numerical model for granular assemblies, *geotechnique,* 29 (1) (1979) 47-65.

[20] G. H. Tattersall, P. Banfill, The rheology of fresh concrete, Pitman London, 1983.

[21] A. K. Schindler, Prediction of concrete setting, in: Proceedings of the RILEM International Symposium on Advances in Concrete through Science and Engineering, Citeseer, 2004.

[22] T.-S. Tan, C.-K. Loh, K.-Y. Yong, et al., Modelling of bleeding of cement paste and mortar, *Advances in cement research,* 9 (33) (1997) 75-91.

[23] R. J. Hunter, Foundations of colloid science, Oxford University Press, 2001.

[24] Z. Li, T. Ohkubo, Y. Tanigawa, Theoretical analysis of time-dependence and thixotropy of fluidity for high fluidity concrete, *Journal of Materials in Civil Engineering,* 16 (3) (2004) 247-256.

[25] D. H. Everett, Basic Principles of Colloid Science, *Royal Society of Chemistry, Kyoto, Japan,* (2000) 23-27.

Chapter 5
Shearing Time-dependent SPH Approach

5.1 Introduction

With development of computer technology, numerical approach has been become a powerful tool to understand the rheological behavior and design the workability of fresh concrete. So far, a lot of numerical simulations have been performed by researchers. Concrete is a kind of heterogeneous multi phase composites that consisted of coarse aggregate and mortar. The physical flocculation, dispersion and hydration of cement particles cause the change in the particle arrangement of fresh concrete. It is considered that the change of fresh concrete's particle arrangement, during the rheological tests, results in that the flow curve of fresh concrete is nonlinear [1, 2], and shearing time-dependent [3]. Due to the same reason, measuring value of yield stress varies with the shearing time [4].

So far, Bingham-type model are usually used as the constitutive equation in the numerical simulation [5, 6]. High fluidity concrete has a fluid flow behavior, and thus its flow behaviors are usually described approximately by Bingham model [2]. However, since fresh concrete is composed of cement and aggregate particles with inter-friction, and its deformation is time-dependent, it has the flow behaviors of both granular material and viscous material. Obviously, Bingham model is unable to describe the nonlinear, and normal stress-dependent flow behaviors of fresh concrete, and it can't describe the change of rheological property with rest time and shearing time, i.e. the time-dependence of rheological property. Therefore, The VGM model was employed as the constitutive equation of fresh concrete in numerical simulation.

Recently, the so-called meshless/mesh free or particle methods have been actively developed and applied to simulate large deformation of continuum or dispersed material. Among these methods, SPH) is the longest established and has matured compared with other meshless or particle methods. SPH has been successfully used by Karihaloo to model the concrete tests, such as slump [5], L-flow [7], J-ring [8] and V-funnel tests [9]. In this paper, The SPH was used as the numerical tool.

In the case of fluid concretes, i.e. low yield stress, these concretes flow behaves just like suspensions, so the assumption of sticky flow is valid and there is shearing resistance at the boundary. In the case of high yield stress, two different trend may exist. On one hand, the amount of cement or fine particles may be high. The colloidal force network that can be built results in the increase of yield stress, the assumption of shearing resistance is also valid. On the other hand, the amount of coarse particles may be high. The behavior of this fresh concrete becomes closer to the

behavior of a cohesive granular material. In this case, the behavior at the boundary may be frictional [10]. Particle collisions in highly sheared and/or highly concentrated zones force particles to migrate from these zones, this is so-called shear induced particle migration. Shear induced particle migration is often strongly localized in highly sheared zones at interfaces [11]. It can therefore strongly affect flow by creating lubricating layers such as the ones observed during concrete pumping processes [12, 13] or during rheometric testing on concrete or mortars [14]. Therefore, it is almost mortar matrix at the boundary. A visco-plastic model of fresh mortar matrix [15] used at the boundaries.

In this chapter, a numerical approach, based on SPH and VGM model was proposed. The parameters of VGM model were measured in chapter 3. Numerical simulations of L-flow of three types fresh mortar with different W/C ratio were conducted. In order to contrast, the numerical simulation using SPH and Bingham model were also performed for the same mortars.

5.2 SPH

SPH method is a mesh free and particle-based method and originally used for continuum scale applications [16]. Besides the applications in astrophysics and solid problems such as dynamic material response [17], high velocity impact (HVI) [18] and explosion simulations [19], SPH method has also been applied to fluid problems, such as Newtonian and non-Newtonian flows with a free surface [20]. In SPH method, a system is represented by a set of discrete particles that possess material properties. Any particle i interacts with the others that are in a spherical domain, of which the radius (kH) is settled by a weight function or a smooth function [21], as shown in Fig. 5.1. The behaviors of discrete particles must obey the mechanical laws of motion, called governing equation.

5.2.1. Governing Equation

The governing equations for granular material consist of the continuity and momentum equations. The continuity equation describes the mass conversation that particles' densities change with the corresponding deformation, while the momentum equation expresses the motion of particles. The mass and momentum conversation equations for a continuum are as follows.

$$\frac{d\rho}{dt} = -\rho \nabla \cdot v \tag{5-1}$$

$$\frac{dv}{dt} = \frac{1}{\rho} \nabla \cdot P + g \tag{5-2}$$

where, ρ is density of particle, v is velocity of particle, t is time, g is gravitational acceleration.

Also, the total stress tensor P in Eq.(2) is expressed by
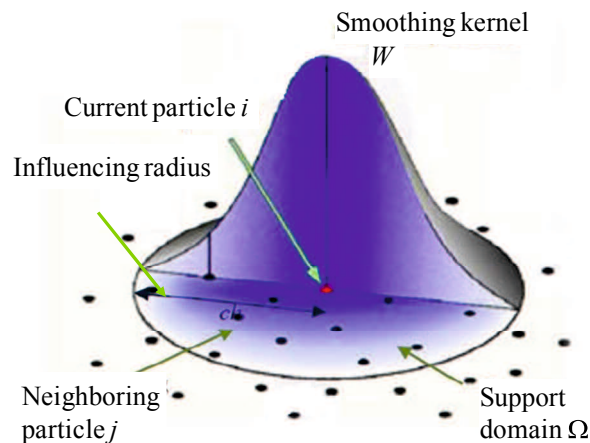
Fig. 5.1 Influential range of particle i

$$P = -pI + \tau \qquad\qquad (5\text{-}3)$$

where p is hydrostatic pressure at equilibrium, I is unit matrix, τ is extra stress tensor.

5.2.2. SPH Approximation of Governing Equations

Two steps are need for obtaining an SPH formulation. The first step is to build a function and/or its derivative in continuous form as integral representation. This step is usually termed as kernel approximation. The second step is usually referred to the particle approximation. In this step, the computational domain is firstly discretized by describing the domain with a set of initial distributions of the particles, which represents an initial state. After the discretization, field variables of a particle i are approximated by a summation of the values of the particles in the influential range of the particle i. The integral of an arbitrary function $f(x)$ in the SPH is based on the kernel function W and is expressed by

$$f(x) \approx \int f(x')W(|x-x'|, H)dx' \qquad\qquad (5\text{-}4)$$

where, H is smoothed length for defining the influential range of kernel function. The kernel function W is usually chosen to be an even function, and should satisfy the conditions, such as the normalization condition (see Eq.(5-5)) and the compact condition (see Eq.(5-6)).

$$\int_{\Omega} W(|x-x'|, H)dx' = 1 \qquad\qquad (5\text{-}5)$$

$$W(|x-x'|, H) = 0, \ x-x' > kH \qquad\qquad (5\text{-}6)$$

where, k is a parameter related to the smooth function. kH is effective radius of the smooth function (see Fig. 1). When H approaches to zero, the kernel function W need to be a delta function. After describing the computational domain with a finite number of particles, the continuous form of kernel approximation shown in Eq.(4) can be written as a discretized form of the summation of the influenced particles as follows.

$$f(x_i) = \sum_j \frac{m_j}{\rho_j} f(x_j)W(|x_i - x_j|, H) \qquad\qquad (5\text{-}7)$$

In this study, we adopted the usually used cubic spine function as kernel function, as follows:

$$W(r,H) = \alpha_d \begin{cases} 1 - \dfrac{3}{2}q_H{}^2 + \dfrac{3}{4}q_H{}^3 & 0 \le q_H \le 1 \\ \dfrac{1}{4}(2 - q_H)^3 & 1 \le q_H \le 2 \\ 0 & q_H \ge 2 \end{cases} \qquad (5\text{-}8)$$

where $r = (r_i - r_j)$, α_d is normalization factor and is equal to $10/7\pi H^2$ in case of two dimensions or $1/\pi H^3$ in case of three dimensions.

In SPH, the movements of all the discrete particles are calculated individually, and further accumulated to clarify the deformation and movement of whole system. Hence, the governing equations need to be discretized for each discrete particle. In this study, we used the most popular SPH approximation forms to discretize the governing equations. Discretized continuity and momentum equations are expressed by Eq.(5-9), and Eq.(5-10), respectively [22]. They were used to calculate the local density, velocity and acceleration of each particle.

$$\frac{d\rho_i}{dt} = \sum_j m_j (v_i - v_j)\nabla_i W_{ij} \qquad (5\text{-}9)$$

$$\frac{dv_i}{dt} = \sum_j m_j \left(\frac{P_i}{\rho_i^2} + \frac{P_j}{\rho_j^2} \right)\nabla_i W_{ij} + g \qquad (5\text{-}10)$$

5.2.3. Equation of State

An equation of state must be used to describe the relationship between pressures and densities of the particles. Fluid is generally incompressible. However, since the incompressible SPH method (ISPH), using the actual equation of state (Pressure Poisson Equation), needs extremely small time step, the solving process is greatly slowed. Hence, in most cases, fluid is treated to be weakly compressible to the advantage of shortening the solving process, called weakly compressible SPH method (WCSPH) here.

Fresh concrete contains tiny air bubbles. Some of them would get out while fresh concrete flows. It is reasonable to consider that fresh concrete has weak compressibility. Shadloo compared the ISPH and the WCSPH, and concluded that the WCSPH can give an accurate and reliable analysis like as the ISPH method does [23]. Thus, we used the WCSPH method in this study, the following thermodynamic equation of state was employed according to Reference [24].

$$P = B\left[\left(\frac{\rho}{\rho_0}\right)^a - 1\right] \tag{5-11}$$

where, $B = c_0^2 \rho_0 / a$, $a = 7$, and c_0 is sound speed under the initial density ρ_0.

5.2.4. Artificial Viscosity

In the SPH method, when the particles are in a tension state, their motions become unstable. As a consequence, the particles tend to clump together and show unrealistic physical behavior. In order to stabilize the numerical scheme and to alleviate the unphysical oscillations, the artificial viscosity approach was adopted in this study, which is expressed by Eq.(5-12) [25].

$$\Pi_{ij} = \begin{cases} \dfrac{-\alpha \bar{c}_{ij}}{\bar{\rho}_{ij}} \cdot \dfrac{h v_{ij} r_{ij}}{r_{ij}^2 + 0.01 H^2} & v_{ij} r_{ij} < 0 \\ 0 & v_{ij} r_{ij} > 0 \end{cases} \tag{5-12}$$

where, α is a free parameter changing with numerical problem, $\bar{c}_{ij} = (c_i + c_j)/2$, $\bar{\rho}_{ij} = (\rho_i + \rho_j)/2$. v_{ij} ($= v_i - v_j$) is relative velocity of particles i and j, and $r_{ij} = (r_i - r_j)$ is relative distance of particles i and j.

5.2.5. Boundary Condition

Two types of boundary conditions need to be taken into account. Firstly, when a particle approaches boundary, the kernel function will be truncated and unphysical penetration will happen. This problem further reduces the accuracy of SPH method. For solving the problem, in this work we employed the repulsive boundary condition developed by Monaghan [25]. Secondly, the discrete particles of fresh concrete may slip at the boundary and thus suffer from slippage resistance. In most case, coarse aggregates are surrounded by mortar matrix. Therefore, it is almost mortar matrix at boundary. The slippage resistance has important effect on flow process of fresh concrete (see Section 4.2). We used the visco-plastic model of fresh mortar matrix to describe the slippage resistance, which was proposed by Murata, as shown in Eq.(5-13) [15]

$$\tau_s = \eta_s v + \tau_{sy} \tag{5-13}$$

where, τ_s is slippage resistant stress at boundary, η_s is plastic viscosity of slippage, τ_{sy} is yield stress of slippage.

5.2.6. Integration Scheme

Predictor-Corrector algorithm [26] was employed to execute the time integration. If considering the mass and momentum conversation equation (Eqs. (5-1) and (5-2)) in the form of $d_\rho/d_t=S$, $d_v/d_t=F$, all the values of time-variant quantities are predicted at the time step n+1, based on the time step n+1/2 as follows:

$$\rho^{n+1/2} = \rho^n + \frac{\Delta t}{2} S^n, \quad v^{n+1/2} = v^n + \frac{\Delta t}{2} F^n \tag{5-14}$$

Then, these values are updated at another half time step.

$$\rho^{n+1/2} = \rho^n + \frac{\Delta t}{2} S^{n+1/2}, \quad v^{n+1/2} = v^n + \frac{\Delta t}{2} F^{n+1/2} \tag{5-15}$$

At the end of the time step, the values are calculated as follows:

$$\rho^{n+1} = 2\rho^{n+1/2} - \rho^n, \quad v^{n+1} = 2v^{n+1/2} - v^n \tag{5-16}$$

The selection of the magnitude of time step Δt is dependent on the Courant Friedrichs Lewy (CFL) condition, the force terms, and the viscous diffusion terms. Δt is expressed by Eq.(5-17) [26]

$$\Delta t = 0.3 \cdot \min(\Delta t_f, \Delta t_{cv}) \tag{5-17}$$

$$\Delta t_f = \min(\sqrt{H/|f|}), \quad \Delta t_{cv} = \min(H/(c_s + \max|Hv_{ij}r_{ij}/r_{ij}^2|)) \tag{5-18}$$

where f is a force acting on per unit mass, c_s is a constant.

5.3. Constitutive Equation

5.3.1. Bingham Model

Present SPH simulations of fresh concrete have generally used Bingham model as constitutive model, as shown in Eq.(5-19).

$$\tau = \left(\eta_b + \frac{\tau_0}{\dot{\gamma}} \right) \dot{\gamma} \qquad (5\text{-}19)$$

where, τ_0 is yield stress, η_b is plastic viscosity, $\dot{\gamma}$ is shear strain rate.

The stress tensor and the shear strain rate tensor are written as

$$\tau = \sqrt{\frac{1}{2} \tau_{ij} \tau_{ij}} , \dot{\gamma} = \sqrt{\frac{1}{2} \dot{\gamma}_{ij} \dot{\gamma}_{ij}} \qquad (5\text{-}20)$$

The constitutive law shown in Eq.(5-19) is discontinuity when shear stress τ approaches to the yield stress τ_0. When subjected to the τ_0, the apparent viscosity ($\eta_{app} = \tau/\dot{\gamma}$) becomes infinite so that numerical divergence occurs in the computation. Hence, it is difficult to introduce directly Bingham model into the SPH simulation. A regularized Bingham model, as shown in Fig. 1(a) and in Eq.(5-21), is usually used in SPH simulations of fresh concrete [27]. In this study, we first used the regularized Bingham model (Fig. 5.2(a)) to do SPH simulations.

$$\tau = \left(\eta_b + \tau_0 \frac{\left[1 - e^{\beta \dot{\gamma}}\right]}{\dot{\gamma}} \right) \dot{\gamma} \qquad (5\text{-}21)$$

where, β is a parameter related to the transition between the solid and fluid regimes. The larger the β, the sharper the transition [28].

5.3.2. VGM Model

As stated above, Bingham model can't exactly describe various reological behaviors of fresh concrete overall since fresh concrete has granular flow behavior. For this reason, Li proposed the VGM model based on a series of theoretical analyses [2, 29] and experimental investigations[30, 31], as shown in Eqs. (5-22) and (5-23) [29, 32]. It was verified that this model is able to describe various rheological flow behaviors of fresh concrete [33]. When shear stress (τ) and shear strain (γ) are smaller than the shear failure limit stress (τ_f) and limit strain (γ_f), fresh concrete is in

visco-elasto-plastic state, and the shear strain γ under a shear stress τ is expressed by Eq.(5-22). When $\tau \geqq \tau_f$ and $\gamma \geqq \gamma_f$, fresh concrete enters into the shear failure state, the τ–$\dot{\gamma}$ relationship is described by Eq.(5-23).

if $\tau < \tau_f,\ \gamma < \gamma_f$

$$\gamma = \frac{c_6\tau}{c_2 + c_3\tau} \cdot \frac{1}{\sigma_n + C_{w2}} \cdot [1 - \exp(-qt)] = \gamma_\infty \cdot [1 - \exp(-qt)]$$

$$\dot{\gamma} = \frac{c_2 c_6 s_1 / (\sigma_n + C_{w2})}{(c_2 + c_3\tau)^2} \cdot \left[1 - \exp\left(-q\frac{\tau}{s_1}\right)\right] + \frac{c_7\tau(c_2 + c_3\tau)}{\exp(q\tau / s_1)}$$

$$c_2 = \phi + \theta_0,\ c_3 = \frac{\theta_f - \theta_0}{\tau_f},\ c_6 = \frac{1}{2} N\Lambda_0$$

$$q = c_8(\sigma_n + C_{w2})\left(\frac{c_2 + c_3\tau}{c_6}\right)^2,\ C_{w2} = N f_{wm}\cos\theta_0$$

$$\gamma_\infty = \frac{c_6\tau}{c_2 + c_3\tau} \cdot \frac{1}{\sigma_n + C_{w2}},\ c_8 = \frac{2\Lambda_c c_6^2}{hNc_2 \exp(E/kT)}$$

(5-22)

if $\tau \geq \tau_f,\ \gamma \geq \gamma_f$

$$\tau = \sigma_n \tan(\theta_f e^{-\kappa\cdot\dot{\gamma}\cdot(t-t_f)} + \phi) + C_{w1} + \frac{\eta}{\cos(\theta_f e^{-\kappa\cdot\dot{\gamma}\cdot(t-t_f)})}\dot{\gamma}$$

$$= \tau_f^* + \eta_t\dot{\gamma}$$

(5-23)

$$\tau_f^* = \sigma_n \tan(\theta_f e^{-\kappa\cdot\dot{\gamma}\cdot(t-t_f)} + \phi) + C_{w1},\ \eta_t = \frac{\eta}{\cos(\theta_f e^{-\kappa\cdot\dot{\gamma}\cdot(t-t_f)})}$$

The shear failure limit stress τ_f is mainly dependent on normal stress σ_n, mean particle contact angle θ_f, and mean inter-particle frictional angle ϕ, and is expressed by Eq.(5-24) [32].

$$\tau_f = \sigma_n \tan(\theta_f + \phi) + C_{w1}$$

(5-24)

Because almost all the present rheometers of fresh concrete adopt the rotational speed sweep control method, it is impossible to evaluate the deformation behavior of fresh concrete before yield. VMG model not only describes the flow behaviors of fresh concrete in shear failure state, i.e. in yielded state, but also provides the information about the deformation before yield.

In order to properly simulate the flow of fresh concrete under various conditions, in this study we incorporated VGM model into the SPH program as constitutive model. For a detailed clarification of material's properties, the description of the deformation behavior before the shear failure, shown in Eq.(5-22), is of great significance, and if using Eq.(5-22) as a constitutive equation before yield, the divergence problem in the numerical analysis mentioned above can be avoided. However, Eq.(5-22) describes the deforming behavior of fresh concrete before yield. A precise
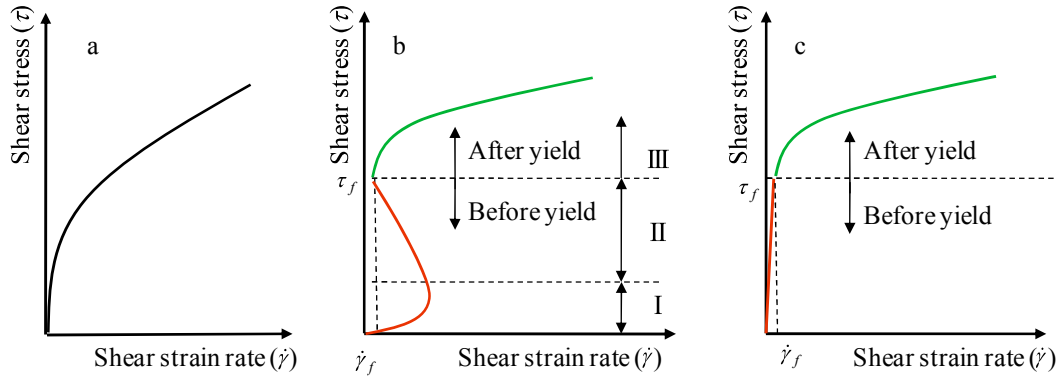
Fig. 5.2 The τ-$\dot{\gamma}$ relationship: (a) Regularized Bingham model, (b) VGM model, and (c) simplified VGM model.

calculation of the shear deformation before yield is not necessary for simulating the flow of fresh concrete during pumping or casting. And, because Eq.(5-22) is nonlinear function, it is extremely difficult to apply directly this complicated equation in the numerical simulation. Therefore, we simplified the flow curve before yield with a straight line, as shown in Fig. 5.2(c). Because the $\dot{\gamma}_f$ is very small, the slope ($\tau_f/\dot{\gamma}_f$) of the line is large, i.e. the viscosity before yield is extremely large. Similar simplification is also found in Reference [34].

$$\tau = \frac{\tau_f}{\dot{\gamma}_f}\dot{\gamma} \qquad (\text{if } \tau < \tau_f) \tag{5-25}$$

where $\dot{\gamma}_f$ is the shear strain rate at the shear failure point.

5.4 Numerical Results and Discussion

The input parameters of VGM and Bingham models (measured at Section 3.6) and the values of boundary parameters in Eq. (5-13) are shown in Table 5.1. In the L-flow test, since normal stress σ_n varies with location, τ_f of samples at different locations are different. Hence, we firstly calculated the σ_n and further the τ_f at different locations. Then, the shear stress τ, acting on the sample at different locations, was calculated according to Eq.(5-20). The stress state (yield or not) of sample was judged by comparing the τ_f and τ. According to the stress state, we selected Eq.(5-23) or Eq.(5-25) to calculate the shear strain rate at every time step.

After yield, the τ_f^* and the η_t shown in Eq.(5-23) vary with shear rate $\dot{\gamma}$ and shearing time t, they were calculated at step n (time interval Δt) on basis of step n-1, as shown in Eq.(5-26).

$$[\tau_f^*]^n = [\sigma_n]^n \, \tan(\theta_f e^{-\kappa \cdot [\dot{\gamma}]^{n-1} \cdot \Delta t} + \phi) + C_{w1}$$

$$[\eta_t]^n = \frac{\eta}{\cos(\theta_f e^{-\kappa \cdot [\dot{\gamma}]^{n-1} \cdot \Delta t})}$$

(5-26)

In our SPH simulations, 2376 discrete particles were used to represent each of the fresh mortar. And the inner walls of the L-flow box and the sliding door were represented by 3234 fixed boundary particles, and 140 mobile boundary particles, respectively. In the beginning, the mobile boundary particles were let to move upward at a speed of 0.1 m/s, and they were stopped after they moved vertically 25 cm. The final flow shapes of three series of mortars obtained by the SPH method are shown in Fig. 5.3. Like the experimental results, the final flow distances increase with the decrease of W/C. In case of series No. 6 and No. 7 mortars, the final flow distance of VGM model is slightly larger than that of Bingham model.

Fig. 5.4 indicates the comparison of the relationships between the flow distance and the standing time, which are obtained by the experiments, and the SPH methods using the two models, respectively (when the flow velocity is less than 0.015 m/s, it is regarded that the flow stopped). As shown in this figure, for series No. 5 and No. 6 mortars, the numerical results using the VGM model are more consistent with the experimental results, the flow distance calculated by Bingham model is

Table 5.1 The input parameters of numerical simulations

Series No.	Parameters in VGM model								Bingham model parameters		Boundary model parameters	
	τ_f(Pa)	$\dot{\gamma}$(s^{-1})	η (Pa·s)	C_{w1}(Pa)	ϕ (rad)	θ_f(rad)	κ	σ_n (Pa)	τ_0 (Pa)	η_b(Pa·s)	τ_{sy} (Pa)	η_s (Pa·s)
1	1538	0.20	772	400	0.157	0.284	2.2	-	1254	833	2.0	100
2	569	0.18	558	150	0.054	0.121	1.5	-	379	560	1.0	40
3	302	0.16	455	90	0.030	0.062	0.7	-	111	457	0.2	5
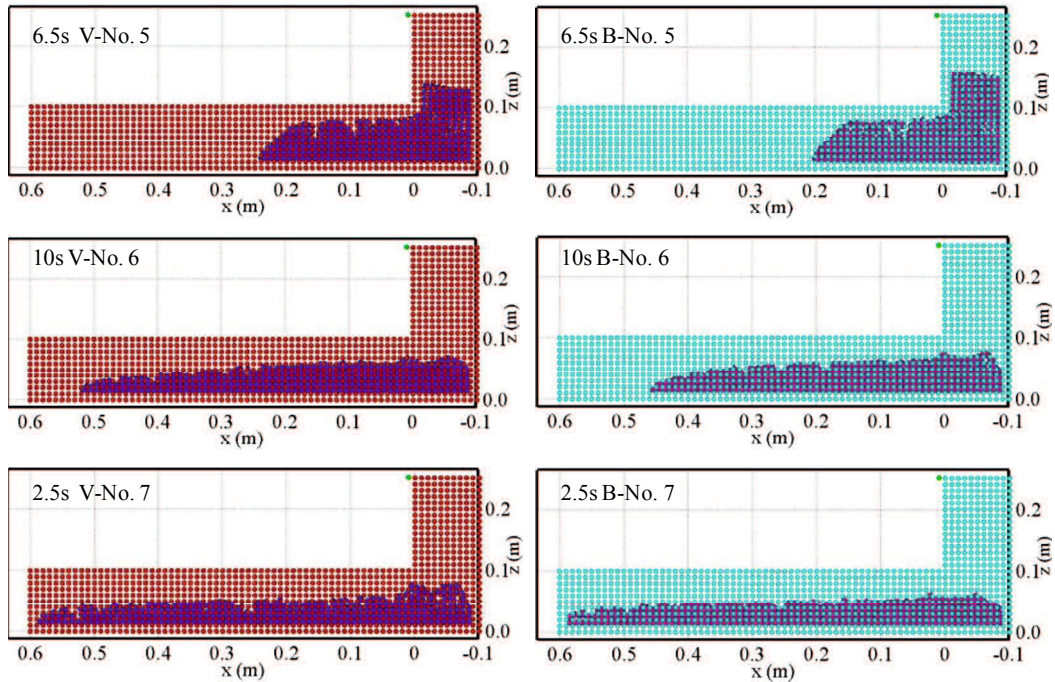
Fig. 5.3 Final shape of L-flow simulation. (V-No. n and B-No. n represent the numerical results using VGM model, and Bingham model, respectively)

smaller than that obtained by the VGM model for the same time. The errors of the numerical results using VGM model to the experimental results are almost within the range of ±12%. But when using Bingham model, the errors are -20~22%. However, in case of series No. 7 mortar, the numerical results using either of the VGM and Bingham models are very close to the experimental results. The errors of the numerical results based on any of the two models are within ±11%.

In order to clarify the effect of slippage resistance, the numerical results without considering the slippage resistance were also shown in Fig. 5.4. The numerical results of series No. 7 mortar, using the VGM model but ignoring the slippage resistance, were close to experimental results. But for series No. 5 and No. 6 mortars, the numerical results were not well consistent with the experimental results when the slippage resistance was not taken into account. This is because that the slippage resistance increases with the decrease of fluidity. Hence, in case of series No. 7 mortar with a lower W/C, even if the slippage resistance was ignored, there was no great difference between the numerical and experimental results, but for series No. 5 and No. 6 mortars, the slippage resistance is needed to consider. It is also concluded that the visco-plastic model is apt to use in SPH approach of fresh concrete.

When the W/C is low, fresh mortar has a low fluidity so that its fluid or suspension flow behavior becomes unobvious. The interaction between the particles or the particles' interlocking gives a prominent influence on the flow resistance of fresh mortar. The VGM model considers the
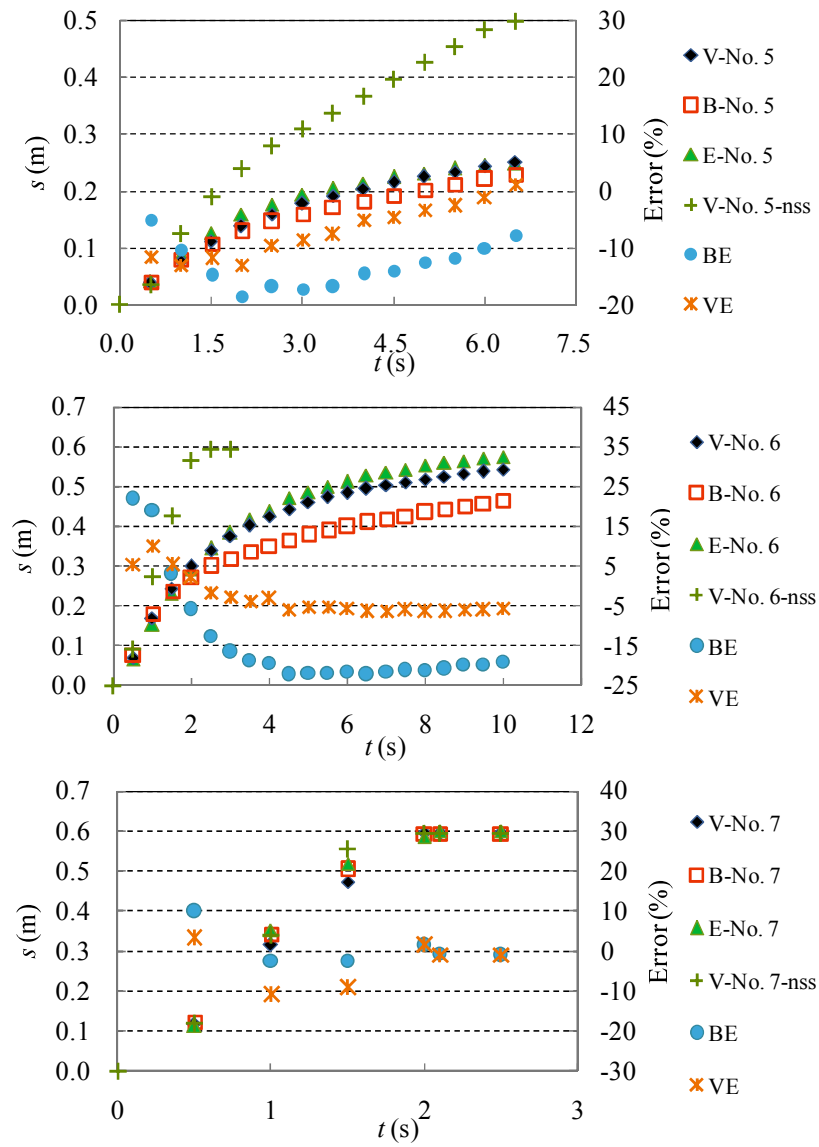
Fig. 5.4 Comparison of the numerical and experimental results of L-flow test. (VE, BE represent the error of numerical results based on VGM, and Bingham model, respectively, to experimental results, V-No. n-nss represents the numerical results using VGM model but not considering the slippage resistance)

change of fresh concrete's particle arrangement during the flow through introducing variable yield stress τ_f^* and plastic viscosity η_t, which vary with shearing time t, as shown in Eq.(5-23). As explained above, the particle arrangement of fresh concrete is expressed by the mean particle contact angle (θ), the variations of τ_f^* and η_t are basically resulted from the change of θ with shearing time. However, for the fresh mortar having high fluidity, its fluid flow behavior is predominant, accordingly the effect of the particle arrangement becomes slight. Hence, in this case, the VGM model has no advantage over Bingham model in the numerical analysis.

Fig. 5.5 shows the relationship between the flow velocity and the flow time. The numerical results are close to the experimental results for three mixtures. The flow velocity decreases with the
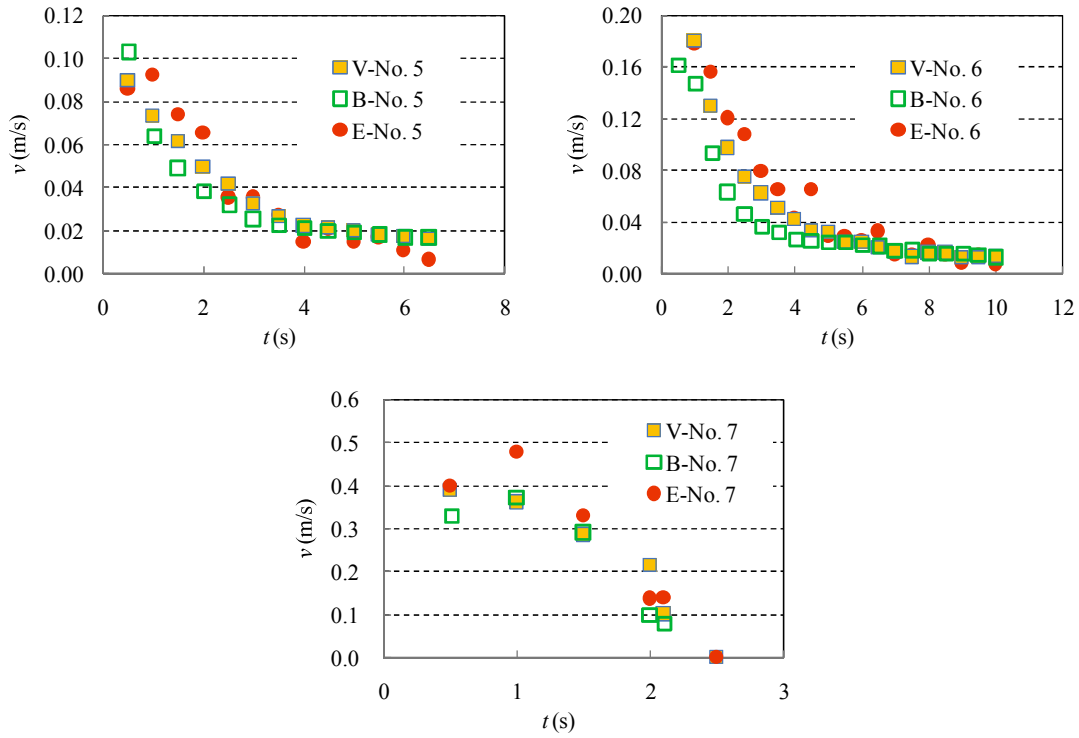
Fig. 5.5 Flow velocity of the mortars in L-flow box

flow W/C. This is because that the viscosity of mortar decreases with the increase of W/C.

Fig. 5.6 and Fig. 5.7 indicate the distributions of τ_f^* and η_t of the moving discrete particles of the mortar samples at the three moments, respectively. As seen from Fig. 5.6 and Fig. 5.7, the τ_f^* and η_t decrease with the increase of W/C. For the same sample and flow moment, the τ_f^* at lower location is larger. This is because the σ_n is larger at the lower location. Moreover, for the same flow moment, the discrete particles moving in the horizontal section of the box have smaller τ_f^* and η_t than that in the left vertical section. The τ_f^* of all the series and the η_t of series No. 5 and No. 6 mortars decrease obviously with the flow time. But series No. 7 mortar has a higher fluidity, thus its η_t is so small that it isn't almost further reduced by the free flow.

Fig. 5.8 shows the variations of the average values of τ_f^* and η_t of the whole moving particles after yield with the flow time. The average τ_f^* decreases with the flow time and finally approaches to a certain value. This is because the particle interlocking is reduced by the free flow. The decrease of normal stress σ_n is another reason, along with the samples moving from the vertical section to the horizontal section of the L-box. But after a long time flow, the particle interlocking approaches to the smallest degree or complete breakdown, and the σ_n at the horizontal section no longer decreases, the τ_f^* doesn't further change. The average η_t of series No. 5 mortar decreases with the flow time. However, the average η_t of any of series No. 6 and No. 7 mortars nearly don't change. Series No. 6 and No. 7 mortars had a larger W/C, accordingly had higher fluidity, the particle interlocking structure in initial state is so weak that it can't be further broken.

98
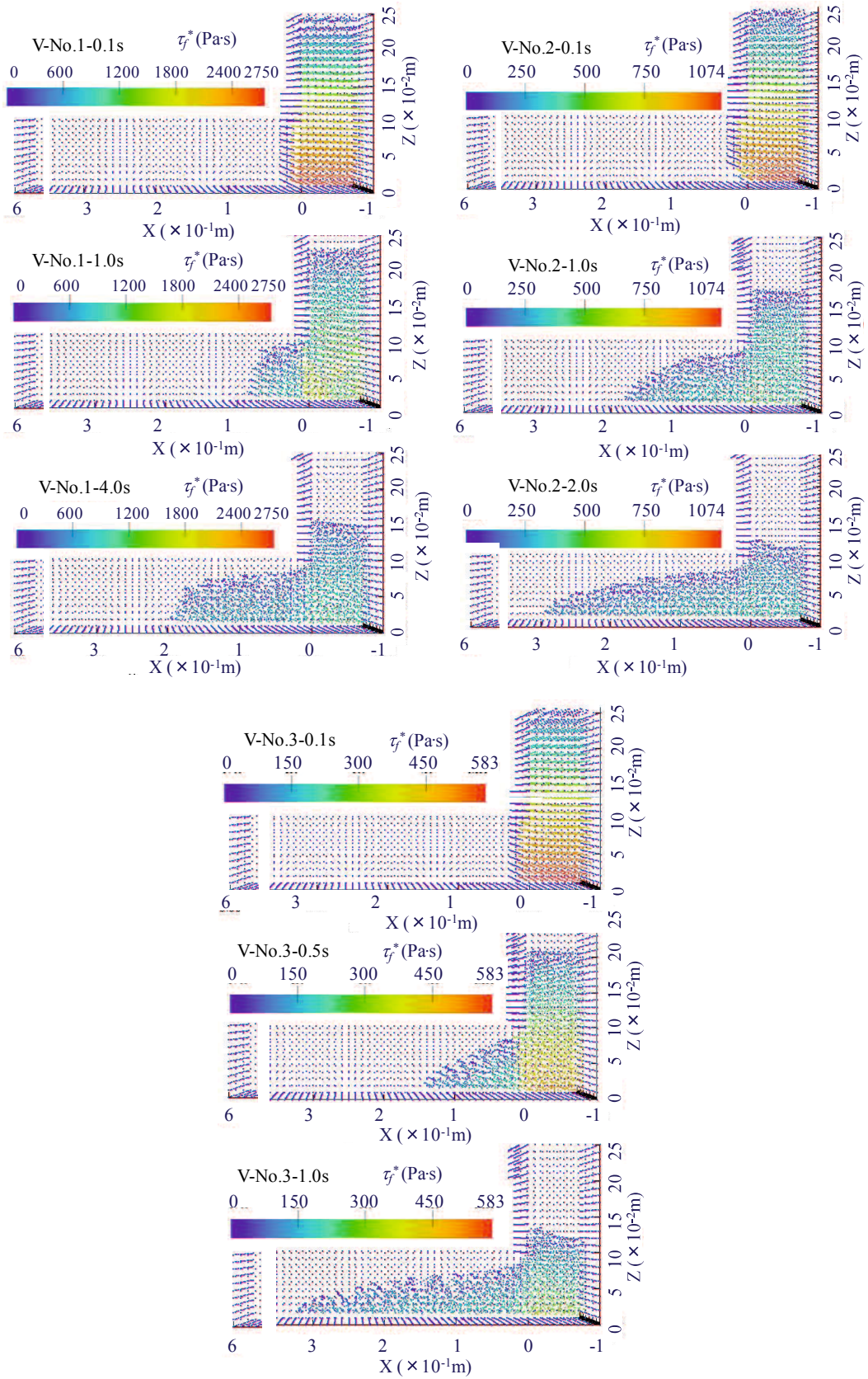
Fig. 5.6 Calculating results of τ_f^* distribution at different moments
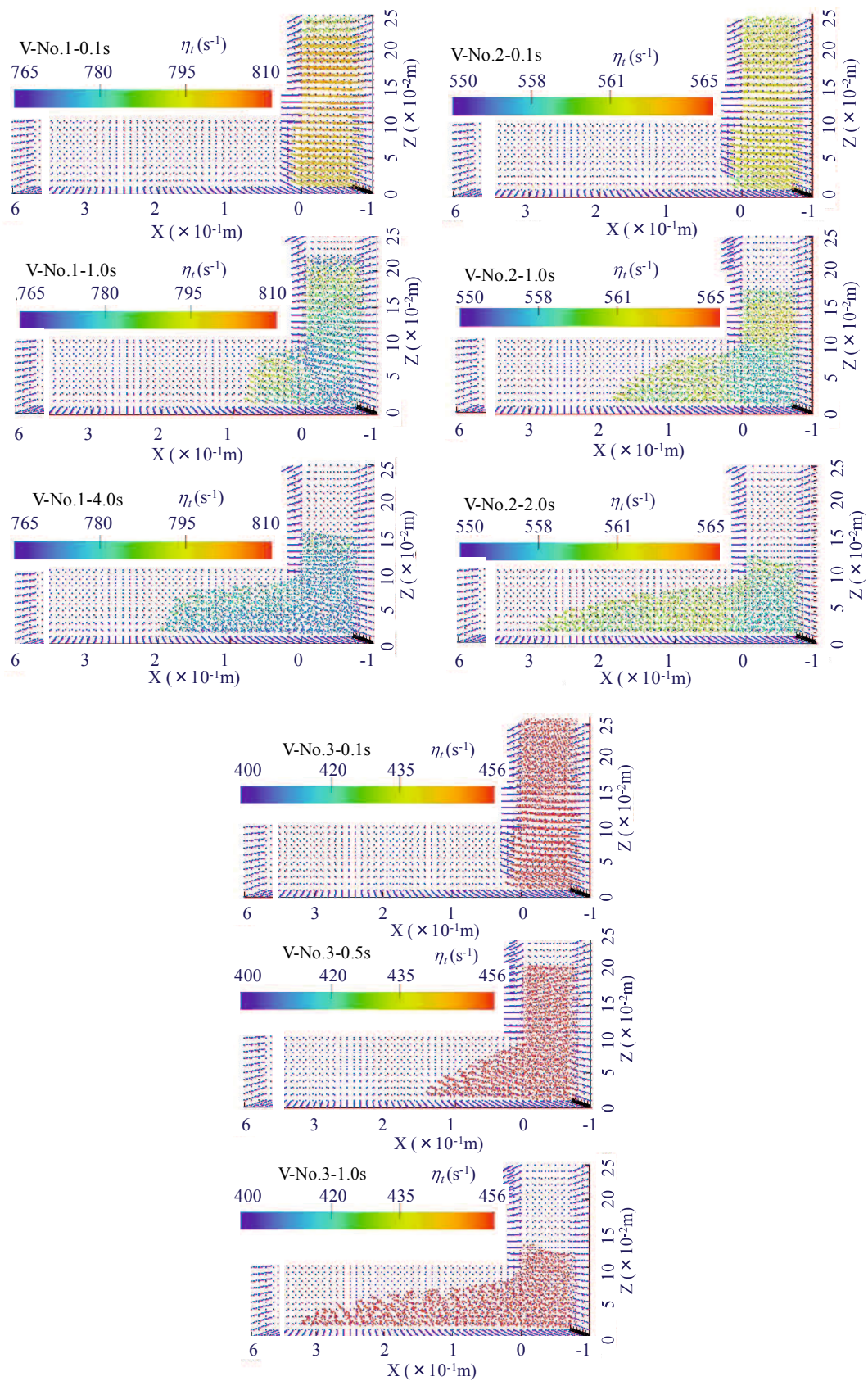
Fig. 5.7 Calculating results of η_f distribution at different moments
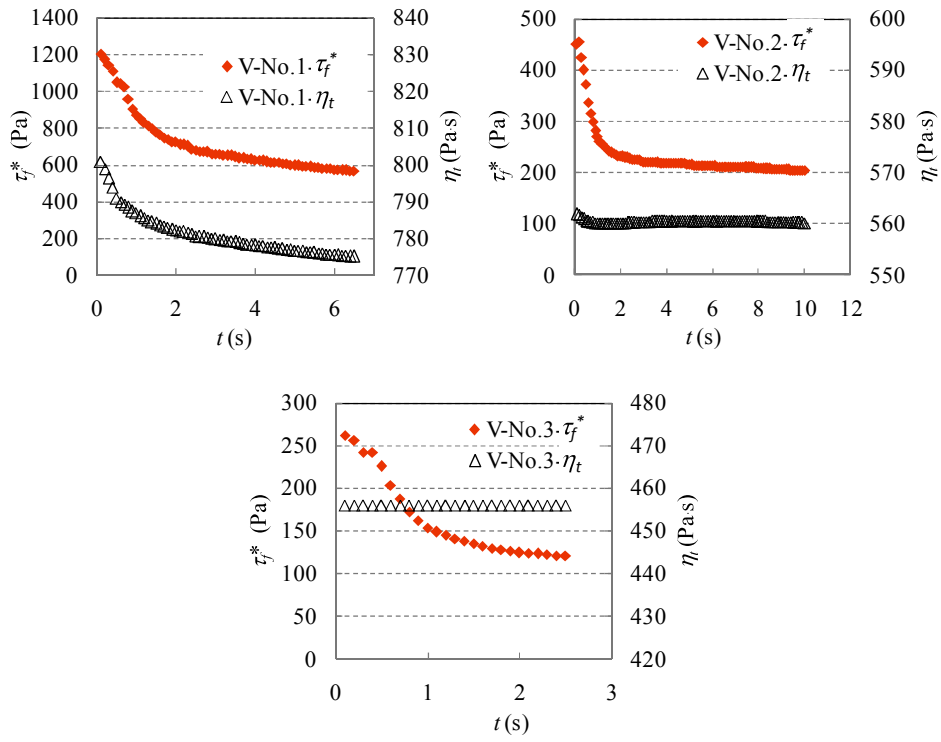
Fig. 5.8 Variations of τ_f^* and η_t in the VGM model with the flow time

5.5 Conclusions

In this paper, a new flow simulation method of fresh concrete was studied on the basis of SPH approach. The VGM model was employed as constitutive model, which can describe the nonlinear, shearing time-dependent, and pressure-dependent flow behaviors of the flow behaviors of fresh concrete. Moreover, a visco-plastic model was incorporated into the SPH approach for describing the slippage resistance of fresh concrete at the boundary. And for making a comparison, the numerical flow simulations with the Bingham model were also conducted.

Fresh concrete has granular flow behavior, including inter-particle friction, dilatant deformation, and particles' interlocking, etc. The degree of particles' interlocking is usually described by mean particle contact angle (θ). For the mixture with low fluidity, the particle contacts increase, and its granular flow behaviors are obvious. The mean inter-particle frictional angle (ϕ) and the normal stress (σ_n) on the shear plane are taken into account in the VGM model, by which the granular flow behaviors of fresh concrete are reflected. Moreover, The VGM model can reflect the flow behaviors affected by the change of θ with shear deformation. Therefore, the numerical results using the VGM model are more consistent with the experimental results than Bingham model. Also, the numerical simulation using the VGM model can reflect the shearing time-dependence of the flow behaviors since the yield stress and viscosity in the VGM model change with the shear flow.

The VGM model can reflect granular flow behavior, it can not only be suited to high fluidity concrete, such as self compacting concrete, but also to low fluidity concrete. However, for the mixture with high fluidity, its granular flow behavior is not obvious, and the particles' interlocking has a little effect on its flow behaviors. Hence, the flow behaviors can be approximately described by Bingham model. Using the VGM model and the Bingham model got close numerical results.

Moreover, combining the VGM model and the visco-plastic model can increase the accuracy of SPH analysis of fresh concrete, especially for low fluidity concrete.

References

[1] J. E. Wallevik, Rheology of Particle Suspensions-Fresh Concrete, *Ph. D Thesis of Norwegian University of Science and Technology,* (2003) 11-47.

[2] Z. Li, T. Ohkubo, Y. Tanigawa, Flow performance of high-fluidity concrete, *Journal of Materials in Civil Engineering,* 16 (6) (2004) 588-596.

[3] Z. Li, T. Ohkubo, Y. Tanigawa, Theoretical analysis of time-dependence and thixotropy of fluidity for high fluidity concrete, *Journal of Materials in Civil Engineering,* 16 (3) (2004) 247-256.

[4] N. Roussel, A thixotropy model for fresh fluid concretes: theory, validation and applications, *Cement and Concrete Research,* 36 (10) (2006) 1797-1806.

[5] R. Deeb, S. Kulasegaram, B. L. Karihaloo, 3D modelling of the flow of self-compacting concrete with or without steel fibres. Part I: slump flow test, *Computational Particle Mechanics,* 1 (4) (2014) 373-389.

[6] H. Lashkarbolouk, A. M. Halabian, M. R. Chamani, Simulation of concrete flow in V-funnel test and the proper range of viscosity and yield stress for SCC, *Materials and Structures,* 47 (10) (2014) 1729-1743.

[7] R. Deeb, S. Kulasegaram, B. L. Karihaloo, 3D modelling of the flow of self-compacting concrete with or without steel fibres. Part II: L-box test and the assessment of fibre reorientation during the flow, *Computational Particle Mechanics,* 1 (4) (2014) 391-408.

[8] M. A. Dhaheer, S. Kulasegaram, B. Karihaloo, Simulation of self-compacting concrete flow in the J-ring test using smoothed particle hydrodynamics (SPH), *Cement and Concrete Research,* 89 (2016) 27-34.

[9] W. Alyhya, S. Kulasegaram, B. Karihaloo, Simulation of the flow of self-compacting concrete in the V-funnel by SPH, *Cement and Concrete Research,* 100 (2017) 47-59.

[10] N. Roussel, Correlation between yield stress and slump: comparison between numerical simulations and concrete rheometers results, *Materials and Structures,* 39 (4) (2006) 501-509.

[11] J. Spangenberg, N. Roussel, J. Hattel, et al., Flow induced particle migration in fresh concrete: theoretical frame, numerical simulations and experimental results on model fluids, *Cement and Concrete Research,* 42 (4) (2012) 633-641.

[12] D. Feys, Interactions between rheological properties and pumping of self-compacting concrete, in, Ghent University, 2009.

[13] S. Jacobsen, L. Haugan, T. A. Hammer, et al., Flow conditions of fresh mortar and concrete in different pipes, *Cement and Concrete Research,* 39 (11) (2009) 997-1006.

[14] H. Hafid, G. Ovarlez, F. Toussaint, et al., Estimating measurement artifacts in concrete rheometers from MRI measurement on model materials, in: Design, Production and Placement of Self-Consolidating Concrete, Springer, 2010, pp. 127-137.

[15] J. Murata, K. Suzuki, Study on grout flow in pipe with slip at wall, *Japan Society of Civil Engineers,*

38 (7) (1987) 129-136.

[16] M. B. Liu, G. R. Liu, Smoothed particle hydrodynamics (SPH): an overview and recent developments, *Archives of Computational Methods in Engineering,* 17 (1) (2010) 25-76.

[17] F. A. Allahdadi, T. C. Carney, J. R. Hipp, et al., High strain Lagrangian hydrodynamics: a three dimensional SPH code for dynamic material response, *Journal of Computational Physics,* 109 (1) (1993) 67-75.

[18] G. R. Johnson, R. A. Stryk, S. R. Beissel, SPH for high velocity impact computations, *Computer Methods in Applied Mechanics and Engineering,* 139 (1-4) (1996) 347-373.

[19] M. B. Liu, G. R. Liu, Z. Zong, et al., Computer simulation of high explosive explosion using smoothed particle hydrodynamics methodology, *Computers and Fluids,* 32 (3) (2003) 305-322.

[20] S. Shao, E. Y. Lo, Incompressible SPH method for simulating Newtonian and non-Newtonian flows with a free surface, *Advances in Water Resources,* 26 (7) (2003) 787-800.

[21] J. Monaghan, A. Kos, Solitary waves on a Cretan beach, *Journal of waterway, port, coastal, and ocean engineering,* 125 (3) (1999) 145-155.

[22] H. H. Bui, R. Fukagawa, K. Sako, et al., Lagrangian meshfree particles method (SPH) for large deformation and failure flows of geomaterial using elastic–plastic soil constitutive model, *International Journal for Numerical and Analytical Methods in Geomechanics,* 32 (12) (2008) 1537-1570.

[23] M. S. Shadloo, A. Zainali, M. Yildiz, et al., A robust weakly compressible SPH method and its comparison with an incompressible SPH, *International Journal for Numerical Methods in Engineering,* 89 (8) (2012) 939-956.

[24] J. J. Monaghan, A. Kos, Solitary waves on a Cretan beach, *Journal of Waterway, Port, Coastal, and Ocean Engineering,* 125 (3) (1999) 145-155.

[25] J. J. Monaghan, Simulating free surface flows with SPH, *Journal of Computational Physics,* 110 (2) (1994) 399-406.

[26] J. J. Monaghan, On the problem of penetration in particle methods, *Journal of Computational Physics,* 82 (1) (1989) 1-15.

[27] T. C. Papanastasiou, Flows of materials with yield, *Journal of Rheology,* 31 (5) (1987) 385-404.

[28] H. Zhu, N. S. Martys, C. Ferraris, et al., A numerical study of the flow of Bingham-like fluids in two-dimensional vane and cylinder rheometers using a smoothed particle hydrodynamics (SPH) based method, *Journal of Non-Newtonian Fluid Mechanics,* 165 (7) (2010) 362-375.

[29] Z. Li, Theoretical investigation on rheological properties of fresh concrete, *Journal of Structural and Construction Engineering, Transaction of Archcitectural Instistue of Japan,* 78 (687) (2013) 895-904.

[30] Z. Li, K. kajiwara, M. Iidaka, Investigation on particle contact angle of fresh concrete using X-ray CT imaging, *Journal of the Society of Matarials Science,* 62 (9) (2013) 585-591.

[31] Z. Li, Y. Tanigawa, Investigation on granular characteristics of fresh concrete based on visualized experiment using alternative materials, *Journal of Structural and Construction Engineering, Transaction*

of Archcitectural Instistue of Japan, 77 (678) (2012) 1175-1184.

[32] Z. Li, Rheological model and rheometer of fresh concrete *Journal of Structural and Construction Engineering, Transaction of Archcitectural Instistue of Japan,* 80 (710) (2015) 527-537.

[33] Z. Li, J. Li, Exterimental investigation on shear defromation of fresh concrete, *Journal of Structural and Construction Engineering, Transaction of Archcitectural Instistue of Japan,* 75 (653) (2010) 1173-1180.

[34] Y. Sakihara, S. Iraha, T. Iribu, et al., Numerical flow simulation of fresh concrete with SPH, *Japan Concrete Institute,* 26 (1) (2004) 1149-1154.

Chapter 6
Conclusions and Future Works

6.1 Conclusions

This paper develops the DEM and SPH simulation to study the standing and shearing time-dependent flow behaviors of fresh concrete. The research findings are concluded as follows:

The all experiments used in this paper were performed in chapter 3. Firstly, the used materials and their mix proportions were given. Then the flow table test, funnel flow, L-flow test and RSNS rheometer test were presented, respectively. The experimental results of these tests were provided.

1) Fresh mortars with same W/C (series No. 2-4), the spread diameter increased with the decrease of cement content. Fresh mortars with different W/C (series No. 5-7), the spread diameter increased with the increase of W/C.

2) Within series No. 1-4 mortars, for the same series, the flow time of funnel flow increased with the standing time. For different series (No. 2-4), the flow time of funnel flow decreased with the decrease of cement content.

3) The flow time of L-flow test decrease with the increase of W/C and τ_f, η in VGM model and τ_0, η_b increased with the decrease of W/C.

In chapter 4, the general DEM was introduced. The mechanism of the time-dependence was discussed, followed by proposing a new numerical approach to predict the standing time-dependent flow behavior on the basis of the Discrete Element Method (DEM). In the proposed standing td-DEM model, both the effects of hydration and physical flocculation were taken into account. The parallel bond model was employed to express the physical dispersed-flocculation behavior of particles, and the clumps of particles were used to represent the bound particles due to the hydration of cement. A viscous damping model was used for the energy dissipation of particle. The changes of the numbers of the clumped particles and the flocculation particles with the standing time were investigated theoretically. Based on these investigations, the time-dependent stiffness coefficients of the parallel bond model were proposed.

The input parameters of standing td-DEM model was calibrated by flow table test. Using these input parameters, the numerical calculation of the gravity-induced funnel flow of fresh mortar were performed. Compared to the experimental results, the DEM approach can accurately predict the standing time-dependence of fresh concrete with or without mineral admixture.

In chapter 5, a numerical approach, based on SPH and VGM model was proposed to study the shearing time-dependence of fresh concrete. A shearing resistance model of fresh mortar was

employed to consider the effect of boundary. Numerical simulations of L-flow of three types fresh mortar with different W/C ratio were conducted. In order to contrast, the numerical simulation using SPH and Bingham model were also performed for the same mortars.

The numerical simulation using the VGM model can reflect the shearing time-dependence of flow behaviors of fresh concrete since the yield stress and viscosity in the VGM model change with the shearing time. Moreover, the VGM model can describe the nonlinear and pressure -dependence of the rheological behaviors of fresh concrete. Hence, The numerical results of VGM model based SPH simulation are more consistent with the experiment.

6.2 Future Works

For rationalizing concrete's design, production and construction, the flow simulation-based workability design is desired. In the future, I will continue to study the numerical simulation method of fresh concrete to make it to have enough accuracy required by the workability design, and to be applied to the vibration state.

1) During the transportation and waiting to cast, due to the hydration of cement, the rheological properties of concrete change with time. I already developed an standing time-dependent DEM. Hence, after developed successfully a more accurate SPH approach through this study, a DEM-SPH coupling numerical method will be developed to predict the workability of fresh concrete at any time point, only using the rheological parameters measured right after mixing.

2) In most cases, concrete is cast under vibration. I would like to develop a numerical flow simulation method for fresh concrete under the vibrated state, based on the achievements of this study. We have investigated the rheological behaviors of fresh concrete under vibration by the RSNS rheometer, quantitatively examined the relationship of shear stress and shear strain rate, and proposed a constitutive model for describing the rheological behaviors of fresh concrete in vibrated state. Using this constitutive model, I would like to further develop a novel numerical SPH approach. Through these researches, I wish to steadily promote the advance of simulation technology and make it fit for practical use.

List of Papers

Referred Papers in Journal etc.

1. <u>G. Cao</u>, Z. Li, Numerical flow simulation of fresh concrete with viscous granular material model and smoothed particle hydrodynamics, *Cement and Concrete Research*, Vol. 100, pp. 263-274, 2017, (***Impact Factor* 4.762**).

2. Z. Li, <u>G. Cao</u>, Y. Tan, Prediction of time-dependent flow behaviors of fresh concrete, *Construction and Building Materials,* Vol. 125, pp. 510-519, 2016, (***Impact Factor*3.169**).

3. <u>G. Cao</u>, Z. Li, K. Guo, Analytical study on the change of fluidity of fresh concrete containing mineral admixture with rest time, *Journal of Advanced Concrete Technology*, Vol.15, pp.713-723. (**IF: 0.835**)

Referred Papers in International Conference Proceedings

4. <u>G. Cao</u>, Z. Li, Rheological model of fresh concrete in vibrated state, *Proceedings of the International Conference on Mechanics, Civil Engineering for Building Material, MCEBM* 2017, China, pp. 480-485, 2017.

Technical Papers

5. <u>G. Cao</u>, Z. Li, Analytical study on flow behaviors of fresh concrete with viscous granular materials model and Smoothed Particle Hydrodynamics, *Summaries of Technical Papers of Annual Meeting*, *Architectural Institute of Japan* (AIJ), August, 2017. (in print)

6. <u>G. Cao</u>, Z. Li, G. Kun, Analytical study on time-dependent fluidity of fresh concrete, Part 1: DEM model, *Proceedings of Annual Research Meeting Chugoku Chapter, Architectural Institute of Japan* (AIJ), Vol. 40, pp, 21-24, March, 2016.

7. G. Kun, Z. Li, <u>G. Cao</u>, Analytical study on time-dependent fluidity of fresh concrete, Part 2: Simulation of funnel test, *Proceedings of Annual Research Meeting Chugoku Chapter, Architectural Institute of Japan* (AIJ), Vol. 40, pp. 25-28, March, 2016.

8. <u>G. Cao</u>, Z. Li, N. Maeda, Experimental study on the effects of mix proportions on the rheological constants of fresh concrete, *Summaries of Technical Papers of Annual Meeting*, *Architectural Institute of Japan* (AIJ), pp. 275-276, August, 2016.

9. N. Maeda, <u>G. Cao</u>, Z. Li, Study on the rheological properties of fresh concrete under vibration state, *Summaries of Technical Papers of Annual Meeting*, *Architectural Institute of Japan* (AIJ), pp. 277-278, August, 2016.

10. <u>G. Cao</u>, Z. Li, A. Ishida, N. Maeda, Test method and influencing factors of rheological performance

of fresh concrete, Part 1: Rheological test method and the used specimens, *Proceedings of Annual Research Meeting Chugoku Chapter, Architectural Institute of Japan* (AIJ), Vol. 39, pp. 45-48, March, 2016.

11. A. Ishida, Z. Li, N. Maeda, <u>G. Cao</u>, Test method and influencing factors of rheological performance of fresh concrete, Part 2: Rheological performance and rheological constants in static state, *Proceedings of Annual Research Meeting Chugoku Chapter, Architectural Institute of Japan* (AIJ), Vol. 39, pp. 49-52, March, 2016.

12. N. Maeda, Z. Li, A. Ishida, <u>G. Cao</u>, Test method and influencing factors of rheological performance of fresh concrete, Part 3: Rheological performance and rheological constants in vibrated state, *Proceedings of Annual Research Meeting Chugoku Chapter, Architectural Institute of Japan* (AIJ), Vol. 39, pp. 53-56, March, 2016.